2024

Design and kinematic testing of a resin artificial Monarch butterfly wing

Thomas Payne Clark

DESIGN AND KINEMATIC TESTING OF A RESIN ARTIFICIAL MONARCH BUTTERFLY WING

Thomas Payne Clark

A THESIS

Submitted in partial fulfillment of the requirements
for the degree of Master of Science in Aerospace Systems Engineering
in
The Department of Mechanical and Aerospace Engineering
to
The Graduate School
of
The University of Alabama in Huntsville
May 2024

Approved by:

Dr. Chang-kwon Kang, Research Advisor, Committee Chair
Dr. Farbod Fahimi, Committee Member
Dr. Ryan Conners, Committee Member
Dr. George Nelson, Department Chair
Dr. Shankar Mahalingham, College Dean
Dr. Jon Hakkila, Graduate Dean

Abstract

DESIGN AND KINEMATIC TESTING OF A RESIN ARTIFICIAL MONARCH BUTTERFLY WING

Thomas Payne Clark

A thesis submitted in partial fulfillment of the requirements for the degree of Master of Science in Aerospace Systems Engineering

Mechanical and Aerospace Engineering

The University of Alabama in Huntsville
May 2024

Due to its ability to travel long distances efficiently, as evidenced by its yearly migration, the monarch butterfly is a strong candidate upon which to base a micro-aerial vehicle. Of primary importance in this venture is designing artificial wings with similar kinematics to a monarch wing. A first attempt produced a wing that differed significantly from a monarch wing in terms of deformation while flapping and empirical force coefficient trends. Using a new resin-based 3D printer, a new wing has been designed and developed to improve upon the issue with the original artificial wing. Both wings are tested using a flapping mechanism and an array of VICON tracking cameras to measure their kinematics while flapping. The new wing proves to be a much closer match to the monarch wing in terms of deformation and empirical force production trends.

Acknowledgements

I would like to thank my advisor Dr. Chang-kwon Kang for his assistance, advice, and support throughout my time as an undergraduate and graduate researcher. I would like to thank Tim Morris, Rachel Twigg, Madhu Sridhar, and Shreyas Raghu for their help with learning how to use the equipment in the ATOM Lab and their support. I would like to thank Dr. Kyung-Ho Roh for the use of his lab space to manufacture the bonded wings. Finally, I would like to thank my family and friends who have offered support and advice throughout this process.

Table of Contents

List of Figures

List of Tables

Chapter 1. Introduction

1.1 Background

During their annual migration to winter in Central Mexico, monarch butterflies travel distances of up to 4000 kilometers [1-5]. This incredible feat of long-distance travel makes the monarch butterfly unique in the *Nymphalidae* family [1]. Little is known about the aerodynamics that allow such a small insect to travel such great distances, but it is assumed that monarchs take advantage of the atmospheric boundary and the low atmospheric densities at high altitudes to decrease aerodynamic drag and improve soaring flight [6]. A monarch butterfly is shown here in Figure 1.1.

Figure 1.1 A single monarch butterfly sitting with its wings extended.

In studying how a monarch butterfly can travel such distances, the logical starting point is a study of its wings. Monarch wings are very flexible and experience

large deformations during flight. This allows the flapping wing of the monarch to generate large forces (relative to its own size) with less power when compared to rigid wings [7-23].

1.2 Insect Wing Aerodynamics and Structure

The aerodynamics of insect flapping wing flight has been researched for years. Studies have attempted to appraise the efficiency of flexible flapping wings using insect wings [8, 9, 12-15, 19, 24] as well as to look into low-Reynolds number vortex dynamics [10, 13, 17, 21, 22, 25, 26]. Insects have also been shown to create large amounts of lift (relative to their bodyweight) and possess great maneuverability [7, 8, 9]. In addition, insects can maintain stable flight despite their small size and weight through coupling their wing flapping and body movement [17, 19, 25].

The flight capabilities of insects are due to how their wings interact with the surrounding unsteady airflow. This interaction is impacted by the material properties of the wings. These properties determine how the wings will structurally react when forces are exerted on them. Thus, these material properties are very important to better understand insect flight dynamics. Several studies have examined the density and flexural stiffness of insect wings [27-32]. Studies by Combes *et al.* [27], Tanaka and Wood [28], and Steppan [29] discovered that the flexibility of the wings changed when the wings were dry versus when they were wet and found that the chordwise and spanwise stiffnesses differed for wings. Additional studies measured the stiffness of various insect wings including bees and blowflies [30-32]. However, the monarch butterfly was not included in these studies.

To better understand the monarch butterfly's long-distance travel capabilities and develop bioinspired micro-aerial vehicles, several studies researched the properties of its wings. Twigg [33] examined the material properties of monarch butterfly wings and developed a first attempt at an artificial reproduction of a monarch fore-wing. A second study by Morris [34] tested the force generation capabilities of a single monarch fore-wing flapping at varying frequencies and a set amplitude. However, the artificial wing suffers from high stiffness and an asymmetric construction that impacts its force generation characteristics. The asymmetric construction results in greater force production in the downstroke than in the upstroke which leads to decreased turning ability in a vehicle using these wings. Figure 1.2 shows a sample empirical lift coefficient curve for the wing developed by Twigg [33].

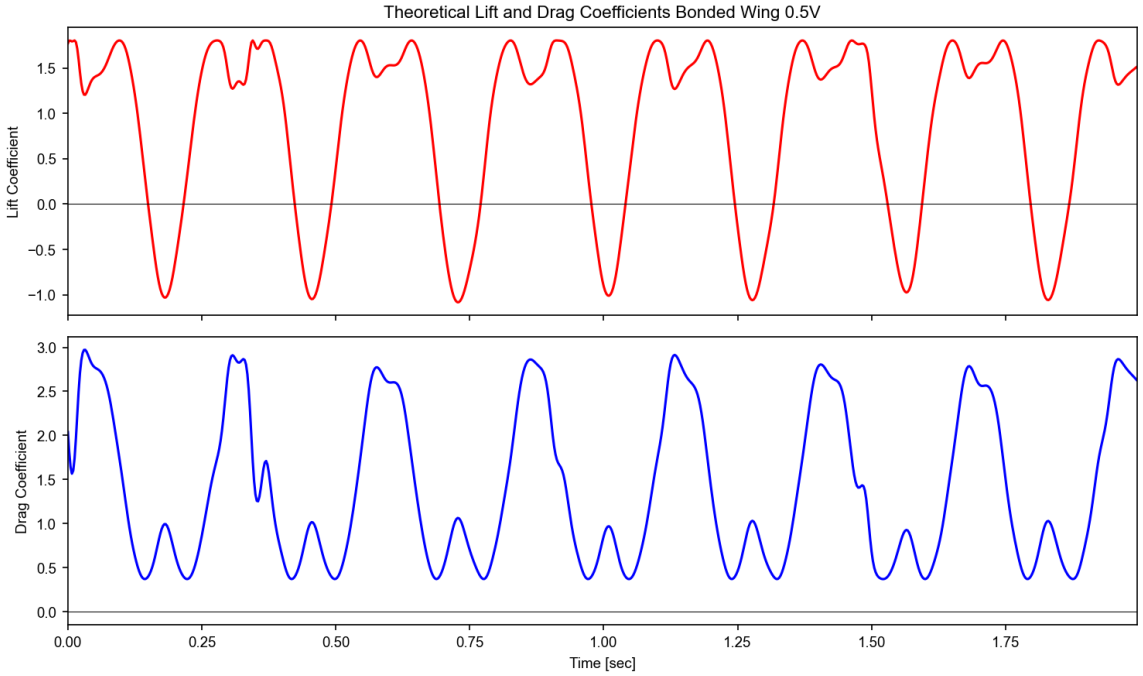

Figure 1.2 Empirical lift and drag curves calculated for the artificial wing developed by Twigg [33]. The lift curve (upper graph) does not oscillate around zero, but shows a bias towards positive lift coefficient.

1.3 Objective

The objective of this project is to develop a new artificial butterfly wing that better mimics the symmetric flapping motion of a monarch butterfly wing. In preparation for designing a bio-inspired micro-aerial vehicle, a new wing needs to be developed that produces symmetric lift in both its upstrokes and downstrokes like a monarch wing. This is especially important when attempting to create a flying vehicle as asymmetries in the force production can decrease the maneuverability of the vehicle.

The goal of this thesis is to demonstrate the improvements made in terms of wing deformation and lift production trends using a new artificial wing. For this, motion capture data of both the newly developed artificial wing and the design by Twigg [33] are taken using a VICON motion-tracking system. These data are collected at a set flapping amplitude across several flapping frequencies. The data are post-processed to determine the feathering angle (a measure of wing deformation while flapping) and empirical force coefficients for both artificial wings. These results are compared to the monarch wing data in the study by Morris [34]. The progress made with the new artificial wing design will aid the development of a bio-inspired micro-aerial vehicle.

1.4 Novel Contributions

The primary contribution of this study is the development of a new artificial wing. New printing methods using a resin-based 3D printer were developed that allowed for integrated printing of both the wing veins and the wing membrane in a single print. The VICON camera setup [34] was updated by removing and replacing two malfunctioning

cameras. In addition, the number of VICON cameras was decreased by one to increase the efficiency of data gathering.

1.5 Outline

Chapter 2 contains a literature study that details monarch wing aerodynamics (Section 2.1), monarch butterfly wing properties (Section 2.2), monarch wing angle and force measurements (Section 2.3), and recent developments in flapping wing micro-aerial vehicles (Section 2.4). Chapter 3 explains the experimental and data processing methodologies. The manufacturing process for the bonded wing and the integrated wing are presented (Section 3.1 and 3.2) as well as the data acquisition process (Section 3.3), the calculations for empirical lift and drag coefficients (Section 3.4), and an overview of the experimental design (Section 3.5). Chapter 4 presents the results for the wing angles and empirical force coefficients for the monarch wing (Section 4.1), bonded wing (Section 4.2), and the integrated wing (Section 4.3) with direct comparisons of the results (Section 4.4). Chapter 5 presents concluding remarks (Section 5.1) as well as recommendations for future studies (Section 5.2).

Chapter 2. Literature Review

2.1 Monarch Wing Aerodynamics

Unsteady aerodynamic mechanisms such as clap and fling, leading-edge vortex generation and shedding, and wake-capture benefit butterflies in their flight [7]. Unfortunately, these phenomena have not been sufficiently studied due to the dynamics of butterflies' coupled wing-body movements and the complicated interactions between a fluid and a large, thin flapping wing. It is known that monarch butterflies have the lowest wing loading among insects [27]. This implies that monarch butterflies have large wings when compared to their small body size. This low wing loading allows the monarch butterfly to have great agility [8, 16-18]. The relative wing loadings of several insects, birds, and aircraft are shown here in Figure 2.1.

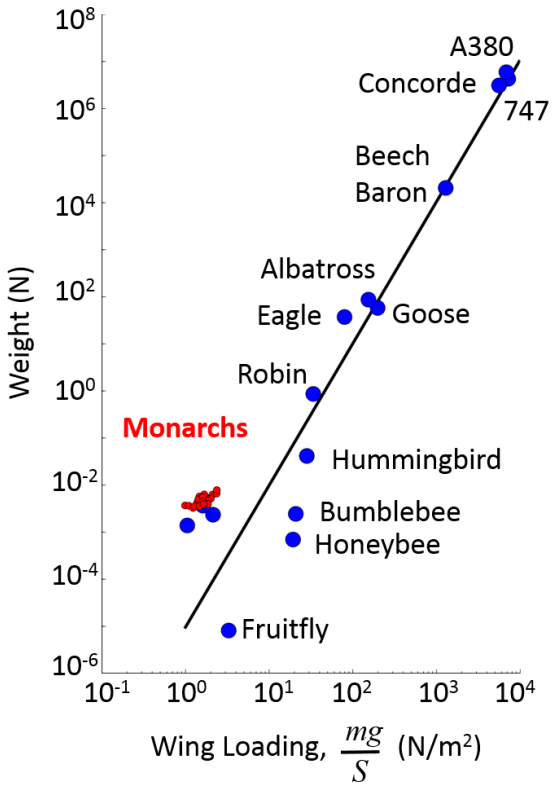

Figure 2.1 Great Flight Diagram. From Kang [37]. Reprinted with permission.

It has been seen with other insects that insect wings have fluid-structure mechanisms that reduce drag and increase lift. For instance, a reverse von Karman street, produced by vortices along the wing's surface that are shed in the downstream direction, increases the thrust produced by a wing [13, 17]. The production and shedding of vortices are the product of passive pitching of the insect's wing as insects are not capable of actively pitching their wings [11]. This passive pitching allows the vortices to remain attached to the wing surface for a longer distance which in turn increases the lift production [12, 25].

One of the most important characteristics of flapping wings is their flexibility. This flexibility minimizes flight disturbances due to wind gusts and allows for anisotropic wing characteristics such as producing different amounts of lift on the upstroke versus the

downstroke [15, 19]. Because of this, it has been assumed that an optimal wing flexibility exists for both lift production and efficiency [8, 9, 12, 23].

2.2 Monarch Butterfly Wing Properties

Twigg *et al*. [33, 39] is the only study so far to produce data about the structure and properties of monarch butterfly wings. Using a micro-CT scan with a spatial resolution of 10 μm, the authors were able to measure the volume of a monarch wing [33]. From this measurement and a measurement of the wing's mass, Twigg *et al.* [33, 39] was able to calculate the density of a monarch wing to be 307 kg/m^3. This differed greatly from the value previously reported by Wainwright *et al*. [31] for insect wing structural densities. In that paper, Wainwright reported the wing's density as 1200 kg/m^3 [31]. However, this value was determined from a blowfly (*Phormia*) whereas Twigg's value was from a monarch (*D. Plexxipus*) [31,33]. The discrepancies can be further explained by the equipment that Twigg *et al.* [33, 39] used. The equipment used by Twigg *et al.* [33, 39] was much more precise than the equipment used by Wainwright [31], giving a much more valid volume measurement.

In addition to determining the density of a monarch wing, Twigg *et al.* [33, 39]also used a finite element method (FEM) to determine the elastic modulus of the wing [33]. Using the CT scan results, Twigg *et al.* [33, 39]developed a SolidEdge model of the butterfly wing and applied an FEM to the model [33]. Several different forces were applied at the 70% chord length point of the model [33]. The tests resulted in an average spanwise elastic modulus of 2.91×10^9 N/m^2 and an average chordwise elastic modulus of 0.36×10^9 N/m^2 [33]. The results from this analysis are displayed below in Table 2.1.

Table 2.1 Elastic modulus of the hollow, tapered vein determined using FEM in both the spanwise and chordwise directions. From Twigg *et al.* [33, 39]. Reprinted with permission.

Spanwise			Chordwise		
Force, F (mN)	**Displacement, δ (mm)**	**Elastic Modulus, E ($\times 10^9$ N/m^2)**	**Force, F (mN)**	**Displacement, δ (mm)**	**Elastic Modulus, E ($\times 10^9$ N/m^2)**
1.02	1.32	2.18	2.03	0.67	0.43
2.00	5.30	4.50	3.03	1.15	0.50
3.00	4.00	2.25	4.01	0.74	0.24
3.99	6.80	2.88	5.03	1.00	0.26
4.99	9.10	3.08	6.03	1.69	0.37
6.00	9.23	2.60			
Average		**2.91**	**Average**		**0.36**

2.3 Monarch Wing Angle and Force Measurements

In addition to studying the wing properties, Twigg [33] did a preliminary study of the angles and force generation of a single flapping monarch wing [33]. Twigg [33] used a Micron 6mm Ornithopter gearbox with a flapping amplitude of 20° [33, 36]. Twigg used 6 VICON T40 cameras to record the wing motion and an ATI Nano 17 Titanium force transducer to record the wing forces. Three reflective markers were placed on the wing while two other markers on the gearbox served as stationary reference points. The VICON cameras recorded at a rate of 200 Hz for 5 seconds while the wing flapped.

The gearbox was given a voltage input of 1.1V for the test [33]. This produced a flapping frequency of 10.3 Hz, which is approximately the free flight flapping frequency of a monarch butterfly [33, 37]. The results for the test are shown in Figure 2.2.

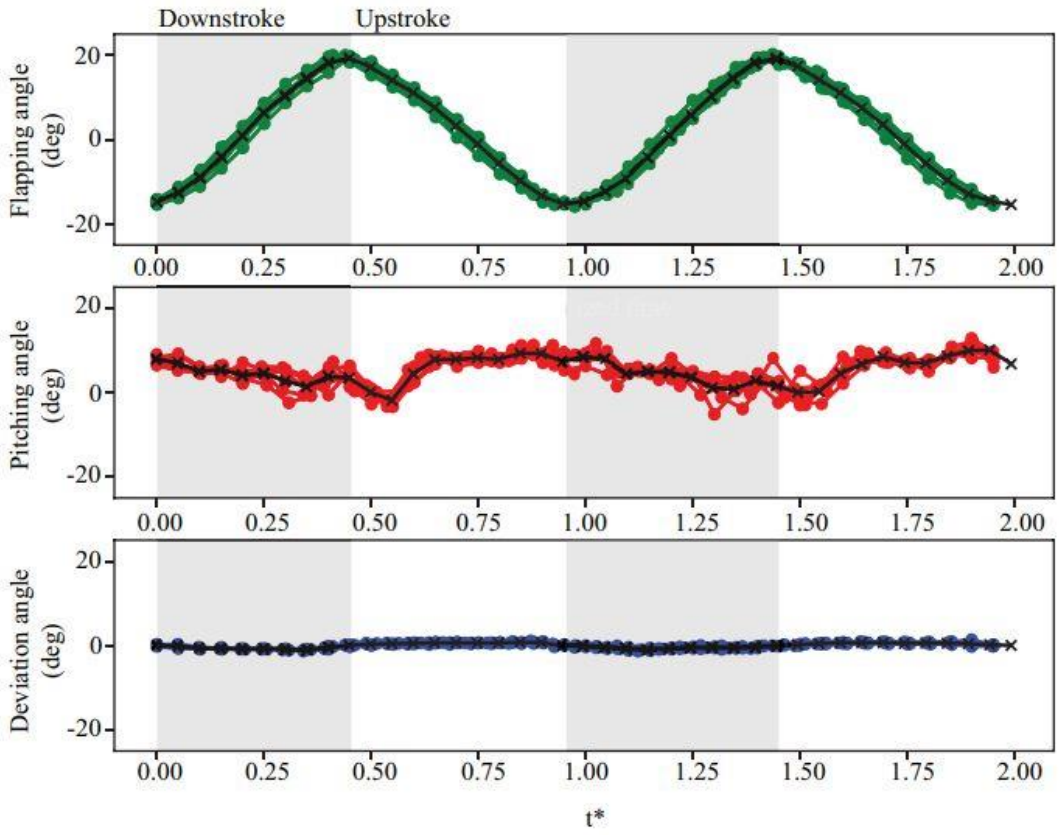

Figure 2.2 Representative time histories of the flapping angle, feathering angle, and deviation angle of a real monarch butterfly wing mounted on the gearbox and operated at an input voltage of 1.1 V. The FFT analysis of the flapping motion indicates that the flapping frequency was 10.3 Hz. The grey bars indicate the downstroke, and the white bars indicate the upstroke. The black line is the average of each subplot (n=6). From Twigg [33]. Reprinted with permission.

The gearbox produced an average flapping amplitude of 20° [33]. This value is much smaller than the average flapping amplitude of a monarch butterfly which is 64° [37]. Here data also showed that the feathering angle followed an approximately sinusoidal trend with a phase lag of 155°-190° behind the flapping angle [33]. This indicates that the pitching of the wing is approximately half a stroke behind the flapping motion.

In a study similar to Twigg's [33], Morris [34] repeated Twigg's wing angle and force generation study for monarch wings, but he used a new gearbox with a flapping amplitude of 55°. Morris [34] found that the increase in flapping amplitude from 20° to

55° had a significant impact on the feathering angle of the wing. These results are shown in Figure 2.3 below.

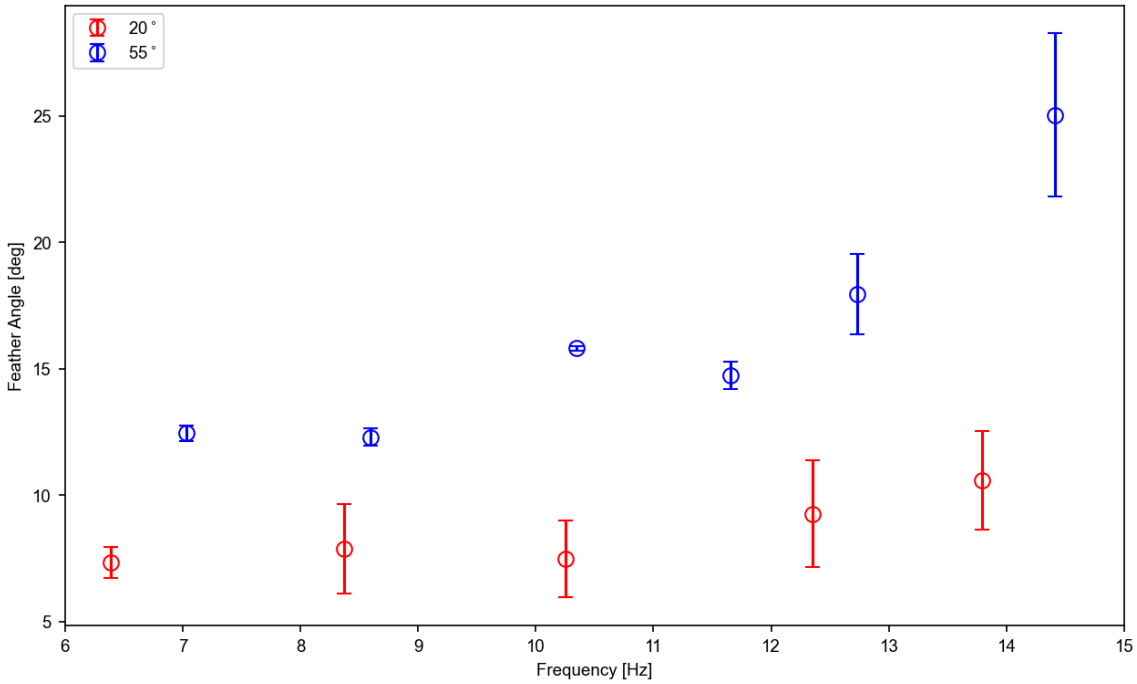

Figure 2.3 The mean feathering angle for 20° (red) and 55° (blue) flapping amplitudes versus frequency. The error bars represent the 95% confidence interval (nred=6, nblue=4). From Morris [34]. Reprinted with permission.

As shown in Figure 2.3, the increase in the flapping amplitude resulted in a larger feathering angle. Because the feathering angle is directly linked to force production, this increase in feathering angle relative to the smaller flapping amplitude also resulted in an increase in generated force as shown in Figure 2.4 below.

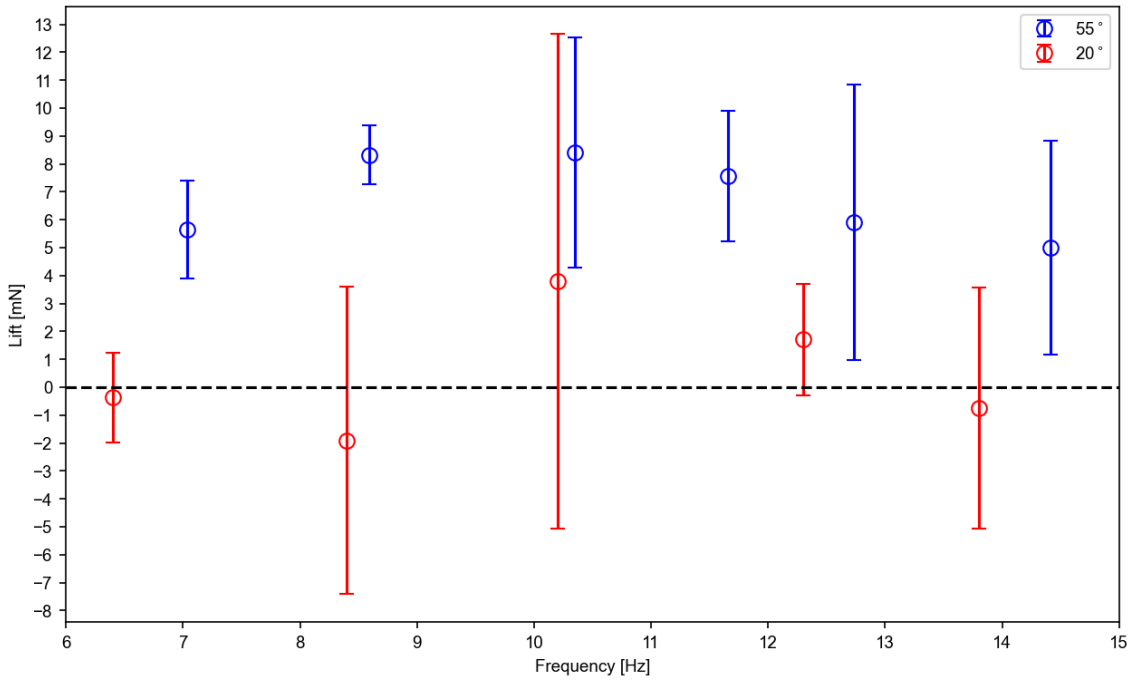

Figure 2.4 Lift forces produced by a monarch wing at 20° and 55° flapping amplitudes for a range of different flapping frequencies. The error bars represent the 95% confidence interval (nred=6, nblue=4). From Morris [34]. Reprinted with permission.

2.4 Recent Developments of Flapping Wing Micro Aerial Vehicles

Flapping wing micro-aerial vehicles are robotic vehicles that draw inspiration from biological fliers such as insects and birds. They seek to benefit from the lift production capabilities and high agility of natural flapping wing creatures. One of the primary issues with these vehicles is generating sufficient forces for flight and controls without a tail [40]. This has led to development of smaller vehicles where less force is required. As a result, wing sizes in the range of insects to hummingbirds have been of particular interest. Several examples of development in this size range exist including the BigBee [41], the AeroVironment Nano hummingbird [42], the DelFly [43], the Harvard RoboBee [44], and the hummingbird inspired vehicles of Texas A&M [45] and Purdue [46]. The Delfly and Robobee are shown here in Figures 2.5 and 2.6.

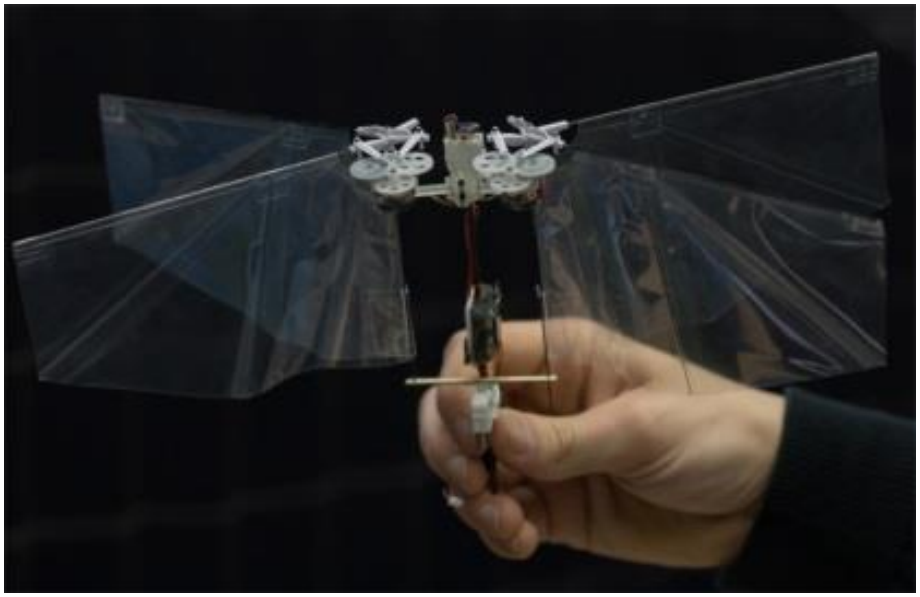

Figure 2.5 The Delfly Nimble presented as an example of a flapping wing micro-aerial vehicle [43].

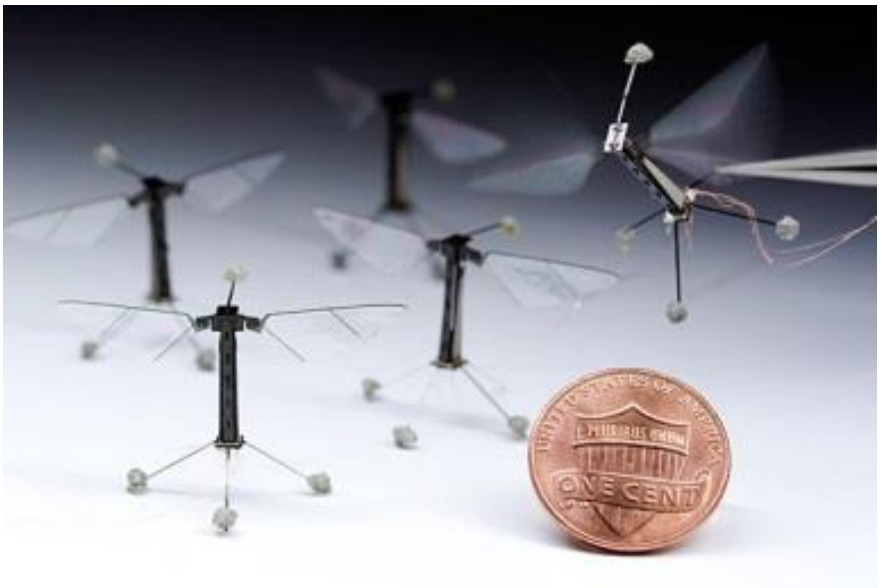

Figure 2.6 Five Harvard Robobees shown with a penny for size reference. The Robobee in the upper right corner is flying, but it must be tethered to an external power source [44].

All of these designs seek to capitalize on the efficiency, agility, and low flight noise levels of their biological counterparts. However, current technology, especially battery technology, is a limiting factor for these vehicles. Additional improvements in lift

production while also reducing vehicle mass will be essential to the further development of flapping wing micro-aerial vehicles.

Chapter 3. Methodology

In this study, the goal is to design a new artificial monarch wing, improving over the version developed by Twigg [33]. The primary focus is on developing a wing that has similar feathering angle and empirical lift production trends to a true monarch wing. Towards this end, both artificial wings were tested at multiple voltage inputs which resulted in multiple flapping frequencies. Both the flapping angles and the feathering angles were measured for both wings.

3.1 Bonded Wing Fabrication

For the purposes of this thesis, the artificial wing that was developed by Twigg [33] will be referred to as the "bonded wing." This name relates to the manufacturing process which requires the vein structure to be chemically bonded to the membrane of the artificial wing.

The vein structure is printed from a three-dimensional model developed from the micro-CT scan of a monarch wing. The veins of a monarch wing have a hollow, circular cross section. Due to the limitation of the 3D printer used to make these veins, the bonded wing has veins that are solid and rectangular in cross section. These veins are also 1 mm thick due to the print resolution of the printer. The veins are printed using a standard Polylactide (PLA) material.

To simulate the membrane of a monarch wing, the vein structure is chemically bonded to a 0.05 mm thick sheet of Poly-L-lactide (PLLA). For this process, one side of

the vein structure was dipped into the organic solvent tetrahydrofuran (THF) for 5 seconds. This partially dissolved the PLA of the vein structure. The veins were then placed on the PLLA sheet and clamped between two metal plates. When the THF evaporated, the PLA of the vein structure reformed and bonded with the PLLA of the membrane. This only occurred because the PLA and PLLA are the same material. The newly formed artificial wings were kept clamped between two slabs of metal for a minimum of two weeks to prevent warping. When the THF interacts with the PLLA sheet, the sheet relaxes and expands slightly. As the THF evaporates, the PLLA sheet will contract and warp the wing unless it is tightly clamped between two flat surfaces. Two of the bonded wings are shown below in Figure 3.1.

Figure 3.1 Two bonded wings shown after the PLA vein structure (green) has been fused to the PLLA membrane (clear).

3.2 Integrated Wing Fabrication

"Integrated wing" is the name given to the new design for the artificial wing. Again, the name relates to the manufacturing process for the wing. As part of her FEM tests, Twigg [33] created a second three-dimensional model of the wing. This model included a membrane material around the veins and used the hollow circular cross section of a real monarch wing. This model was used to develop the integrated wing and is shown below in Figure 3.2.

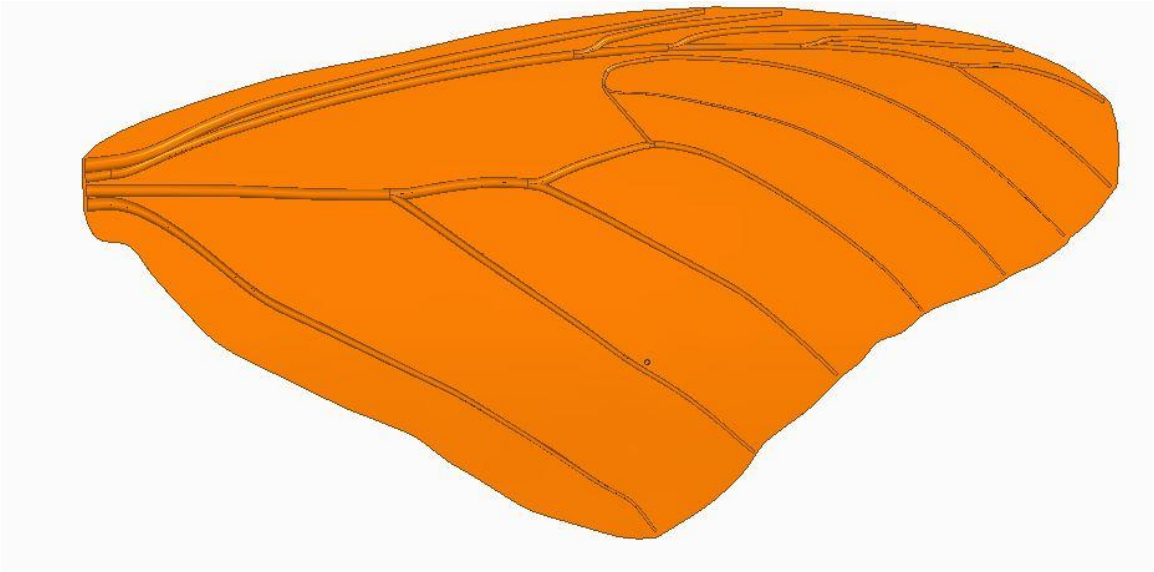

Figure 3.2 Artificial wing CAD model developed by Twigg [33].

To improve the print quality and allow for the membrane and veins to be printed as one part, an Anycubic Photon S resin-based printer was used. This printer uses a photopolymer resin and a UV screen to make three-dimensional prints. The Photon S has an XY resolution of 47 µm and a Z resolution of 1.25 µm. This resolution allows the integrated wing to have the same vein cross section at the same scale as a monarch butterfly wing. The resin printing of the Photon S also allows the membrane to be printed

directly on the wings in a single print. This gives the new design its name of “integrated wing.” A picture of the integrated wing is shown here in Figure 3.3.

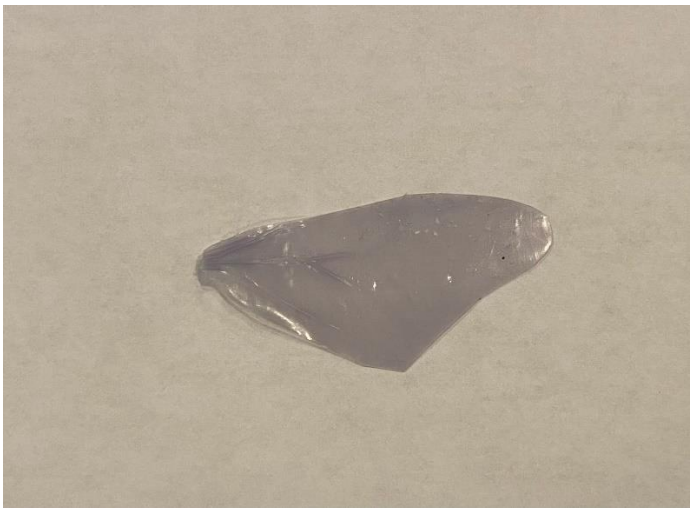

Figure 3.3 A single integrated wing printed from grey photopolymer resin.

3.3 Wing Motion Measurements

The test setup for this study consisted of an in-house designed flapper similar to the one that Morris [34] used in his study and an array of VICON T40 cameras. The flapper was mounted on an ATI Nano 17 Titanium force transducer which was itself mounted on an in-house designed vibration dampener. The mounting set up is shown in Figure 3.4 below.

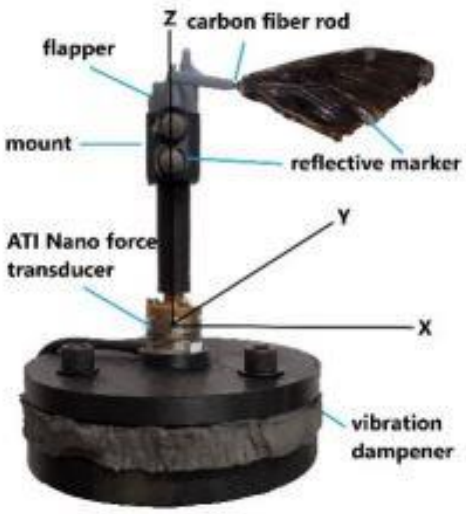

Figure 3.4 Flapping wing mount showing the in-house designed flapping mechanism and vibration dampening base. The wing is attached to the flapper using a circular 1 mm diameter carbon fiber rod. From Morris [34]. Reprinted with permission.

As shown in Figure 3.4, reflective markers were placed upon the wing. These markers served as reference points which are detected and tracked by the VICON cameras. A total of three markers were placed upon the wing with two additional markers on the mount itself. The two markers on the mount served as stationary reference points for the later calculations with the VICON data. To make the three reflective markers on the wings stand out and to minimize interference with them, the artificial wings were colored black with a felt-tip pen before the markers were added. An integrated wing and a bonded wing that were used in testing are shown in Figure 3.5 below.

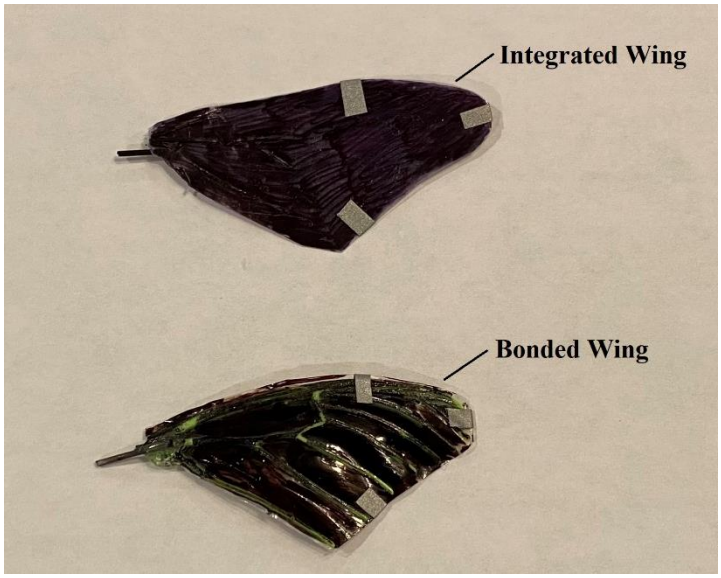

Figure 3.5 An integrated wing and a bonded wing shown in testing configuration with the wings colored black and reflective markers attached.

The VICON cameras were placed in a roughly semicircular shape around the mount to ensure that the complete flapping range of the wing was captured. For VICON to record position data, at least three cameras must be seeing the wing markers at a given time. Eleven VICON cameras were used to ensure that at least three cameras could see the wing markers at any point. To further minimize interference in the cameras' views, all test equipment was either colored black or covered with black construction paper to reduce the number of reflective surfaces. In addition, part of the wall behind the test area was covered with black construction paper to further reduce reflective points. The camera array and test area are shown in Figure 3.6.

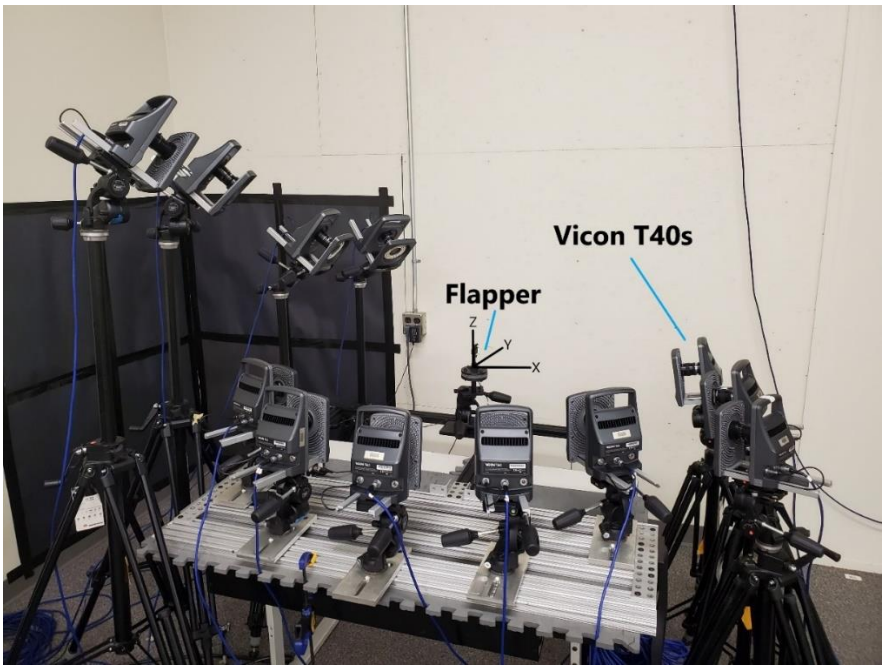

Figure 3.6 VICON camera array and test area with the flapper on its mount in the center.

The VICON cameras recorded at a frequency of 400 Hz for two seconds. This resulted in 800 data points per test which gives an accurate portrayal of the wing's movements. The data were processed through the VICON Nexus system to recreate and record the positions of each marker throughout the motion of the wing. These data were then exported to an ASCII file. The ASCII file was read by a PYTHON code which converts the VICON position data into flapping and feathering angle values throughout the motion of the wing.

A Fast-Fourier Transform (FFT) approach was used to calculate the flapping frequency for the test from the marker motion data. The wing angles were calculated by assuming that the wing forms a rigid plane under the three reflective markers. The two markers on the test stand were used as stationary reference points against which the positions of the wing markers were measured. From these measurements, the Euler angles were calculated.

3.4 Empirical Lift and Drag Coefficients

As mentioned in Section 3.3, the flapper is mounted onto an ATI Nano 17 Titanium force transducer. This was intended to provide force generation data for this study similar to the data that Morris [34] reported. Unfortunately, the force transducer started to malfunction at the end of Morris' study, and it has not been repaired. Because of this, no direct force measurements were collected as part of this study. To replace this missing data, the lift and drag coefficients were calculated from the quasi-steady model by Dickinson *et al.*[38].

The quasi-steady model by Dickinson *et al.*[38] predicts the force coefficients based on the instantaneous angle of attack α. In the case of insect wings, the angle of attack is the feathering angle which is calculated as shown in Section 3.3. The two equations are presented here as Equations 1 and 2:

$$C_L = 0.225 + 1.58\sin(2.13\alpha - 7.20) \text{ and} \quad (1)$$

$$C_D = 1.92 - 1.55\cos(2.04\alpha - 9.82). \quad (2)$$

In Equations 1 and 2, C_L is the coefficient of lift and C_D is the coefficient of drag. The coefficients were empirically determined from dynamically scaled insect wing measurements.

3.5 Design of Experiments

The experiments conducted during this study were designed to closely match the experiments run during the study by Morris [34] and to enable the accurate comparison of the monarch wing data with the artificial wing data collected here. As such, the same range of voltage inputs were used with the flapper. The input voltages were increased by 0.1 V and ran from the minimum power with which the flapper could smoothly move the wing (0.5 V) to the highest voltage before the failure of the monarch wings (1.0 V). The input voltages are displayed below in Table 3.1.

Table 3.1 Input voltages used in the testing of the artificial wings.

Input Voltage (V)	0.5	0.6	0.7	0.8	0.9	1.0

Chapter 4. Results and Discussion

The real monarch wing data that is presented in this thesis was collected during Morris' study [34]. The integrated and the bonded wing data were collected during this project. To maintain consistency across the three different sets of data (one set for each wing type), the monarch wing data has been recalculated using the same post-processing code as described in Section 3.2.

The wing morphology data for all three of the wings are displayed here in Table 4.1.

Table 4.1 Morphological data recorded for a real monarch wing [34] and two artificial wings.

Wing Type	Wing Mass (g)	Span ($\times 10^{-3}$ m)	Chord ($\times 10^{-3}$ m)
Monarch	0.019	53.11	27.04
Integrated	0.318	57.01	26.00
Bonded	0.305	52.00	25.00

The most important parameter in the morphological data is the weight of the wing. The artificial wings have approximately the same dimensions as the real wing since they were designed using a monarch wing. However, due to material properties and limitations, the artificial wings are about 50% heavier. This affects the flapping frequency that the gearbox can achieve for each wing. As a result, the artificial wings have lower flapping frequencies than the monarch wing at the same voltage input.

For comparison purposes in this paper, two representative data sets are presented for each wing. The first will be at an input voltage of 0.7V. Voltage is the only experimental

parameter that is directly controlled. As such, comparisons are made at a constant voltage even though the wings have different flapping frequencies. The second data set presented are at a set flapping frequency of approximately 6 Hz. Both the bonded and the integrated wing have flapping frequencies of approximately 6 Hz at a voltage input of 0.9V while the monarch has this flapping frequency at an input of 0.5V. All other data for each of the wings at the other input voltages will be presented in the appendix.

4.1 Wing Angles and Empirical Force Coefficients for a Monarch Wing

The plots of the two representative data sets for the real monarch wing are shown in Figures 4.1 and 4.2. Figure 4.1 shows the 0.7 V (constant voltage) data while Figure 4.2 shows the 6 Hz (constant frequency) data. In the figures, an upstroke is defined as the region between a local minimum point of the flapping angle and a local maximum point. The downstroke is defined as the region between a local maximum point of the flapping angle and a local minimum point.

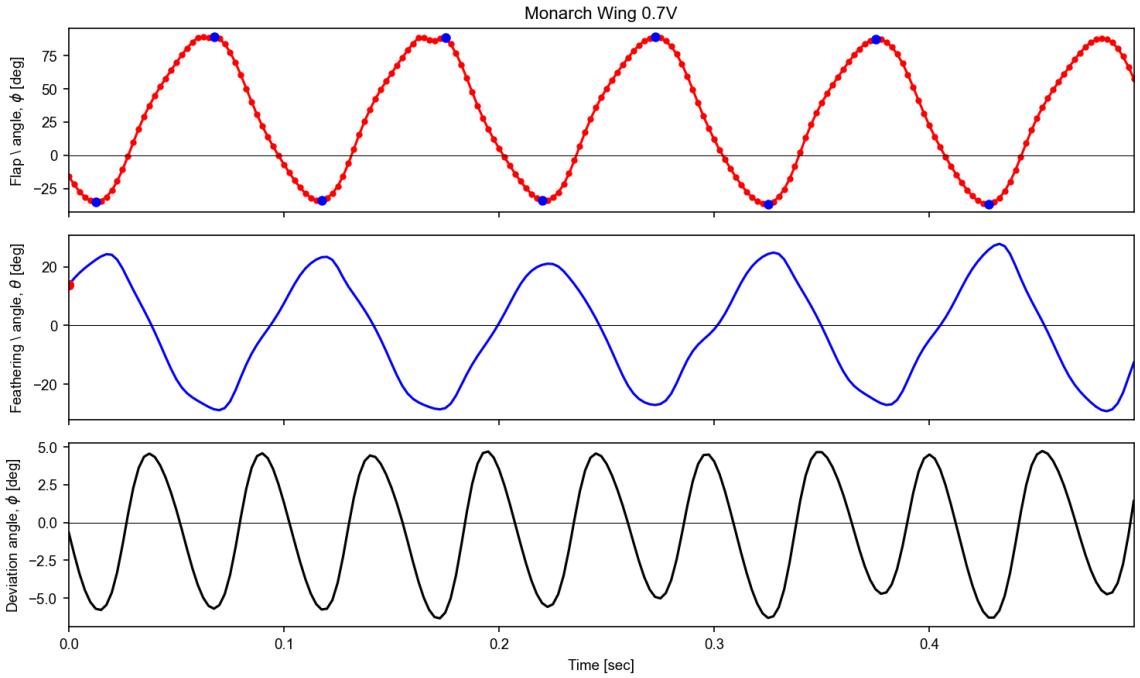

Figure 4.1 Representative time history for the monarch wing taken at a constant input voltage of 0.7 V. The average feathering angle is -2.27° while the flapping frequency is 10.05 Hz. The peak-to-peak flapping amplitude is 126.11° while the peak-to-peak feathering amplitude is 56.87°.

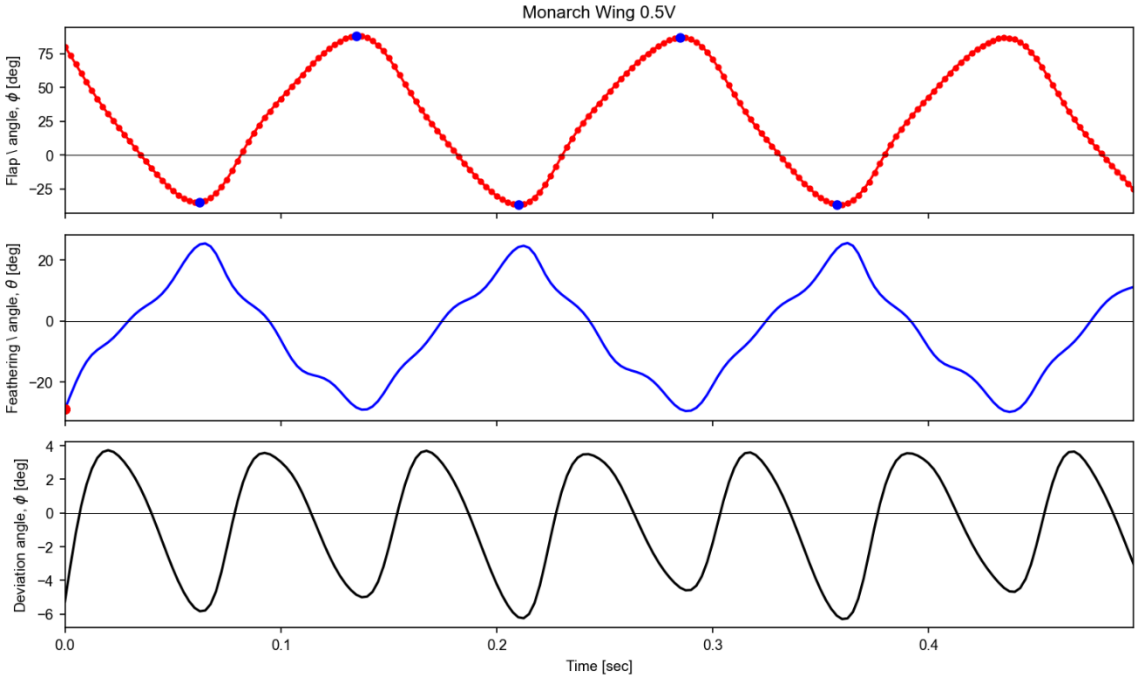

Figure 4.2 Representative time history for the monarch wing flapping at 6 Hz flapping frequency with a 0.5 V input voltage. The average feathering angle is -3.65° while the flapping frequency is 6.03 Hz. The peak-to-peak flapping amplitude is 124.97° while the peak-to-peak feathering amplitude is 55.30°.

Three angles are shown in Figures 4.1 and 4.2. The flapping angle (top plot in the subplot) and the deviation angle (bottom plot in the subplot) are not focused on in this study. The flapping angle is simply a measure of how far the wing traverses during its motion, and this is determined solely by the flapping mechanism. While the flapping angle is of importance when studying the aerodynamics of the flapping wing, this study focuses on the kinematics of the wing. The deviation angle measures if the wing has any unexpected changes from an expected motion.

The third and most important of the three measurements shown in Figures 4.1 and 4.2 (flapping angle, feathering angle, and deviation angle) is the feathering angle. The feathering angle is a measurement of how much the trailing edge of the wing lags the leading edge as the wing flaps. This can also be referred to as the wing deforming during flapping. As mentioned above in Section 3.4, the feathering angle for a flapping wing is analogous to the angle of attack for a stiff wing. As such, the feathering angle has a direct impact on the force generation characteristics and thus performance of the wing.

In both the 0.7 V trial and the 6 Hz trial, the average feathering angle is near (~4°) zero. This indicates that when a monarch wing is flapped in a linear plane with no pitching or body coupling acting on it, the wing deformation during both the upstroke and the downstroke will be approximately symmetrical. In other words, the wing deforms approximately the same amount regardless of which direction it is flapping. This seems to contradict the discussion of the asymmetry of a monarch's wings in flight that was presented in Chapter 2. However, during flight, the wings are experiencing passive pitching and body coupling effects that can stiffen and relax the wing during its flapping

motion. In its normal state without outside forces, the monarch wing's deformation is approximately symmetric.

This can be better seen by examining the half cycle average feathering angles for a monarch wing. The half cycles can be defined as the upstrokes and downstrokes. For this, two cycles will be examined giving two upstrokes and two downstrokes. The cycles are shown in Figures 4.3 (0.7 V) and Figure 4.4 (6 Hz), and the corresponding average feathering angles half-cycles are shown in Tables 4.2 and 4.3 respectively.

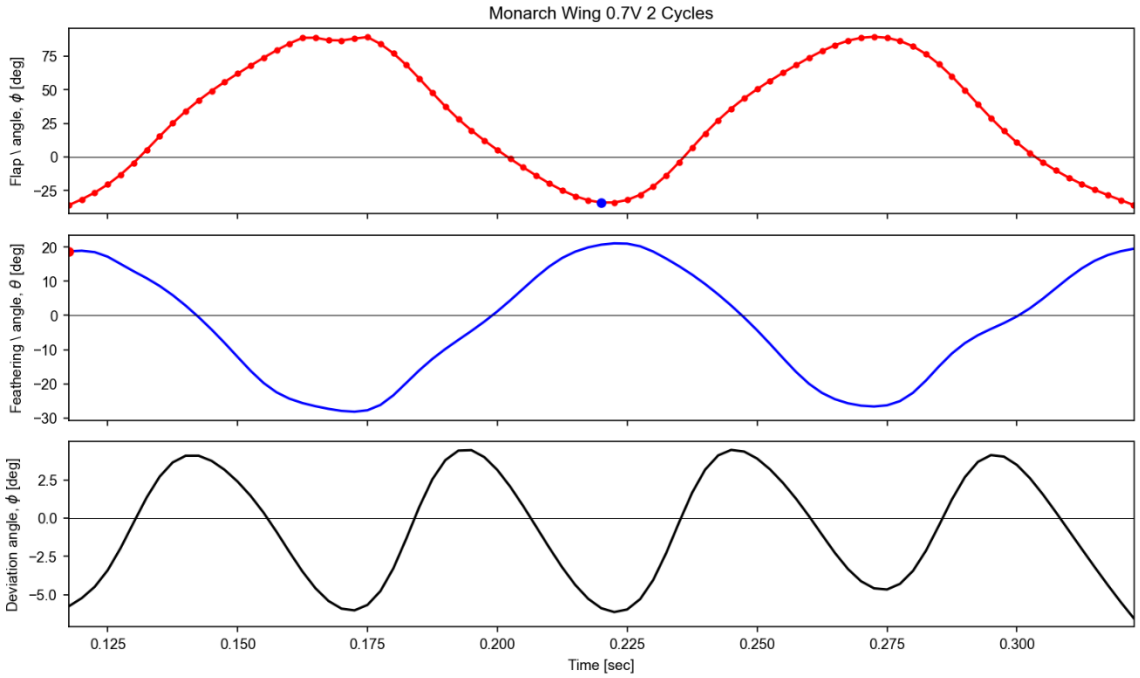

Figure 4.3 Representative time history for 2 cycles of a monarch wing flapping with an input voltage of 0.7 V. The average feathering angle is -2.20° while the flapping frequency is 9.64 Hz. The peak-to-peak flapping amplitude is 125.84° while the peak-to-peak feathering amplitude is 51.50°.

Table 4.2 Average feathering angles for the half-cycles of the two cycles for a monarch wing flapping with an input voltage of 0.7 V.

	Upstroke 1	Downstroke 1	Upstroke 2	Downstroke 2
Average Feathering Angle (°)	-1.24	-2.70	-0.67	-4.30

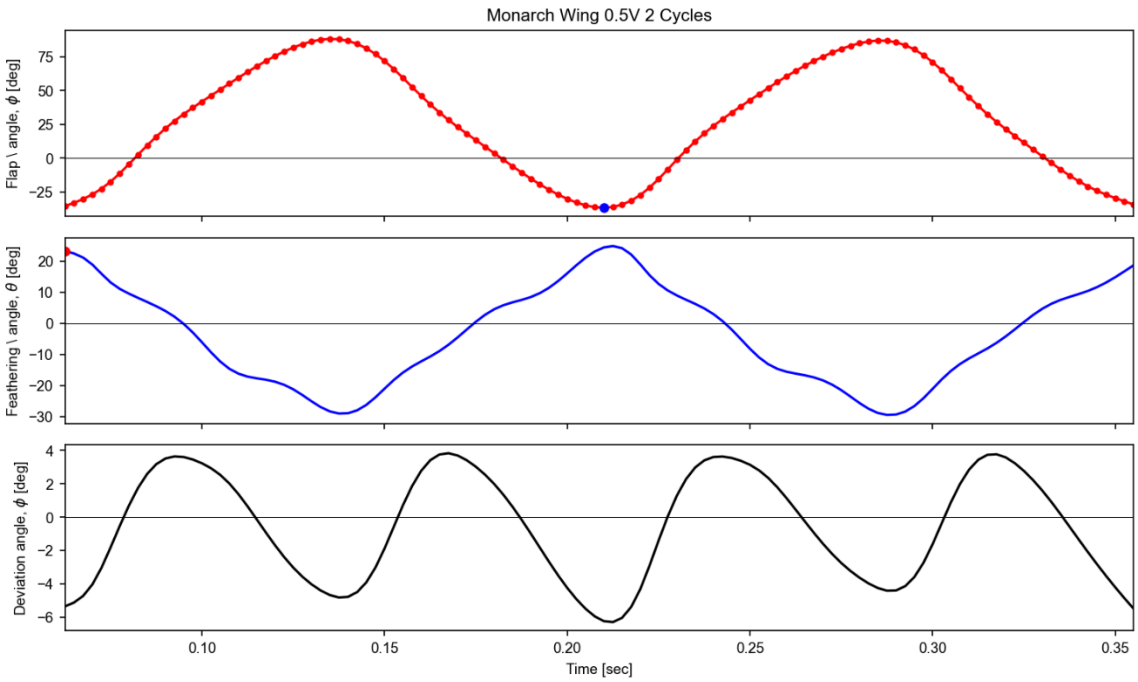

Figure 4.4 Representative time history for 2 cycles for a monarch wing flapping with a frequency of approximately 6 Hz with a 0.5 V voltage input. The average feathering angle is -3.76° while the flapping frequency is 6.78 Hz. The peak-to-peak flapping amplitude is 124.97° while the peak-to-peak feathering amplitude is 54.34°.

Table 4.3 Average feathering angles for the half-cycles of the two cycles for a monarch wing flapping with a frequency of approximately 6 Hz.

	Upstroke 1	Downstroke 1	Upstroke 2	Downstroke 2
Average Feathering Angle (°)	-3.90	-2.57	-4.21	-4.40

In Figures 4.3 and 4.4, the flapping frequency values differ slightly from those in Figures 4.1 and 4.2 despite the graphs being generated from the same data. In Figures 4.3 and 4.4, the values are generated from only the shown portion of the data rather than the entire data set as in Figures 4.1 and 4.2. Thus, the average flapping frequencies for the two data sets are the flapping frequencies shown in Figures 4.1 and 4.2.

In Tables 4.2 and 4.3, the values are once again within a few degrees of zero. This shows that during the upstrokes and downstrokes the feathering angle is roughly symmetrical about zero. In addition, the average feathering angles for the upstrokes and following downstrokes are very nearly the same except for Upstroke 2 and Downstroke 2 in Table 4.2 which is most likely due to some slight deviation in the flapping system. The wing does show a slight bias toward negative feathering angles. All the half-cycle averages are negative as well as the full time series averages. This does indicate a slight asymmetry in the bending of the wing; however, since the values are within a few degrees of zero the wing can still be said to deform symmetrically.

Because the empirical lift coefficient, calculated using Equation 1, is dependent on the feathering angle, it too exhibits a strong symmetry. The empirical lift and drag coefficients for the two representative data sets are shown here in Figures 4.5 and 4.6.

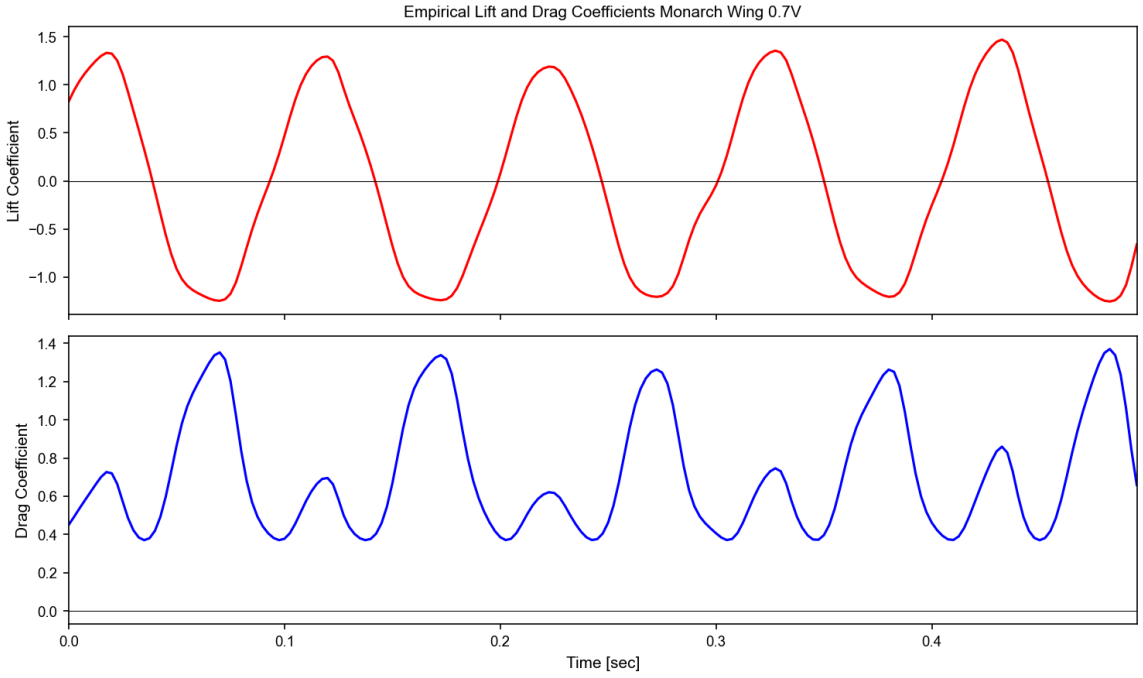

Figure 4.5 Empirical lift and drag coefficient curves calculated from the feathering angle of a monarch wing flapping with an input voltage of 0.7 V. The average lift coefficient is -0.04, and the average drag coefficient is 0.71. The maximum lift coefficient is 1.5.

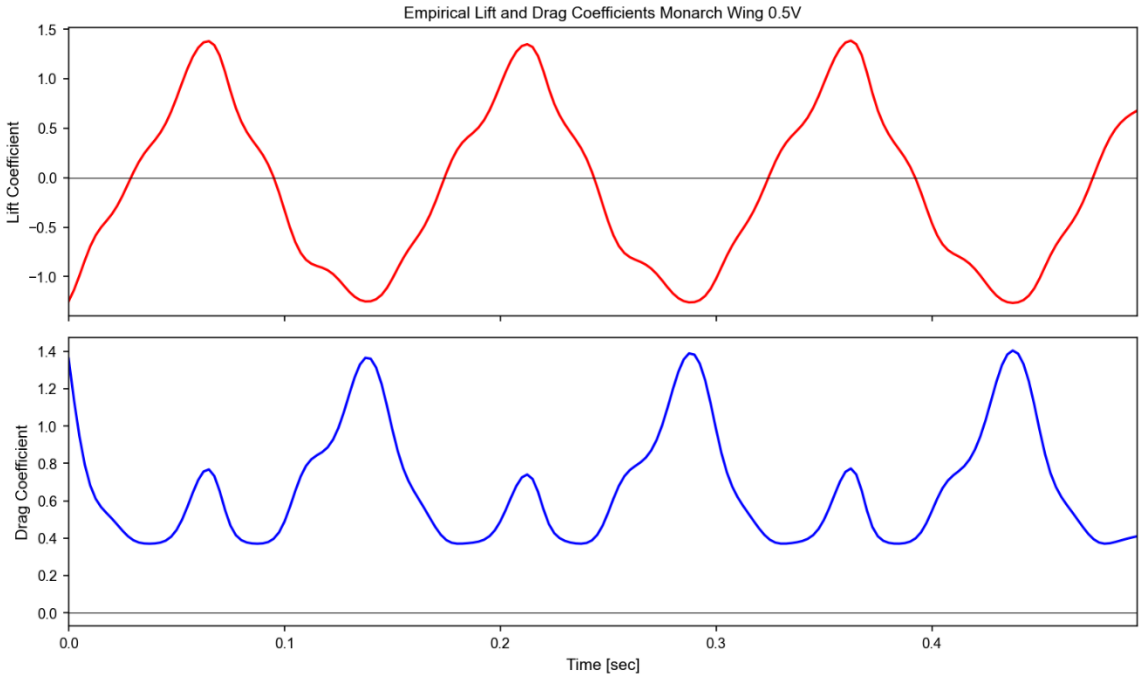

Figure 4.6 Empirical lift and drag coefficient curves calculated from the feathering angle of a monarch wing flapping with a frequency of approximately 6 Hz with a 0.5V voltage input. The average lift coefficient is -0.12, and the average drag coefficient is 0.67. The maximum lift coefficient is 1.4.

In both Figure 4.5 and Figure 4.6, the average lift coefficient is approximately zero. This shows that the monarch wing can produce the same amount of force during both its upstroke and its downstroke when not acted upon by outside forces.

4.2 Wing Angles and Empirical Force Coefficients for the Bonded Wing

The two plots of the representative data for the bonded wing are shown here in Figures 4.7 and 4.8. Figure 4.7 is the constant voltage (0.7 V) data while Figure 4.8 is the constant flapping frequency data (6 Hz).

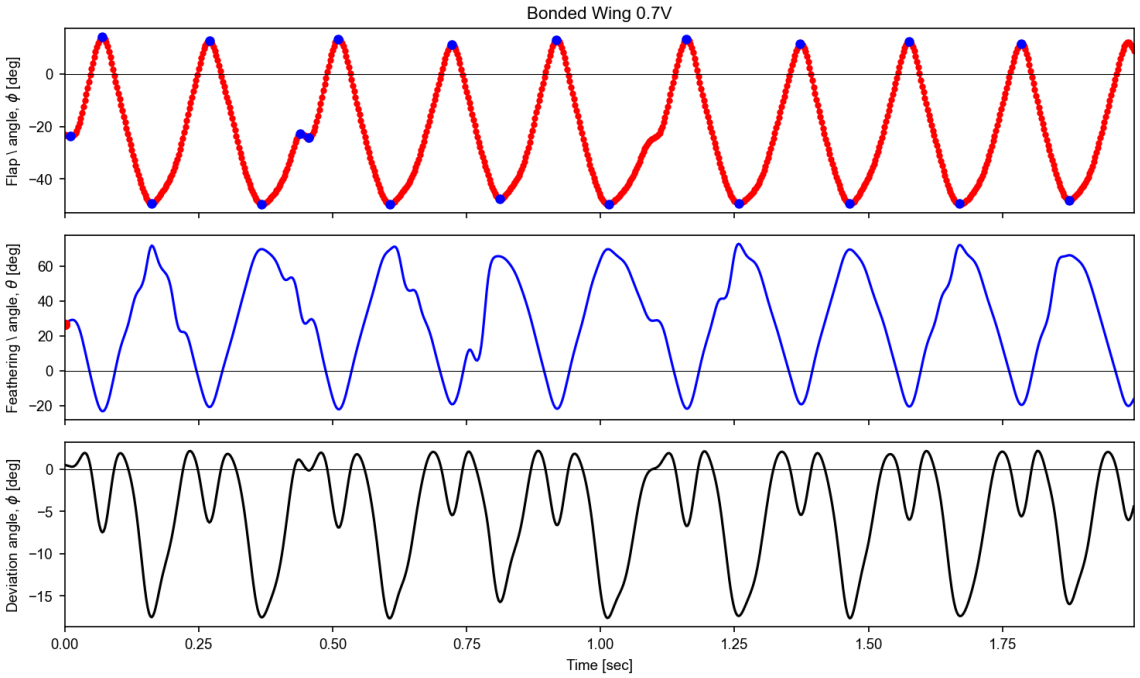

Figure 4.7 Representative time history for the bonded artificial wing flapping with a voltage input of 0.7 V. The average feathering angle is 27.86° while the flapping frequency is 4.51 Hz. The peak-to-peak flapping amplitude is 63.71° while the peak-to-peak feathering amplitude is 96.04°.

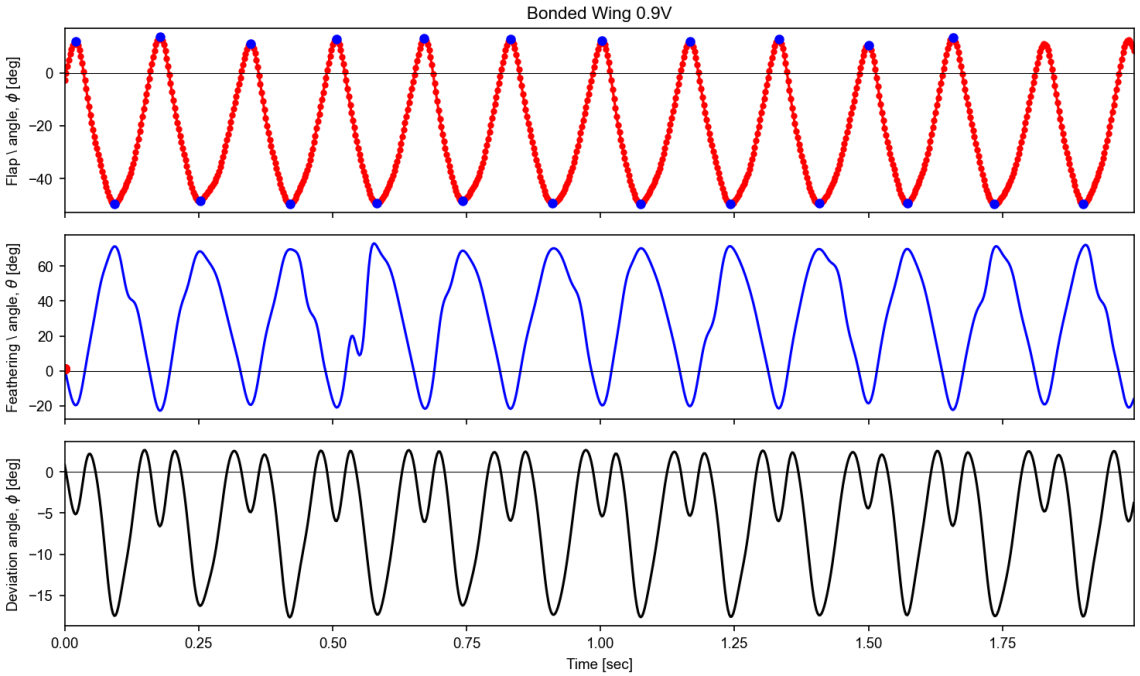

Figure 4.8 Representative time history for the bonded artificial wing flapping with a frequency of 6 Hz at a voltage input of 0.9 V. The average feathering angle is 28.75° while the flapping frequency is 6.01 Hz. The peak-to-peak flapping amplitude is 63.29° while the peak-to-peak feathering amplitude is 95.92°.

In Figures 4.7 and 4.8, the average feathering angles for the bonded wing are 28° and 29°, respectively. This indicates that the bonded wing is highly asymmetric in its deformation characteristics. In fact, the bonded wing shows a distinct preference to deform in the positive direction. This is further shown by examining the half-cycle average feathering angles for the bonded wing. Like the real monarch wing data in Section 4.1, the time history data for the bonded wing is narrowed down to two cycles which are divided into their upstrokes and downstrokes. The data is presented in Figures 4.9 and 4.10 while the average feathering angles are shown in Tables 4.4 and 4.5.

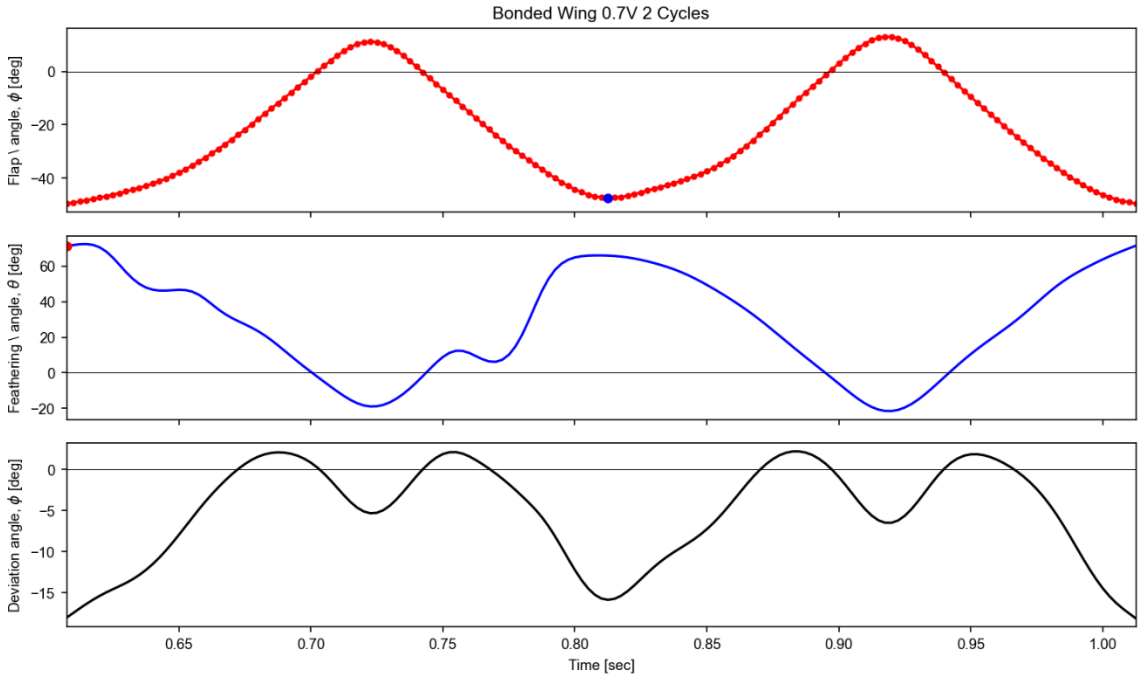

Figure 4.9 Representative time history of two cycles of the bonded wing flapping with a constant voltage input of 0.7 V. The average feathering angle is 27.67° while the flapping frequency is 4.91 Hz. The peak-to-peak flapping amplitude is 62.72° while the peak-to-peak feathering amplitude is 93.89°.

Table 4.4 Average feathering angles for the half-cycles of the two cycles for the bonded wing flapping with an input voltage of 0.7 V.

	Upstroke 1	Downstroke 1	Upstroke 2	Downstroke 2
Average Feathering Angle (°)	37.93	15.47	32.21	25.03

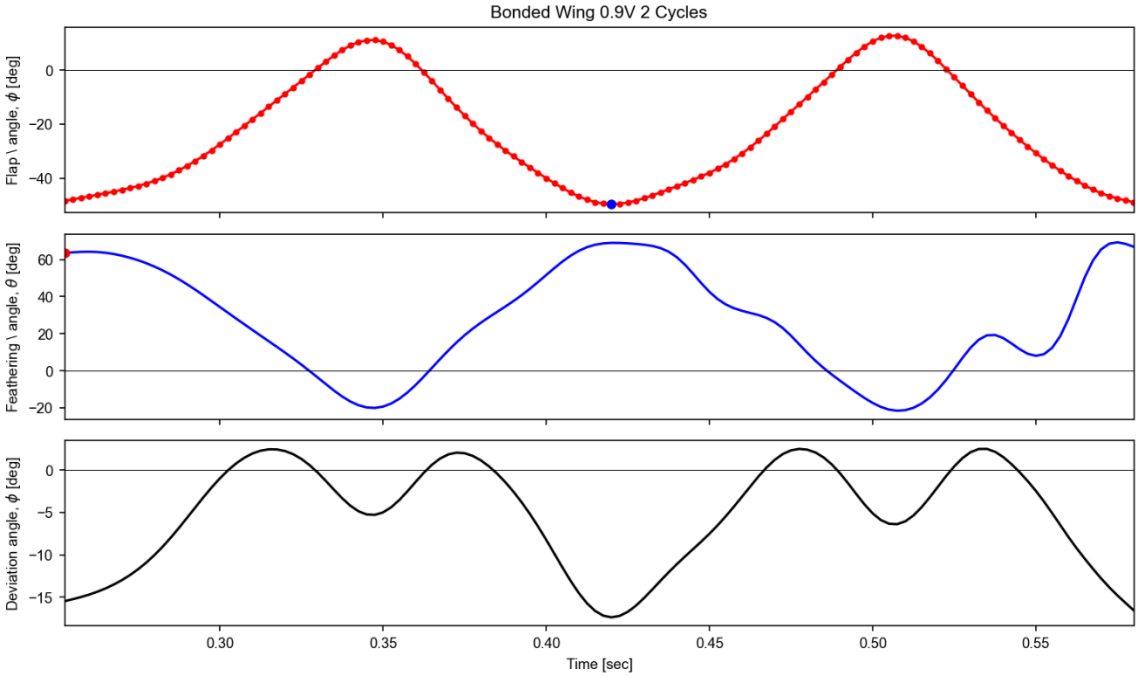

Figure 4.10 Representative time history of two cycles of the bonded wing flapping with a frequency of approximately 6 Hz at an input voltage of 0.9 V. The flapping frequency is 6.06 Hz with a flapping amplitude of 62.38°. The feathering amplitude is 90.88° with an average feathering amplitude of 27.00°.

Table 4.5 Average feathering angles for the half-cycles of the two cycles for the bonded wing flapping with a frequency of approximately 6 Hz at an input voltage of 0.9 V.

	Upstroke 1	Downstroke 1	Upstroke 2	Downstroke 2
Average Feathering Angle (°)	38.31	18.78	35.05	15.87

Upon examination of Figures 4.9 and 4.10, it is evident that the feathering angle time history does not follow a smooth curve between peaks and valleys. Rather, the curves have intermediate local minima and maxima which is indicative of the bonded wing's

asymmetrical deformation. In addition, the average feathering angle values show a definite skewing towards positive feathering angle and a distinct difference between the average values for upstrokes and those for downstrokes.

This asymmetry is expected with the bonded wing due to its construction. As discussed in Section 3.1, the bonded wing is made by adhering a PLLA membrane to a PLA vein structure. In this process, the membrane only adheres to one side of the vein structure. This lends additional stiffness to the side of the wing on which the membrane is adhered. As a result, the wing will resist deforming in the direction of the membrane (compressing the membrane). Also, because the membrane is elastic, it will resist deformation in either direction and will pull the wing back towards its initial shape. This results in the intermediate local maxima and minima between peaks and troughs in the feathering angle time histories.

The bonded wing's tendency to skew toward positive feathering angles and its inconsistent feathering angle time histories lead it to have somewhat inconsistent force generation. The empirical lift and drag coefficients for the two representative data sets are shown here in Figures 4.11 and 4.12.

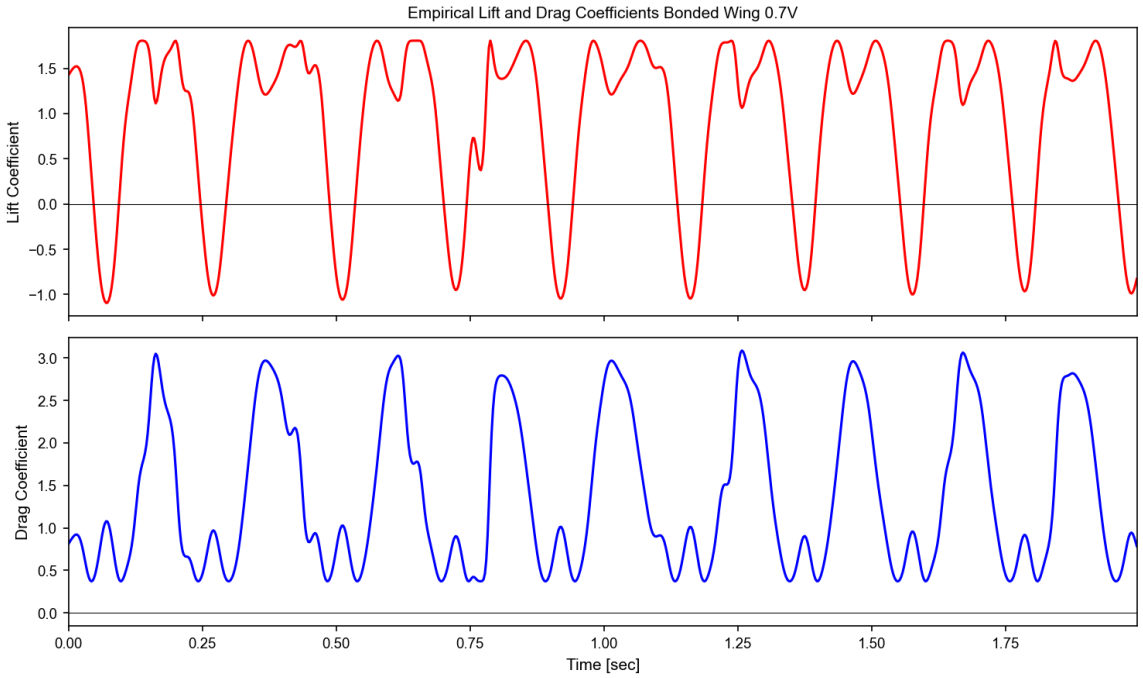

Figure 4.11 Empirical lift and drag coefficient time histories calculated from the feathering angle time history of the bonded wing flapping with a constant voltage input of 0.7 V. The average lift coefficient is 0.88. The average drag coefficient is 1.37. The maximum lift coefficient is 1.8.

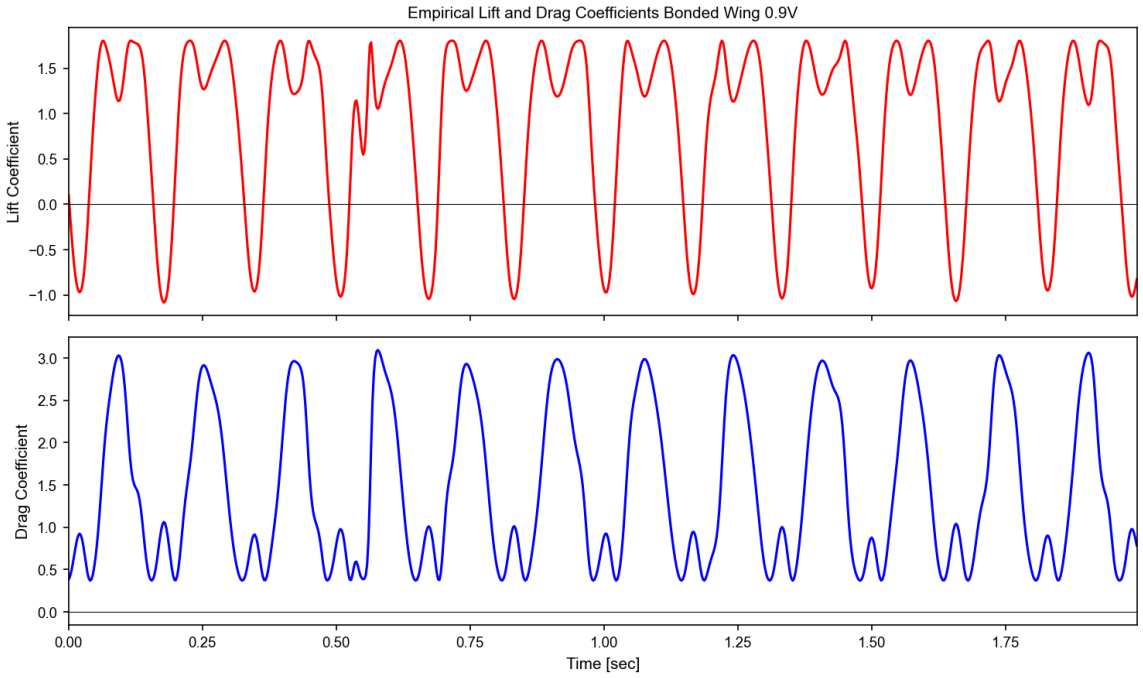

Figure 4.12 Empirical lift and drag coefficient time histories calculated from the feathering angle time history of the bonded wing flapping with a frequency of approximately 6 Hz and at an input voltage of 0.9 V. The average lift coefficient is 0.86. The average drag coefficient is 1.44. The maximum lift coefficient is 1.8.

In both Figures 4.11 and 4.12, the average lift coefficient is greater than 0.8. This shows a definite skewing towards positive lift coefficients due to the feathering angle. In addition, the lift coefficient time histories show sudden changes in the lift coefficient rather than smooth curves between peaks. This is due to the intermediate local minima and maxima in the wing's feathering angle time histories. Some of the dips at the peaks are likely also caused by sharp transitions between upstrokes and downstrokes due to the flapper itself. This likely causes some vibration of the wing that produces a small dip at each peak. The drag coefficient also displays similar sudden changes in its time history, but it does remain a positive value as expected.

4.3 Wing Angles and Empirical Force Coefficients for the Integrated Wing

The two representative time history plots for the integrated artificial wing are shown here in Figures 4.13 (0.7 V) and 4.14 (6 Hz).

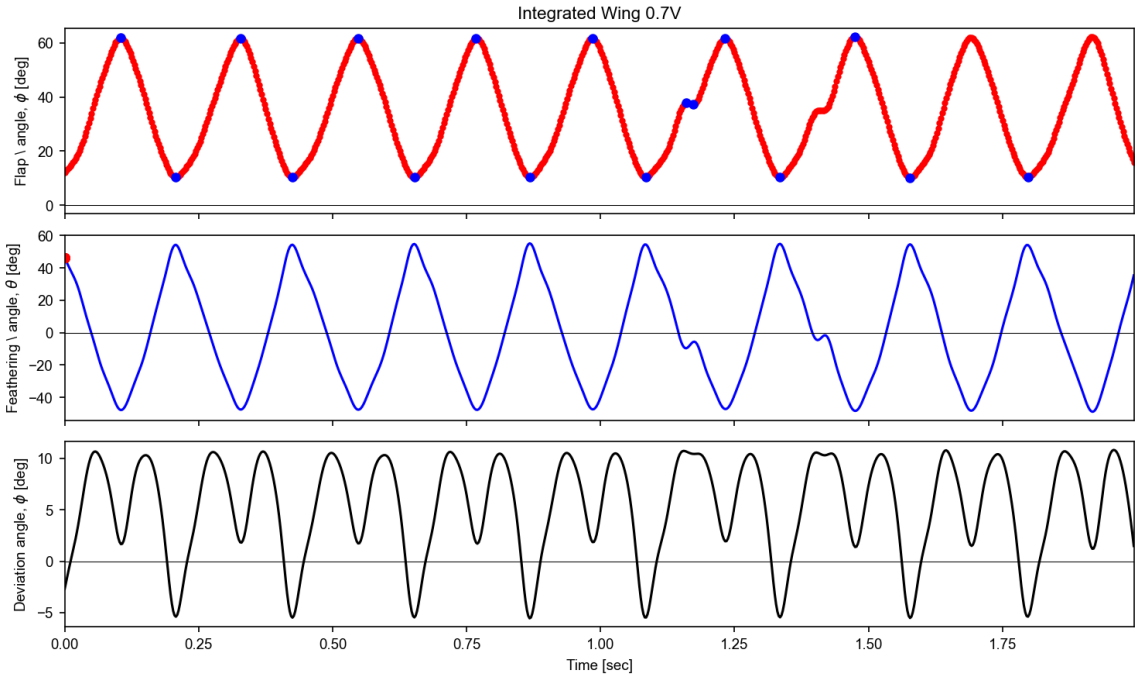

Figure 4.13 Representative time history data for the integrated wing flapping with a constant input voltage of 0.7 V. The average feathering angle is -0.15° while the flapping frequency is 4.51 Hz. The peak-to-peak flapping amplitude is 52.02° while the peak-to-peak feathering amplitude is 103.99°.

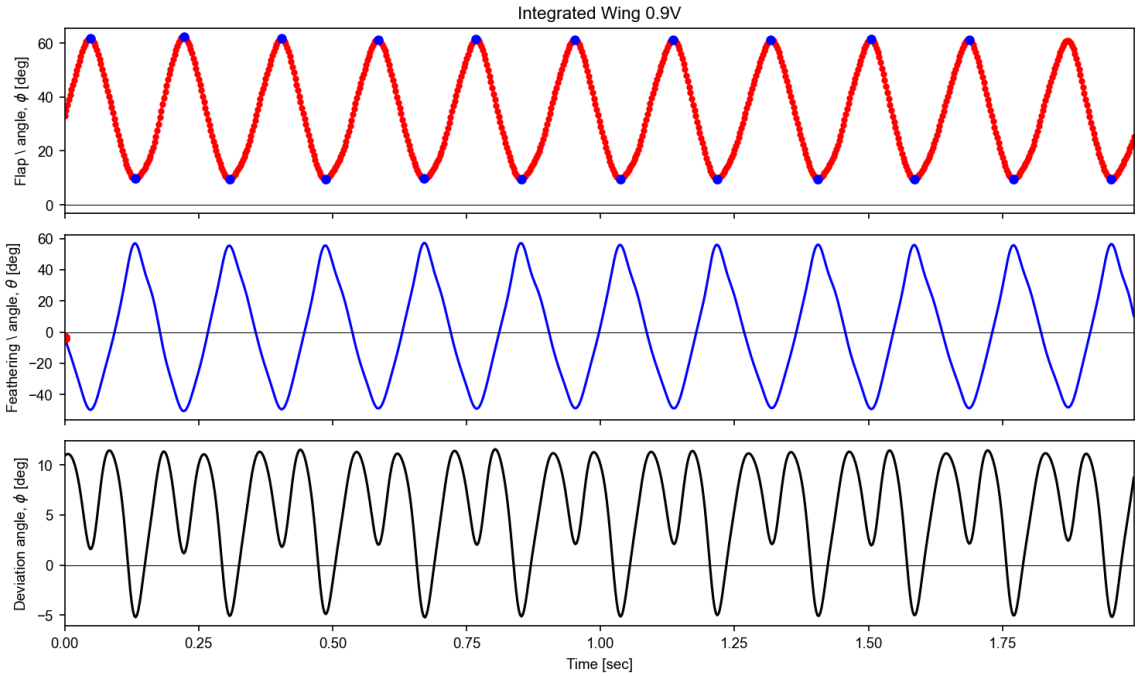

Figure 4.14 Representative time history data for the integrated wing flapping with a frequency of approximately 6 Hz and a voltage input of 0.9 V. The average feathering angle is 0.74° while the flapping frequency is 6.01 Hz. The peak-to-peak flapping amplitude is 52.77° while the peak-to-peak feathering amplitude is 107.90°.

From Figures 4.13 and 4.14, the integrated wing shows a very strong symmetry in its feathering angle measurements. In both cases, the average feathering angle is less than 1°. Also, the integrated wing has very smooth feathering angle time history curves. This shows that the integrated wing is capable of smoothly transitioning between flapping directions and is flexible enough to not try to maintain its regular shape while flapping. The only exceptions to this trend are two small local maxima towards the end of the 0.7 V time history. These irregularities are most likely attributable to the flapping mechanism catching or slowing slightly. The input voltage of 0.7 V is towards the lower end of the range that the flapping mechanism could support for the integrated wing. Thus, if anything happened during the flapping motion, such as a gear slip, the mechanism would catch or slow before powering through the issue.

The symmetry of the integrated wing's feathering angles can be further seen by examining the average values for the half-cycles of the motion. As before in Sections 4.1 and 4.2, two cycles are split into half-cycles giving two upstroke and two downstroke average feathering angle values. The two cycles for the 0.7 V case are shown in Figure 4.15, and the corresponding average feathering angles are shown in Table 4.6. The two cycles for the 6 Hz case are shown in Figure 4.16, and the corresponding average feathering angles are shown in Table 4.7.

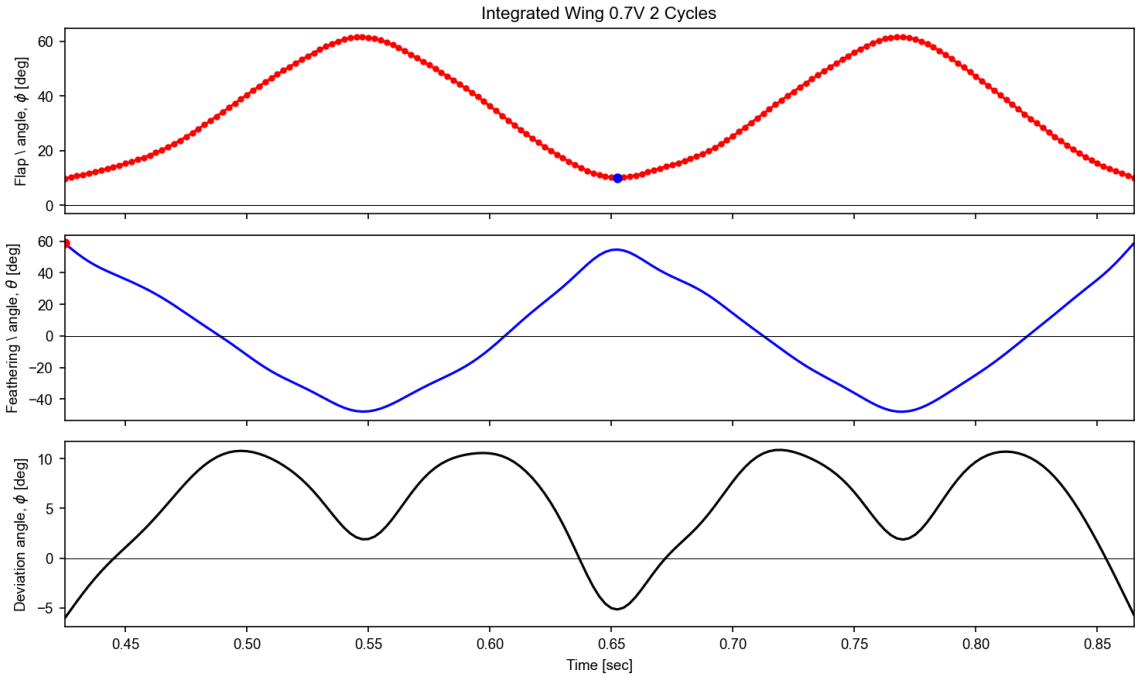

Figure 4.15 Representative time history of two cycles of the integrated wing flapping with a constant voltage input of 0.7 V. The average feathering angle is 0.25° while the flapping frequency is 4.49 Hz. The peak-to-peak flapping amplitude is 51.87° while the peak-to-peak feathering amplitude is 107.01°.

Table 4.6 Average feathering angles for the half-cycles of the two cycles for the integrated wing flapping with an input voltage of 0.7 V.

	Upstroke 1	Downstroke 1	Upstroke 2	Downstroke 2
Average Feathering Angle (°)	7.85	-5.51	6.53	-10.45

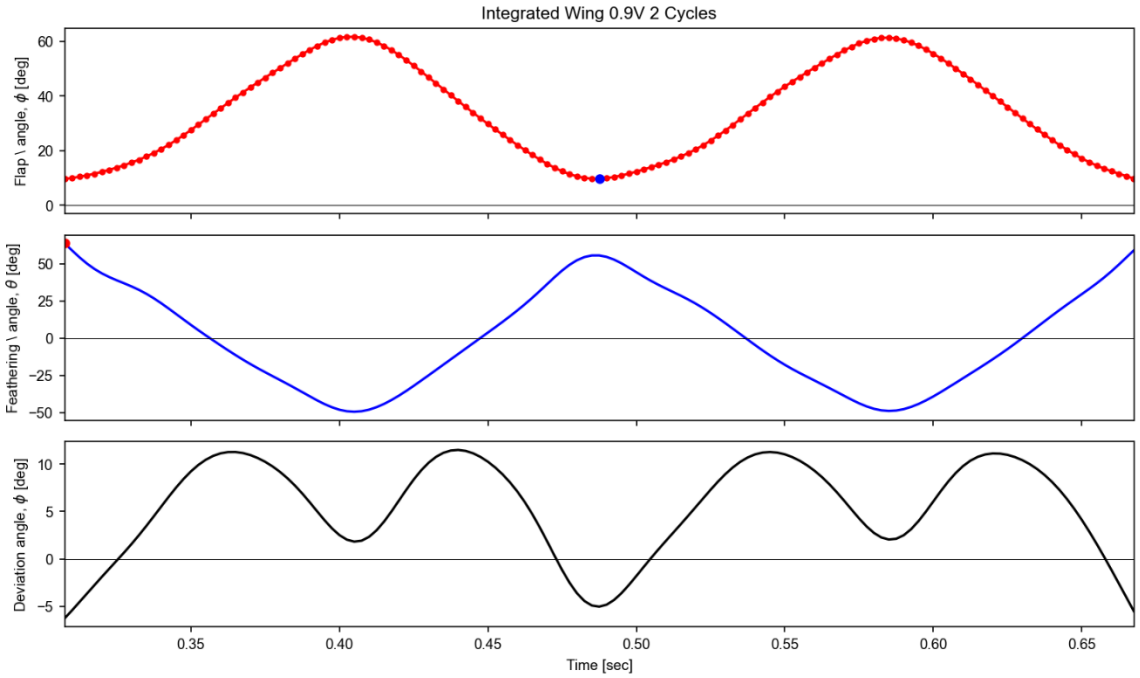

Figure 4.16 Representative time history of two cycles of the integrated wing flapping at a frequency of approximately 6 Hz with a voltage input of 0.9 V. The average feathering angle is 0.73° while the flapping frequency is 6.01 Hz. The peak-to-peak flapping amplitude is 52.04° while the peak-to-peak feathering amplitude is 113.19°.

Table 4.7 Average feathering angles for the half-cycles of the two cycles for the integrated wing flapping at a frequency of approximately 6 Hz with an input voltage of 0.9 V.

	Upstroke 1	Downstroke 1	Upstroke 2	Downstroke 2
Average Feathering Angle (°)	3.08	1.16	1.91	-2.19

Once again, the average feathering angles for the two cycles are close to zero. The half-cycle angles do differ from zero by a few degrees; however, they do still show relative symmetry in the deformation of the wing during the flapping motion. Interestingly, the half-cycle averages are closer to zero for the 6 Hz case than they are for the 0.7 V case. This is likely due to the increased power that was given to the flapper for the 6 Hz case (0.9 V). This allowed for a smoother flapping motion because the motor could simply power through imperfections or slipping in the gears. This allowed the

integrated wing to follow a more natural flapping motion with smoother deformation changes.

In the case of the integrated wing, the upstroke average feathering angles tend to have a positive sign while the downstroke angles in most cases are negative. This is a further example of the symmetric nature of the wing. The feathering angle being positive or negative merely indicates the direction of the deformation. As such, a symmetric wing would be expected to have a positive half-cycle value followed by a negative half-cycle value. The symmetrical nature of the integrated wing can be attributed to its construction. Since the integrated wing is made using resin printing that allows the veins to be encased in the membrane material, the integrated wing experiences no build asymmetries. The same amount of material is on the right side of the veins as is on the left side of the veins.

The symmetrical nature of the feathering angle results in a nearly symmetrical empirical lift production for the integrated wing. The empirical force coefficients for the 0.7 V case are shown in Figure 4.17 while the empirical force coefficients for the 6 Hz case are shown in Figure 4.18.

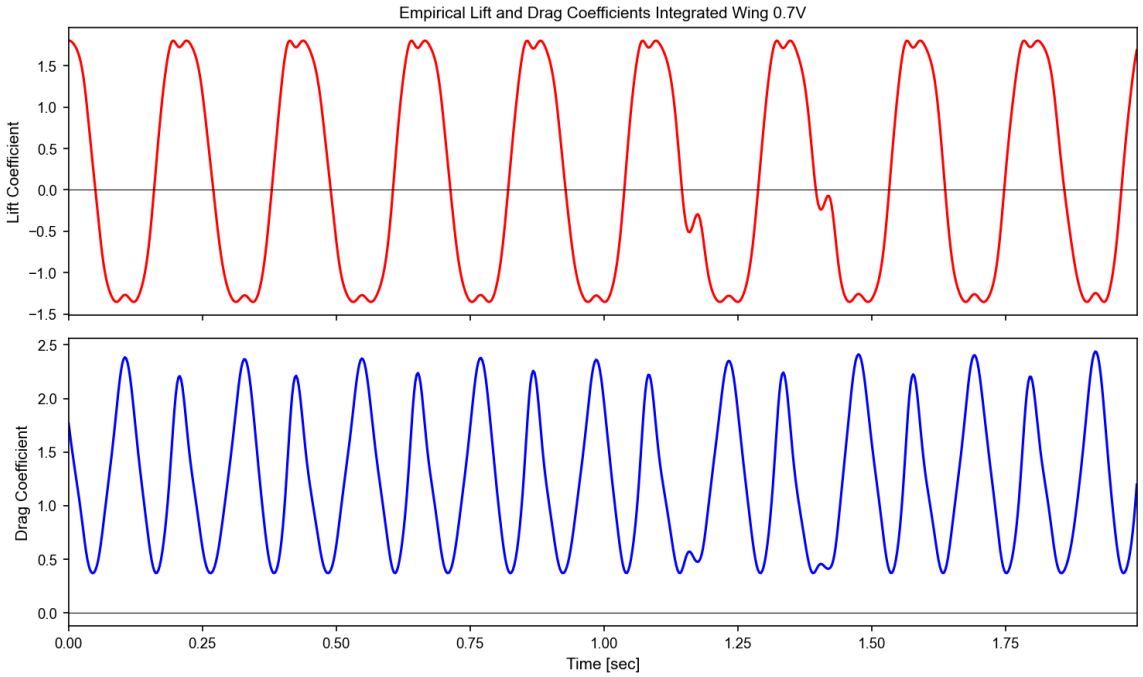

Figure 4.17 Empirical lift and drag coefficient time histories calculated from the feathering angle time history of the integrated wing flapping with a constant voltage input of 0.7 V. The average lift coefficient is 0.09. The average drag coefficient is 1.22. The maximum lift coefficient is 1.8.

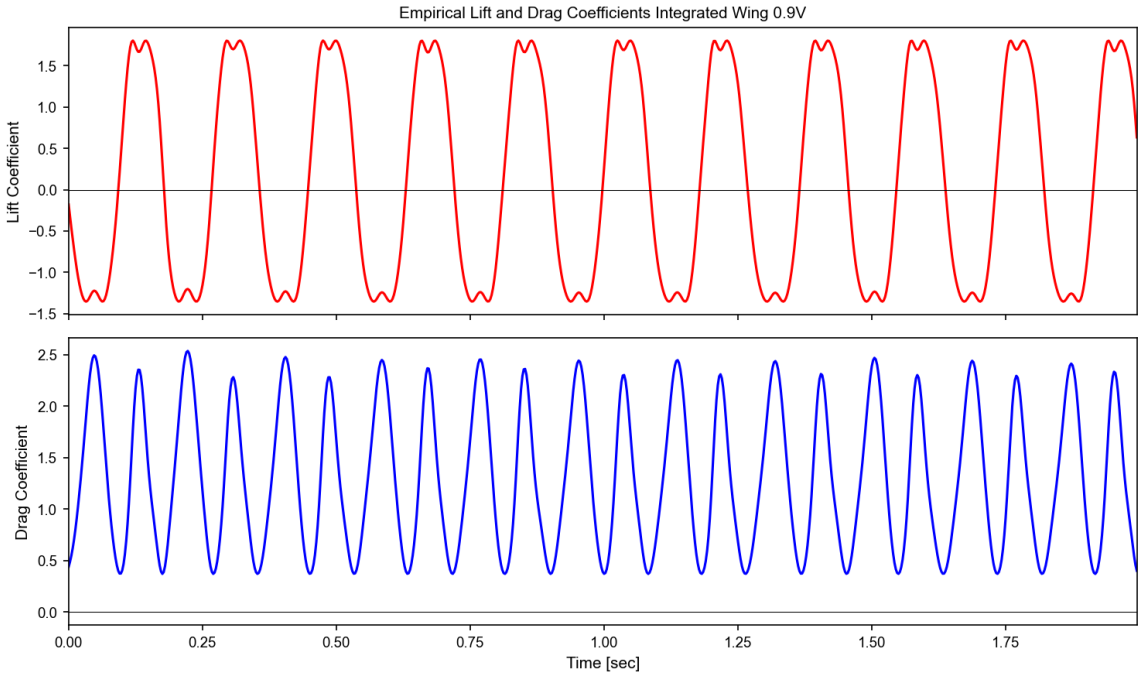

Figure 4.18 Empirical lift and drag coefficient time histories calculated from the feathering angle time history of the integrated wing flapping with a frequency of approximately 6 Hz and at an input voltage of 0.9 V. The average lift coefficient is 0.13. The average drag coefficient is 1.30. The maximum lift coefficient is 1.8.

The average lift coefficients for both cases are nearly zero. This indicates that the integrated wing can generate approximately the same amount of force independent of its flapping direction. There are small dips at the peaks and valleys of the lift curves. Due to the uniformity of these dips, they are most likely due to the flapping mechanism not transitioning smoothly between upstrokes and downstrokes. This results in the wing vibrating or oscillating slightly at the transition point and thus small changes in the lift production. The drag shows a largely symmetric trend as well. It is always positive, which was expected.

4.4 Comparisons of the Three Wings

The primary focus of the comparisons in this study is on the trends and averages for the feathering angles of each of the three wings presented. The magnitudes are largely ignored in this discussion. The reason for this is differences in the testing setup between the monarch wing tests and the artificial wings tests. Since the monarch wing data was collected in a previous study [34], there is some uncertainty about the collection methods. However, it does still provide a solid baseline for monarch performance. In addition, the flapper mechanism has been rebuilt since the monarch study. While every attempt was made to make the same mechanism, some small changes did occur that affected the flapping amplitude of the mechanism. In addition, a new motor was used that had a different efficiency and power output than the motor used during the monarch study. This along with the heavier mass of the artificial wings relative to the monarch wing prevented one-to-one comparison based on flapping frequency. Morris [34] showed in his study that the flapping amplitude and flapping frequency can affect the magnitude of the feathering

angle but do not significantly affect the trends that the feathering angle follows. As such, the primary focus of this paper is on the trends followed by the feathering angles rather than the magnitudes.

In Sections 4.1 and 4.3, the trends followed by the monarch wing and the integrated wing, respectively, are very similar. Both have average feathering angles within a few degrees of zero. In fact, the integrated wing shows a greater tendency towards symmetry when compared to the monarch wing. Overall, both exhibit strong symmetry in their feathering angle time histories. This carries over to their empirical lift production. Both wings exhibit symmetric sinusoidal lift production curves. The average lift coefficients for the monarch wing and the integrated wing are also very similar as shown here in Table 4.8.

Table 4.8 Average lift coefficient values calculated for the monarch wing and the integrated wing.

	0.7 V Case	6 Hz Case
Monarch Wing Lift Coefficient	-0.04	-0.12
Integrated Wing Lift Coefficient	0.09	0.13

In the 0.7 V case, both averages are within a magnitude of 0.1 of zero while both averages are within a magnitude of 0.2 of zero for the 6 Hz case. This indicates that the two wings follow approximately the same lift production trends.

By contrast, the bonded wing exhibits a distinct asymmetry in its feathering angle time histories. In both cases the average feathering angles are larger than 25°. This shows a distinct bias towards positive feathering angles. As mentioned in Section 4.2, this is due to the asymmetric nature of the wing's construction and the elastic effects of the membrane material. These effects are also seen in the lift production histories for the

bonded wing. The average lift coefficients for the bonded wing are presented in Table 4.9.

Table 4.9 Average lift coefficient values calculated for the bonded wing.

	0.7 V Case	6 Hz Case
Bonded Wing Lift Coefficient	0.88	0.86

These values are significantly closer to one than zero, and thus show a large asymmetry in the lift production capabilities of the bonded wing. In addition, the lift production curves for the bonded wing showed more disturbances in the form of intermediate local maxima and minima than the curves for the monarch or the integrated wing. These disturbances, caused by the elastic properties of the membrane, result in sudden decreases and increases in force production that could be disastrous for a flying vehicle. Additionally, while the large positive lift coefficients may seem advantageous for designing a flying vehicle, they are detrimental to its performance. Monarchs achieve their asymmetric force production through body coupling and passive wing pitching rather than built-in asymmetric wing flexibility [11, 12, 15]. This allows monarchs to maneuver with great agility as they can produce sudden force with their wing upstrokes to aid in turning. The bonded wing would not be able to produce such a maneuver because it cannot produce adequate negative lift force on demand.

Based on the gathered data, the integrated wing represents a much closer approximation of the kinematics performance of a monarch wing when compared to the bonded wing. It also offers a higher performance and more predictable wing platform to use in building a bio-inspired micro-aerial vehicle.

Chapter 5. Conclusion

5.1 Conclusion

The purpose of this study was to determine whether a new artificial monarch wing printed using resin-based 3D printing was an improvement upon a PLA printed and chemically bonded artificial wing. The focus was to develop and test a wing that provided a better approximation of the kinematics trends of a monarch wing. The knowledge gained during this study will help with the development of future bio-inspired micro-aerial vehicles. This study directly compared the motion capture data of the wing kinematics for a monarch wing, a bonded artificial wing, and the integrated artificial wing.

It was determined that the integrated wing was an improvement over the bonded wing due to the greater symmetry of the integrated wing's feathering angle. The feathering angle trends of the integrated wing were much more closely aligned with the trends of the monarch wing than those of the bonded wing. Both the monarch wing and the integrated wing had average feathering angles within a few degrees of zero while the average feathering angle of the bonded wing was in excess of 25°. These differences were further seen in the empirical lift coefficient time histories for the wings. Both the monarch wing and the integrated wing had average lift coefficients very close to zero while the bonded wing was close to one. The bonded wing also exhibited sudden changes in lift production due to the elastic nature of the membrane material. This elasticity leads

to unpredictable lift generation. The integrated wing, on the other hand, exhibited a predictable and repeatable lift generation curve. Overall, the integrated wing was found to be a better approximation of the kinematics of a monarch wing as well as a better wing platform for micro-aerial vehicle development than the bonded wing.

5.2 Future Work

There is still additional work to be performed on the development and testing of the integrated wing. The potential tasks include the following:

1. Repeat the testing of the monarch and integrated wings on the same flapping system. This would allow for direct magnitude comparisons in addition to trend comparisons.
2. Collect force data for both a monarch wing and the integrated wing.
3. Conduct wind tunnel testing of both the integrated wing and the monarch wing to examine changes in kinematics and force production. The current test setup emulates hovering flight with no freestream flow. However, butterflies do not hover.
4. Conduct wind tunnel PIV measurements for both the monarch wing and the integrated wing.
5. Develop a model for the hindwing of a monarch butterfly and perform kinematic and force production tests of artificial wings in a forewing and hindwing configuration.
6. Develop a micro-aerial vehicle using the integrated wing.

References

[1] Brower, L. P. Monarchs. In *Encyclopedia of Insects*, Elsevier, 2003, pp. 739–743.

[2] Brower, L. P. "Monarch Butterfly Orientation: Missing Pieces of a Magnificent Puzzle." *Journal of Experimental Biology*, Vol. 199, No. Pt 1, 1996, pp. 93–103.

[3] Brower, L. P., Fink, L. S., and Walford, P. "Fueling the Fall Migration of the Monarch Butterfly." *Integrative and Comparative Biology*, Vol. 46, No. 6, 2006, pp. 1123–1142. https://doi.org/10.1093/icb/icl029.

[4] Froy, O., Gotter, A. L., Casselman, A. L., and Reppert, S. M. "Illuminating the Circadian Clock in Monarch Butterfly Migration." *Science*, Vol. 300, 2003, pp. 1303–1306.

[5] Merlin, C., Gegear, R. J., and Reppert, S. M. "Sun Compass Orientation in Migratory." *Cycle*, Vol. 325, No. 6, 2009, pp. 1700–1705.

[6] Gibo, D. L., "Flight Strategies of Migrating Monarch Butterflies (Danaus Plexippus L.) in Southern Ontario." In *Insect Flight*, Springer, Berlin, 1986.

[7] Shyy, W., Aono, H., Kang, C., and Liu, H. *An Introduction to Flapping Wing Aerodynamics*. Cambridge University Press, New York, 2013.

[8] Spagnolie, S. E., Moret, L., Shelley, M. J., and Zhang, J. "Surprising Behaviors in Flapping Locomotion with Passive Pitching." *Physics of Fluids*, Vol. 22, No. 4, 2010.

[9] Eldredge, J. D., Toomey, J., and Medina, A. "On the Roles of Chord-Wise Flexibility in a Flapping Wing with Hovering Kinematics." *Journal of Fluid Mechanics*, Vol. 659, 2010, pp. 94–115.

[10] Wu, P., Stanford, B. K., Sällström, E., Ukeiley, L., and Ifju, P. G. "Structural Dynamics and Aerodynamics Measurements of Biologically Inspired Flexible Flapping Wings." *Bioinspiration & Biomimetics*, Vol. 6, 2011. https://doi.org/10.1088/1748-3182/6/1/016009.

[11] Vargas, A., Mittal, R., and Dong, H. "A Computational Study of the Aerodynamic Performance of a Dragonfly Wing Section in Gliding Flight." *Bioinspiration & Biomimetics*, Vol. 3, No. 2, 2008.

[12] Dewey, P. A., Boschitsch, B. M., Moored, K. W., Stone, H. A., and Smits, A. J. "Scaling Laws for the Thrust Production of Flexible Pitching Panels." *Journal of Fluid Mechanics*, Vol. 732, 2013, pp. 29–46.

[13] Michelin, S., and Llewellyn Smith, S. G. “Resonance and Propulsion Performance of a Heaving Flexible Wing.” *Physics of Fluids*, Vol. 21, No. 7, 2009.

[14] Vanella, M., Fitzgerald, T., Preidikman, S., Balaras, E., and Balachandran, B. “Influence of Flexibility on the Aerodynamic Performance of a Hovering Wing.” *Journal of Experimental Biology*, Vol. 212, No. 1, 2009, pp. 95–105.

[15] Gordnier, R. E., and Attar, P. J. “Impact of Flexibility on the Aerodynamics of an Aspect Ratio Two Membrane Wing.” *Journal of Fluids and Structures*, Vol. 45, 2014, pp. 138–152.

[16] Shelley, M. J., and Zhang, J. “Flapping and Bending Bodies Interacting with Fluid Flows.” *Annual Review of Fluid Mechanics*, Vol. 43, 2011, pp. 449–465.

[17] Alben, S., and Shelley, M. “Coherent Locomotion as an Attracting State for a Free Flapping Body.” *Proceedings of the National Academy of Sciences*, Vol. 102, No. 32, 2005.

[18] Quinn, D. B., Lauder, G. V, and Smits, A. J. “Scaling the Propulsive Performance of Heaving Flexible Panels.” *Journal of Fluid Mechanics*, Vol. 738, 2013, pp. 250–267.

[19] Masoud, H., and Alexeev, A. “Resonance of Flexible Flapping Wings at Low Reynolds Number.” *Physical Review E*, Vol. 81, No. 5, 2010.

[20] Shahzad, A., Tian, F.-B., Young, J., and Lai, J. C. S. “Effects of Flexibility on the Hovering Performance of Flapping Wings with Different Shapes and Aspect Ratios.” *Journal of Fluids and Structures*, Vol. 81, 2018, pp. 69–96.

[21] Kang, C., and Shyy, W. “Scaling Law and Enhancement of Lift Generation of an Insect-Size Hovering Flexible Wing.” *Journal of The Royal Society Interface*, Vol. 10, No. 85, 2013.

[22] Yin, B., and Luo, H. “Effect of Wing Inertia on Hovering Performance of Flexible Flapping Wings.” *Physics of Fluids*, Vol. 22, No. 11, 2010.

[23] Ramananarivo, S., Godoy-Diana, R., and Thiria, B. “Rather than Resonance, Flapping Wing Flyers May Play on Aerodynamics to Improve Performance.” *Proceedings of the National Academy of Sciences*, Vol. 108, No. 15, 2011.

[24] Wootton, R. J. “Support and Deformability in Insect Wings.” *Journal of Zoology, London*, Vol. 193, 1981, pp. 447–468.

[25] Shyy, W., Aono, H., Chimakurthi, S. K., Trizila, P., Kang, C. K., Cesnik, C. E. S., and Liu, H. "Recent Progress in Flapping Wing Aerodynamics and Aeroelasticity." *Progress in Aerospace Sciences*, Vol. 46, No. 7, 2010, pp. 284–327. https://doi.org/10.1016/j.paerosci.2010.01.001.

[26] Nakata, T., Liu, H., Tanaka, Y., Nishihashi, N., Wang, X., and Sato, A. "Aerodynamics of a Bio-Inspired Flexible Flapping-Wing Micro Air Vehicle." *Bioinspiration & Biomimetics*, Vol. 6, No. 4, 2011.

[27] Combes, S. A., and Daniel, T. L. "Flexural Stiffness in Insect Wings I. Scaling and the Influence of Wing Venation." *Journal of Experimental Biology*, Vol. 206, No. 17, 2003. https://doi.org/10.1242/jeb.00523.

[28] Tanaka, H., and Wood, R. J. "Fabrication of Corrugated Artificial Insect Wings Using Laser Micromachined Molds." *Journal of Micromechanics and Microengineering*, Vol. 20, No. 7, 2010.

[29] Steppan, S. J. "Flexural Stiffness Patterns of Butterfly Wings (Papilionoidea)." *Journal of Research on the Lepidoptera*, Vol. 35, 1996, pp. 61–77.

[30] Song, F., Lee, K. L., Soh, A. K., Zhu, F., and Bai, Y. L. "Experimental Studies of the Material Properties of the Forewing of Cicada (Homóptera, Cicàdidae)." *Journal of Experimental Biology*, Vol. 207, 2004. https://doi.org/10.1242/jeb.01122.

[31] Wainwright, S. A., Biggs, W. D., Gosline, J. M., and Currey, J. D. *Mechanical Design in Organisms*. Princeton University Press, 1976.

[32] Jensen, M., and Weis-Fogh, T. "Biology and Physics of Locust Flight. V. Strength and Elasticity of Locust Cuticle." *Philosophical Transactions of the Royal Society B: Biological Sciences*, Vol. 245, No. 721, 1962, pp. 137–169.

[33] Twigg, R., Sridhar, M. K., Pohly, J., Hildebrant, N., Kang, C. K., Landrum, D. B., Roh, K. H., and Salzwedel, S. "Aeroelastic Characterization of Real and Artificial Monarch Butterfly Wings." *AIAA Scitech 2020 Forum*, Vol. 1 PartF, 2020. https://doi.org/10.2514/6.2020-2002.

[34] Morris, T., Sridhar, M., Clark, T., Schulze, F., Kang, C. K., Landrum, D. B., Roh, K. H., Lee, T., and Aono, H., "Experimental Measurements of the Wing Deformation and Force Production of a Real Monarch Butterfly Wing," AIAA-2022-0308, *AIAA SciTech Forum*, 2022.

[35] Gibo, D. L., and Pallett, M. J. "Soaring Flight of Monarch Butterflies, Danaus Plexippus (Lepidoptera: Danaidae), during the Late Summer Migration in Southern Ontario." *Canadian Journal of Zoology*, Vol. 57, 1979. https://doi.org/10.1139/z79-180.

[36] Sridhar, M. K., Kang, C. K., and Lee, T. “Geometric Formulation for the Dynamics of Monarch Butterfly with the Effects of Abdomen Undulation.” *AIAA Scitech 2020 Forum*, Vol. 1 PartF, No. January, 2020, pp. 1–24. https://doi.org/10.2514/6.2020-1962.

[37] Kang, C. K., Cranford, J., Sridhar, M. K., Kodali, D., Landrum, D. B., and Slegers, N. “Experimental Characterization of a Butterfly in Climbing Flight.” *AIAA Journal*, Vol. 56, No. 1, 2018, p. 15–24. https://doi.org/10.2514/1.J055360.

[38] Dickinson, M. H., Lehmann, F. O., and Sane, S. P. “Wing Rotation and the Aerodynamic Basis of Insect Flight.” *Science*, Vol. 284, 1999.

[39] Kang, C. K., Sridhar, M., Twigg, R., Pohly, J., Lee, T., and Aono, H. “Power Benefits of High-Altitude Flapping Wing Flight at the Monarch Butterfly Scale.” *Biomimetics*, Vol. 8, No. 4, 2023. https://www.mdpi.com/2313-7673/8/4/352

[40] Phan, H. V., and Park, H. C. “Insect-Inspired, Tailless, Hover-Capable Flapping-Wing Robots: Recent Progress, Challenges, and Future Directions.” *Progress in Aerospace Sciences*, 111:100573, 2019.

[41] Ma, J., Yu, W., Liang, P., Li, C., and Jiang, J. “Fusiongan: A Generative Adversarial Network for Infrared and Visible Image Fusion.” *Information Fusion*, 48:11–26, 2019.

[42] Keennon, M., Klingebiel, K., and Won, H. “Development of the Nano Hummingbird: A Tailless Flapping Wing Micro Air Vehicle.” *AIAA-2012- 588*, pages 1–24, 2012.

[43] De Croon, G., Groen, M. A., De Wagter, C., Remes, B., Ruijsink, R., and Van Oudheusden, B. W. “Design, Aerodynamics and Autonomy of the Delfly.” *Bioinspiration & Biomimetics*, 2012.

[44] Wood, R. J. “The First Takeoff of a Biologically Inspired At-Scale Robotic Insect.” *IEEE Transactions on Robotics*, 24:341–347, 2008.

[45] Coleman, D., Benedict, M., Hirishikeshaven, V., and Chopra, I. “Development of a Robotic Hummingbird Capable of Controlled Hover.” *Journal of the American Helicopter Society*, 62(3):1–9, 2017.

[46] Tu, Z., Fei, F., Zhang, J., and Deng, X. “An At-Scale Tailless Flapping-Wing Hummingbird Robot. I. Design, Optimization, and Experimental Validation.” *IEEE Transactions on Robotics*, 36(5):1511–1525, 2020.

Appendix A. Additional Time Histories

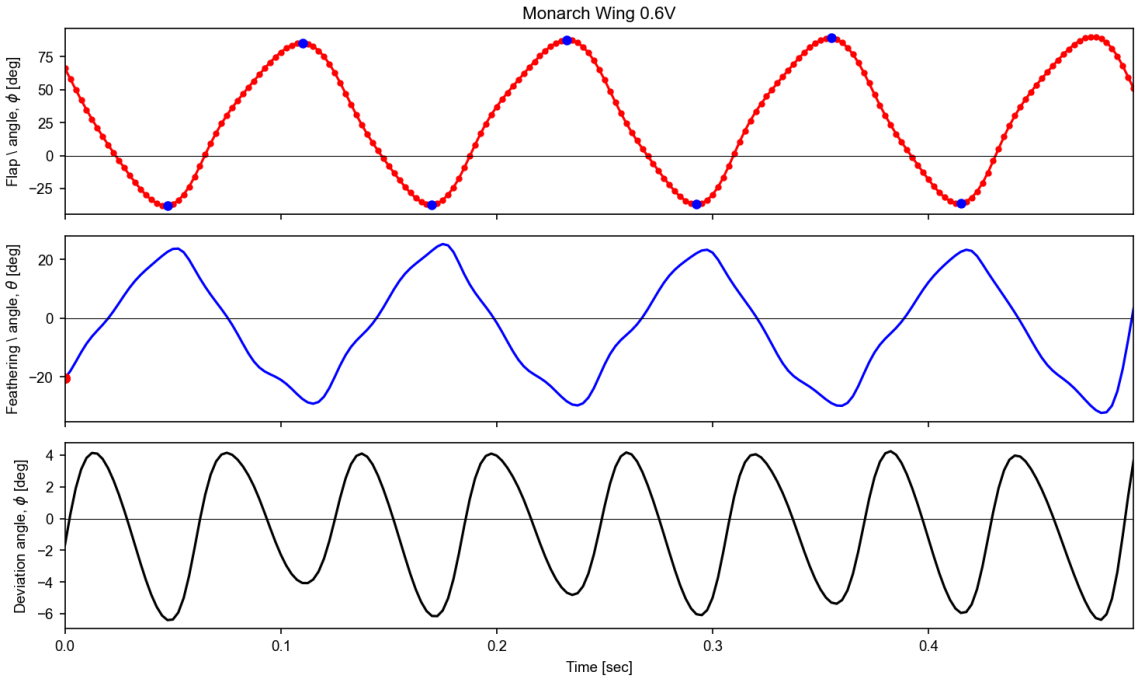

Figure A.1 Representative time history data for the monarch wing flapping with a constant input voltage of 0.6 V. The average feathering angle is -3.43° while the flapping frequency is 8.04 Hz. The peak-to-peak flapping amplitude is 128.06° while the peak-to-peak feathering amplitude is 57.66°.

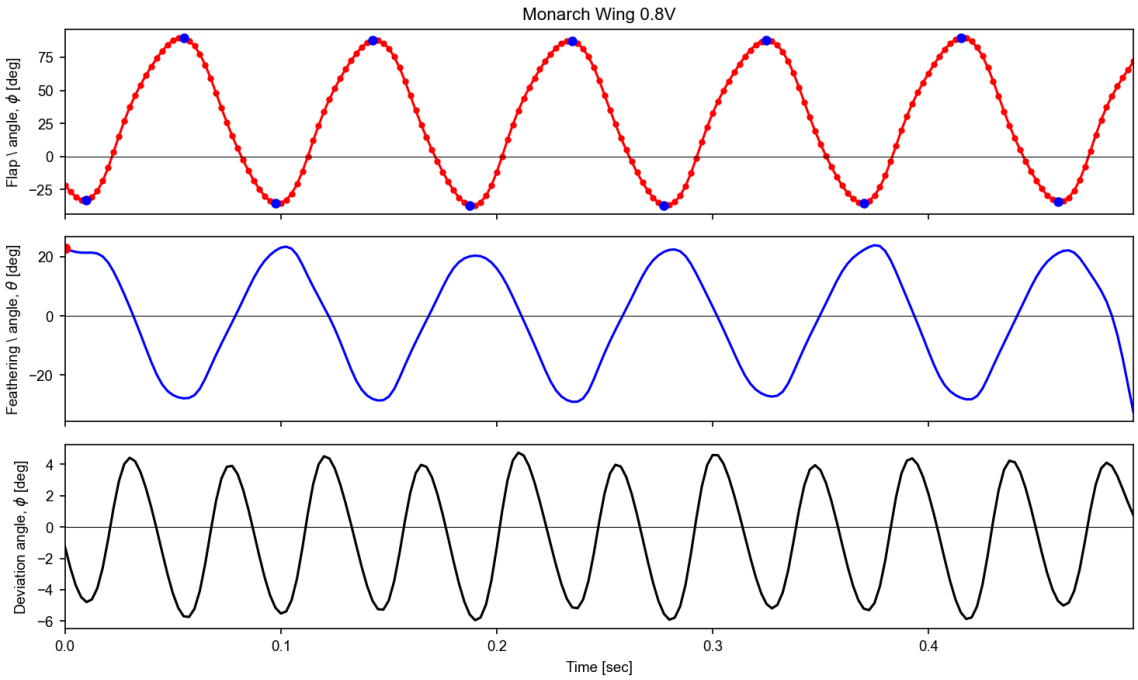

Figure A.2 Representative time history data for the monarch wing flapping with a constant input voltage of 0.8 V. The average feathering angle is -1.29° while the flapping frequency is 12.06 Hz. The peak-to-peak flapping amplitude is 124.54° while the peak-to-peak feathering amplitude is 56.70°.

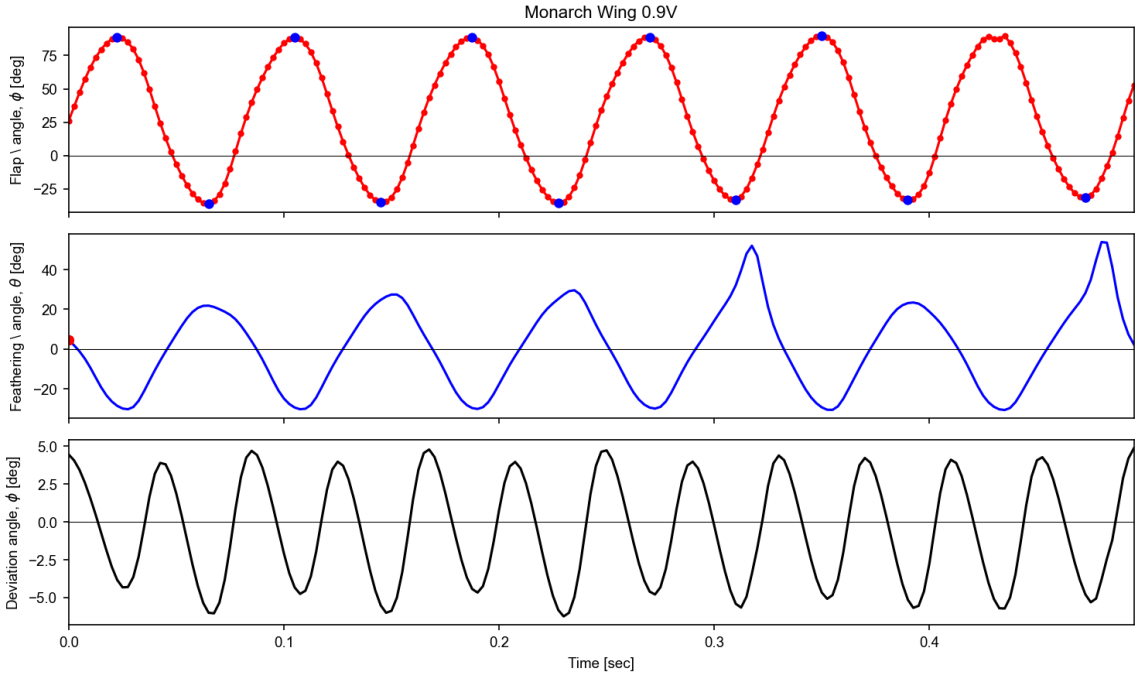

Figure A.3 Representative time history data for the monarch wing flapping with a constant input voltage of 0.9 V. The average feathering angle is 0.34° while the flapping frequency is 12.06 Hz. The peak-to-peak flapping amplitude is 125.83° while the peak-to-peak feathering amplitude is 84.54°.

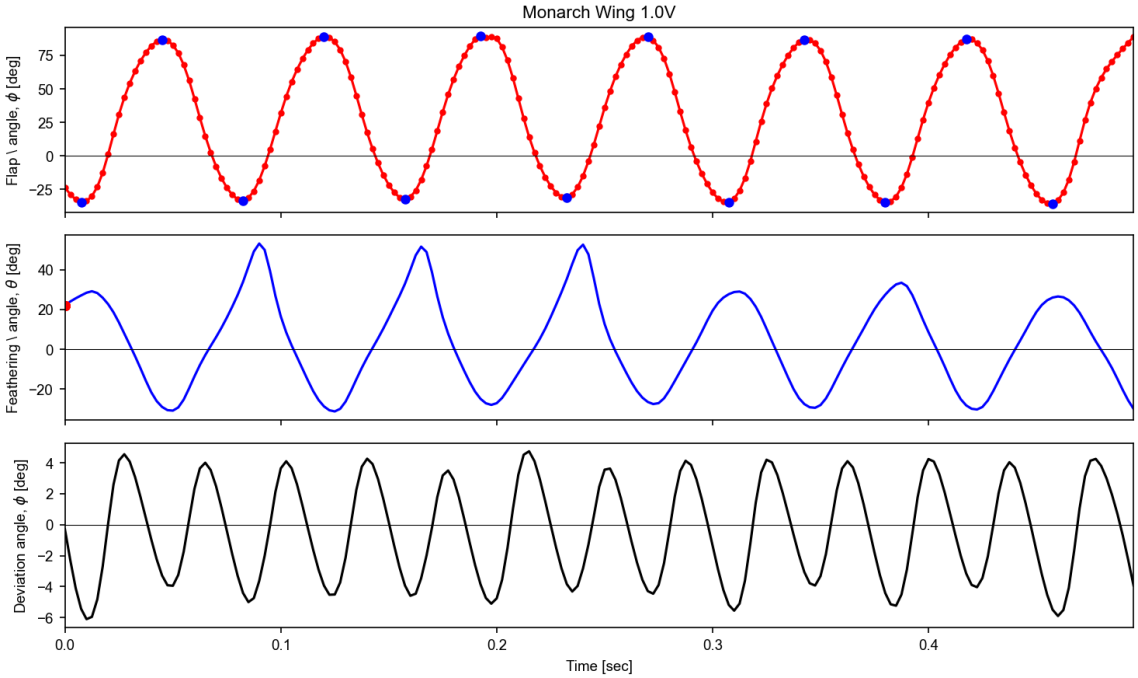

Figure A.4 Representative time history data for the monarch wing flapping with a constant input voltage of 1.0 V. The average feathering angle is 3.36° while the flapping frequency is 14.07 Hz. The peak-to-peak flapping amplitude is 125.23° while the peak-to-peak feathering amplitude is 84.36°.

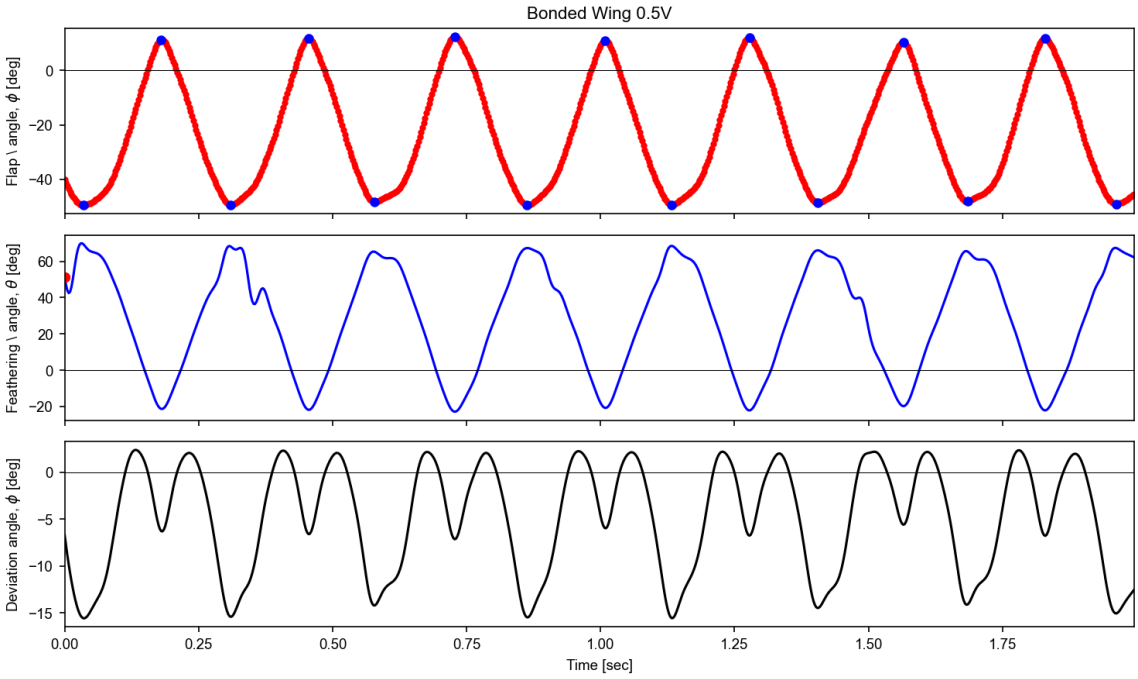

Figure A.5 Representative time history data for the bonded wing flapping with a constant input voltage of 0.5 V. The average feathering angle is 27.57° while the flapping frequency is 3.50 Hz. The peak-to-peak flapping amplitude is 61.94° while the peak-to-peak feathering amplitude is 92.72°.

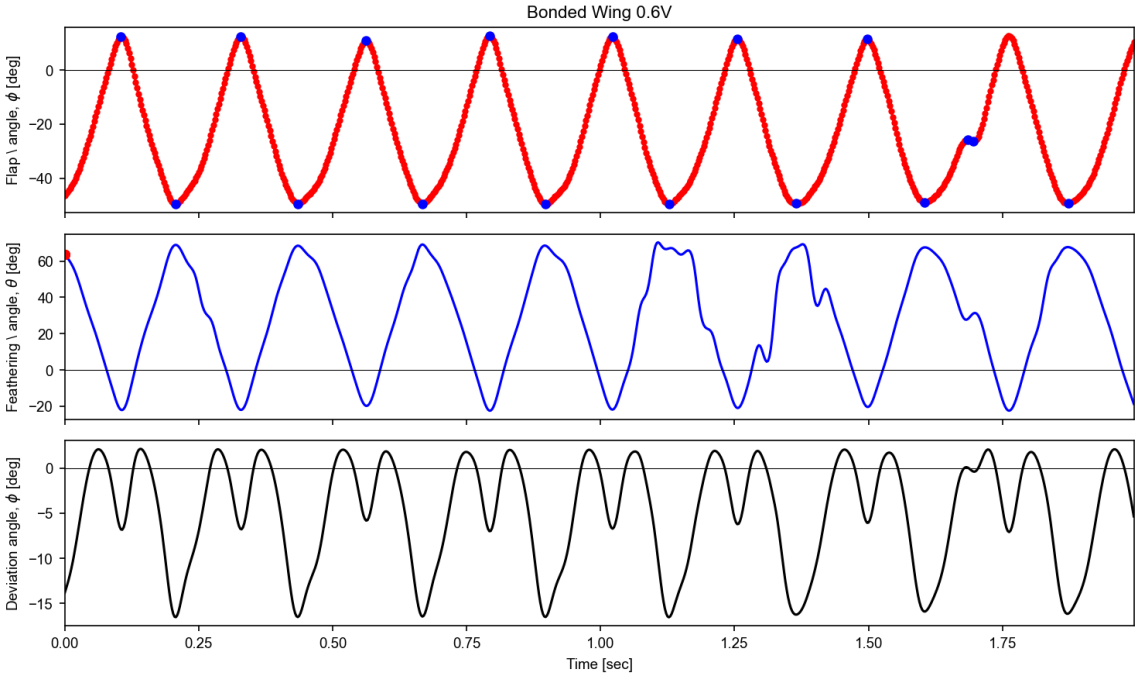

Figure A.6 Representative time history data for the bonded wing flapping with a constant input voltage of 0.6 V. The average feathering angle is 27.69° while the flapping frequency is 4.01 Hz. The peak-to-peak flapping amplitude is 62.32° while the peak-to-peak feathering amplitude is 92.79°.

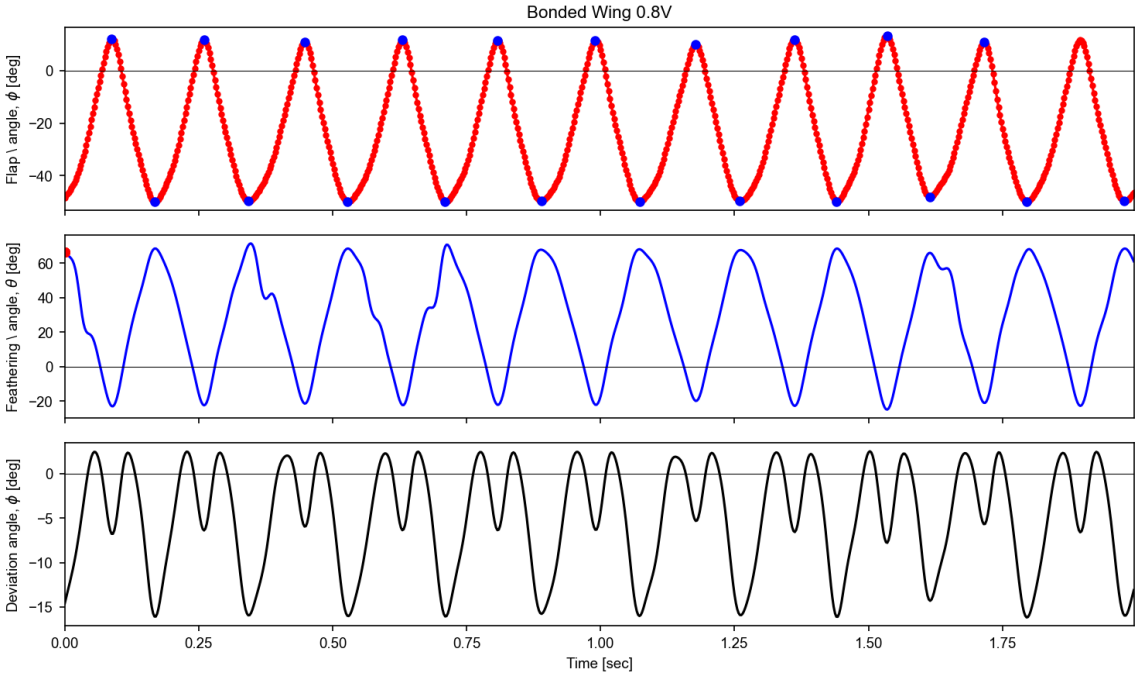

Figure A.7 Representative time history data for the bonded wing flapping with a constant input voltage of 0.8 V. The average feathering angle is 27.37° while the flapping frequency is 5.51 Hz. The peak-to-peak flapping amplitude is 63.39° while the peak-to-peak feathering amplitude is 96.20°.

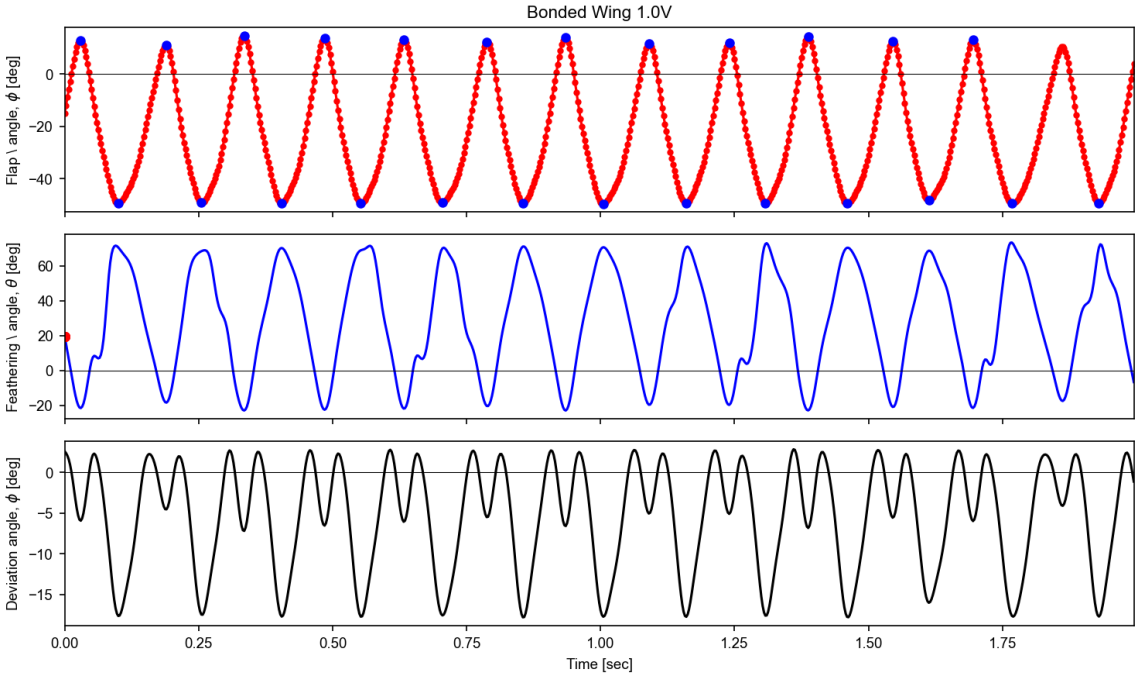

Figure A.8 Representative time history data for the bonded wing flapping with a constant input voltage of 1.0 V. The average feathering angle is 27.77° while the flapping frequency is 6.51 Hz. The peak-to-peak flapping amplitude is 64.23° while the peak-to-peak feathering amplitude is 96.49°.

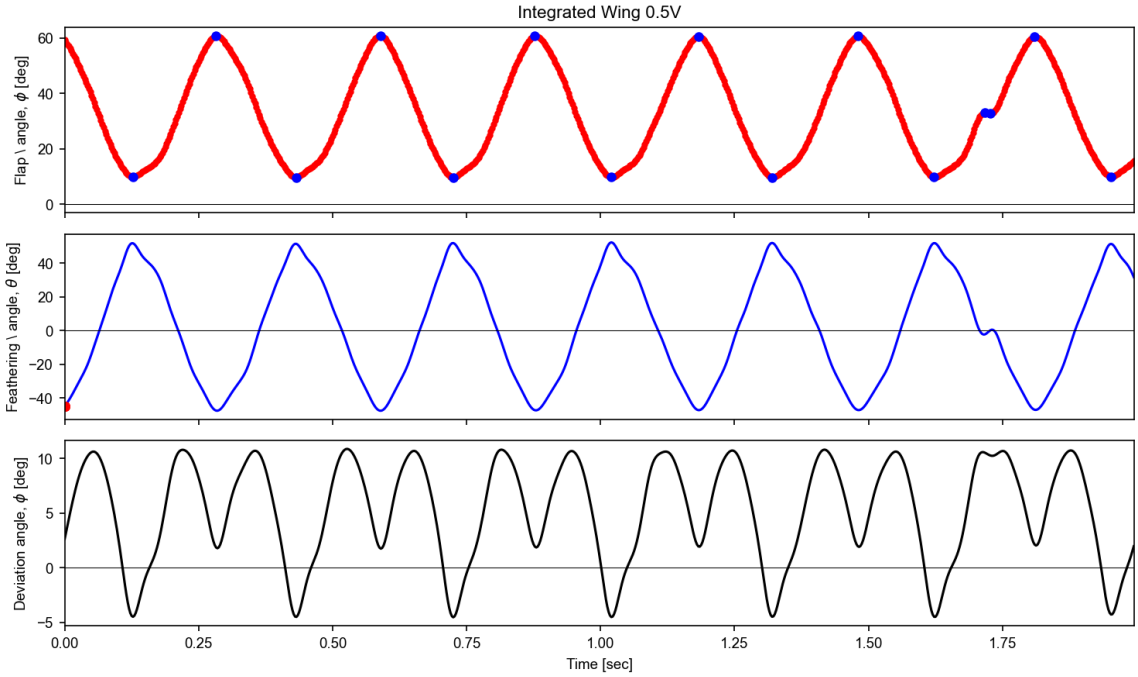

Figure A.9 Representative time history data for the integrated wing flapping with a constant input voltage of 0.5 V. The average feathering angle is 1.69° while the flapping frequency is 3.50 Hz. The peak-to-peak flapping amplitude is 51.07° while the peak-to-peak feathering amplitude is 99.89°.

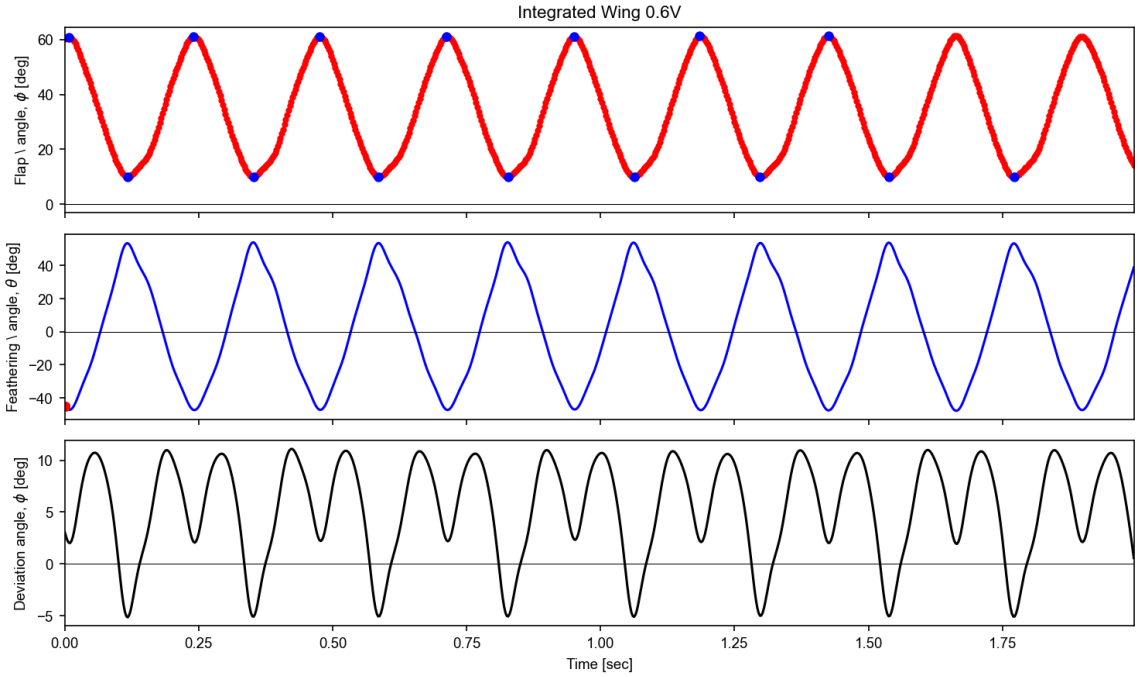

Figure A.10 Representative time history data for the integrated wing flapping with a constant input voltage of 0.6 V. The average feathering angle is 0.18° while the flapping frequency is 4.01 Hz. The peak-to-peak flapping amplitude is 51.41° while the peak-to-peak feathering amplitude is 101.73°.

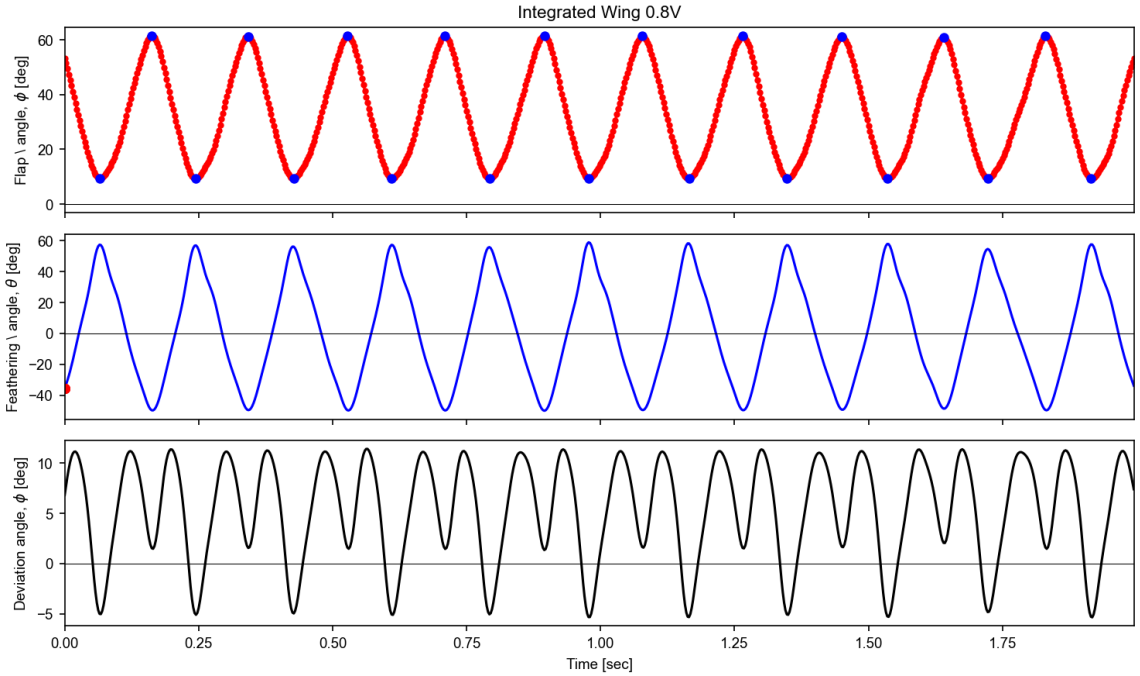

Figure A.11 Representative time history data for the integrated wing flapping with a constant input voltage of 0.8 V. The average feathering angle is 1.43° while the flapping frequency is 5.51 Hz. The peak-to-peak flapping amplitude is 52.15° while the peak-to-peak feathering amplitude is 109.00°.

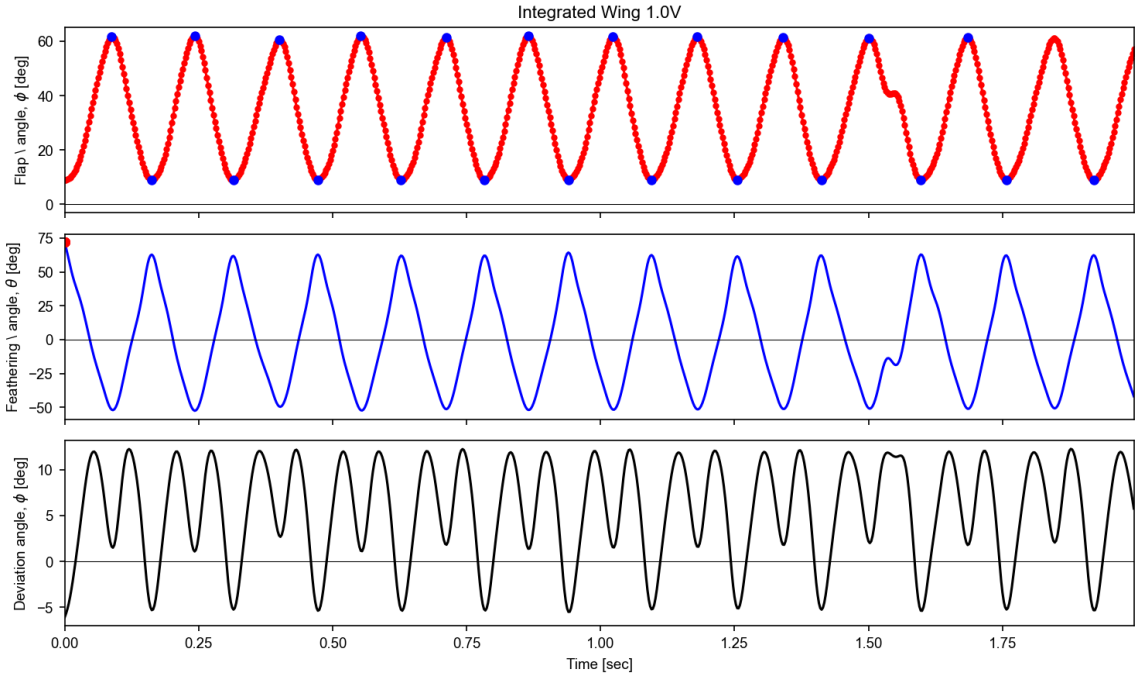

Figure A.12 Representative time history data for the integrated wing flapping with a constant input voltage of 1.0 V. The average feathering angle is 1.57° while the flapping frequency is 6.51 Hz. The peak-to-peak flapping amplitude is 53.11° while the peak-to-peak feathering amplitude is 124.41°.

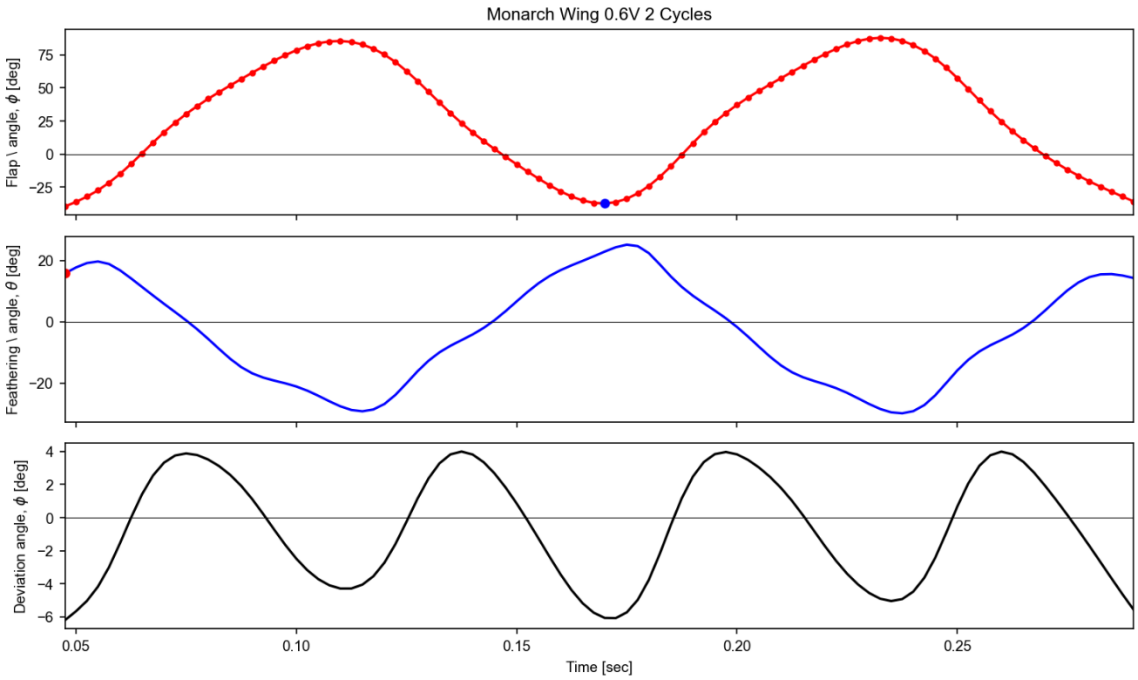

Figure A.13 Representative time history for 2 cycles of a monarch wing flapping with an input voltage of 0.6 V. The average feathering angle is -3.50° while the flapping frequency is 8.16 Hz. The peak-to-peak flapping amplitude is 127.55° while the peak-to-peak feathering amplitude is 54.98°.

Table A.1 Average feathering angles for the half-cycles of the two cycles for a monarch wing flapping with a voltage input of 0.6 V.

	Upstroke 1	Downstroke 1	Upstroke 2	Downstroke 2
Average Feathering Angle (°)	-1.42	-6.93	1.90	-9.05

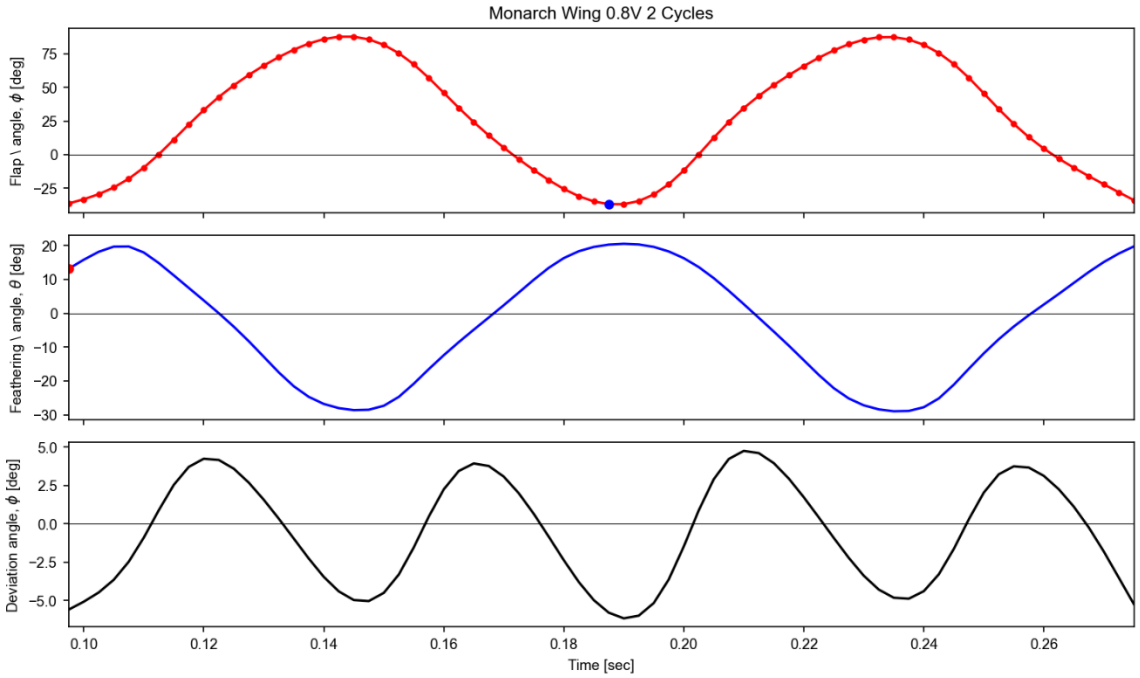

Figure A.14 Representative time history for 2 cycles of a monarch wing flapping with an input voltage of 0.8 V. The average feathering angle is -2.55° while the flapping frequency is 11.11 Hz. The peak-to-peak flapping amplitude is 124.54° while the peak-to-peak feathering amplitude is 49.42°.

Table A.2 Average feathering angles for the half-cycles of the two cycles for a monarch wing flapping with a voltage input of 0.8 V.

	Upstroke 1	Downstroke 1	Upstroke 2	Downstroke 2
Average Feathering Angle (°)	1.43	-6.43	1.40	-6.61

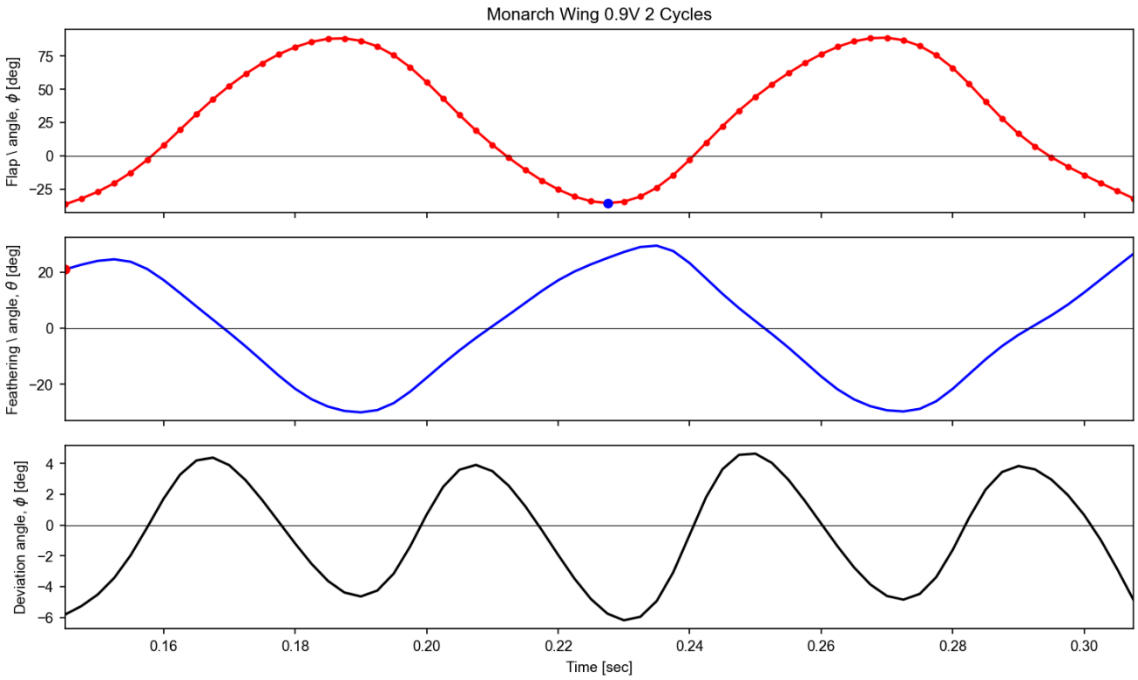

Figure A.15 Representative time history for 2 cycles of a monarch wing flapping with an input voltage of 0.9 V. The average feathering angle is -0.26° while the flapping frequency is 12.12 Hz. The peak-to-peak flapping amplitude is 125.36° while the peak-to-peak feathering amplitude is 59.61°.

Table A.3 Average feathering angles for the half-cycles of the two cycles for a monarch wing flapping with a voltage input of 0.9 V.

	Upstroke 1	Downstroke 1	Upstroke 2	Downstroke 2
Average Feathering Angle (°)	5.88	-8.94	10.26	-11.33

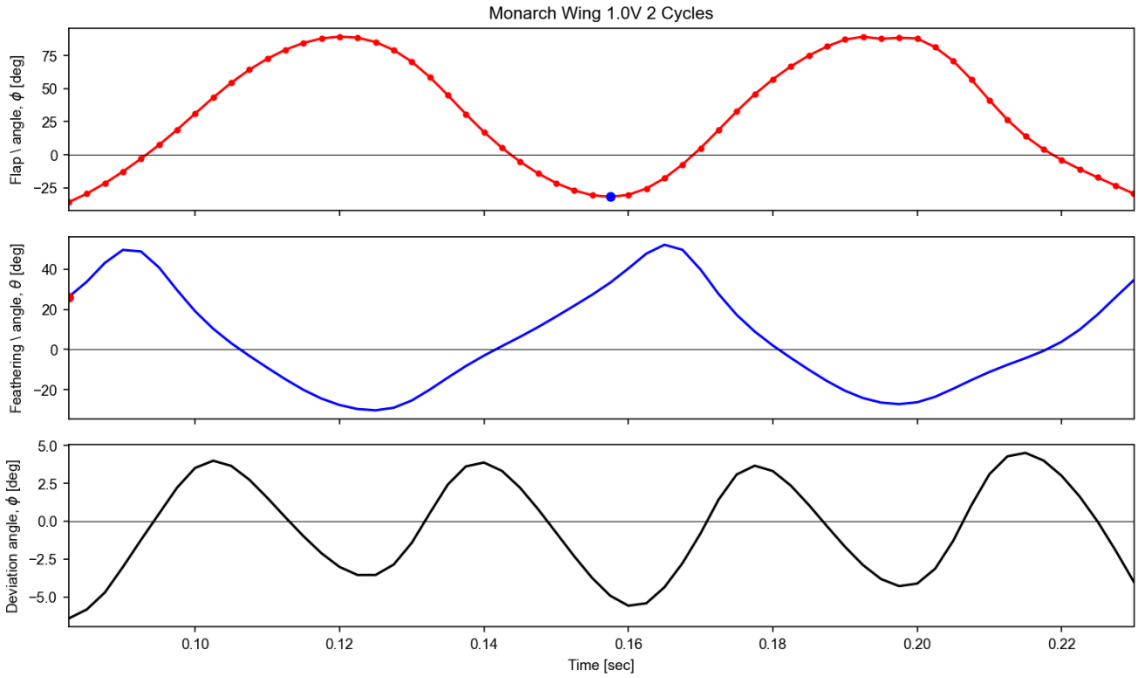

Figure A.16 Representative time history for 2 cycles of a monarch wing flapping with an input voltage of 1.0 V. The average feathering angle is 0.75 °while the flapping frequency is 13.33 Hz. The peak-to-peak flapping amplitude is 126.83° while the peak-to-peak feathering amplitude is 63.47°.

Table A.4 Average feathering angles for the half-cycles of the two cycles for a monarch wing flapping with a voltage input of 1.0 V.

	Upstroke 1	Downstroke 1	Upstroke 2	Downstroke 2
Average Feathering Angle (°)	4.56	-3.55	6.99	-5.01

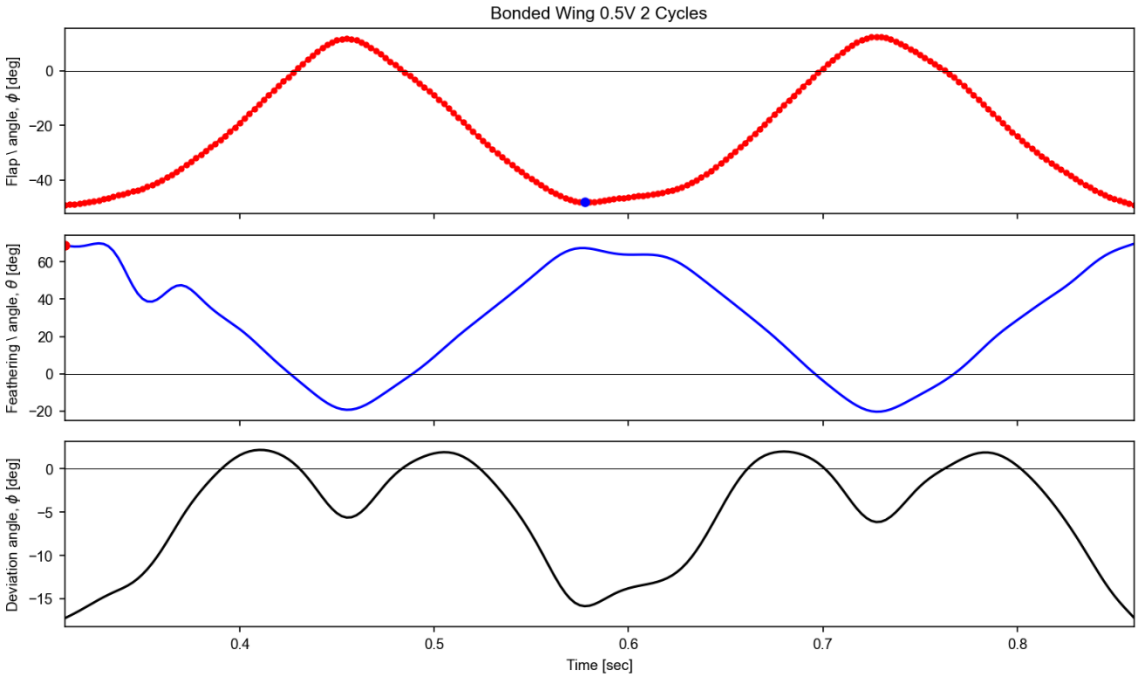

Figure A.17 Representative time history for 2 cycles of the bonded wing flapping with an input voltage of 0.5 V. The average feathering angle is 26.11° while the flapping frequency is 3.69 Hz. The peak-to-peak flapping amplitude is 61.33° while the peak-to-peak feathering amplitude is 90.90°.

Table A.5 Average feathering angles for the half-cycles of the two cycles for the bonded wing flapping with a voltage input of 0.5 V.

	Upstroke 1	Downstroke 1	Upstroke 2	Downstroke 2
Average Feathering Angle (°)	36.13	16.84	35.56	15.14

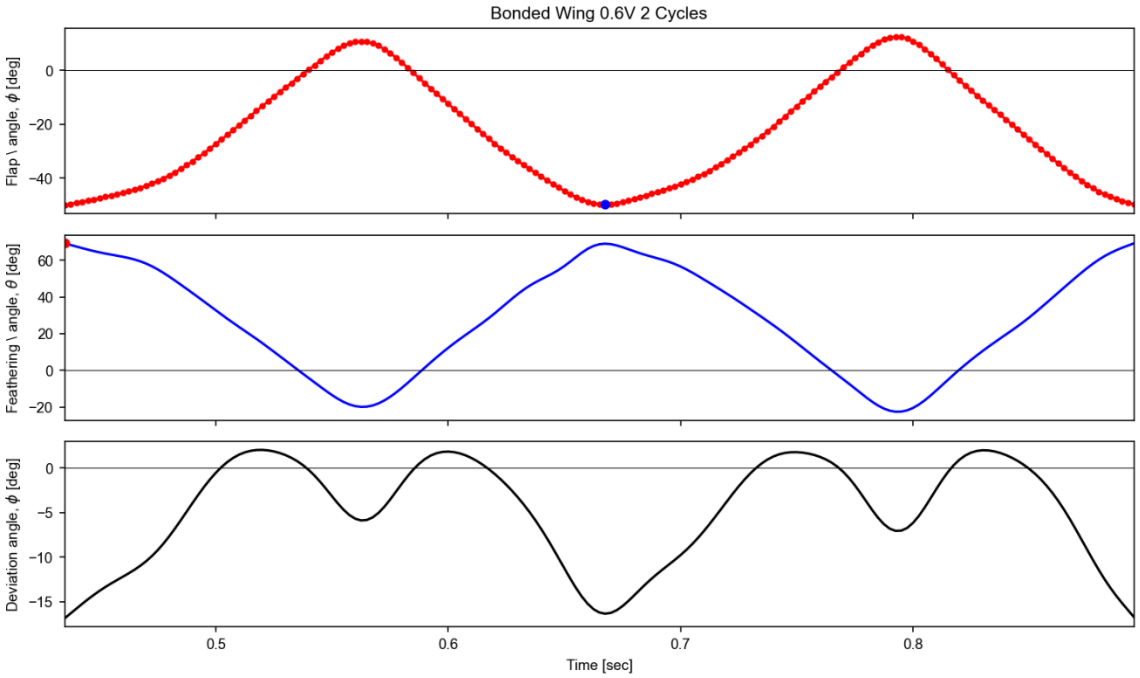

Figure A.18 Representative time history for 2 cycles of the bonded wing flapping with an input voltage of 0.6 V. The average feathering angle is 27.20° while the flapping frequency is 4.35 Hz. The peak-to-peak flapping amplitude is 62.26° while the peak-to-peak feathering amplitude is 92.60°.

Table A.6 Average feathering angles for the half-cycles of the two cycles for the bonded wing flapping with a voltage input of 0.6 V.

	Upstroke 1	Downstroke 1	Upstroke 2	Downstroke 2
Average Feathering Angle (°)	30.96	22.29	34.97	20.60

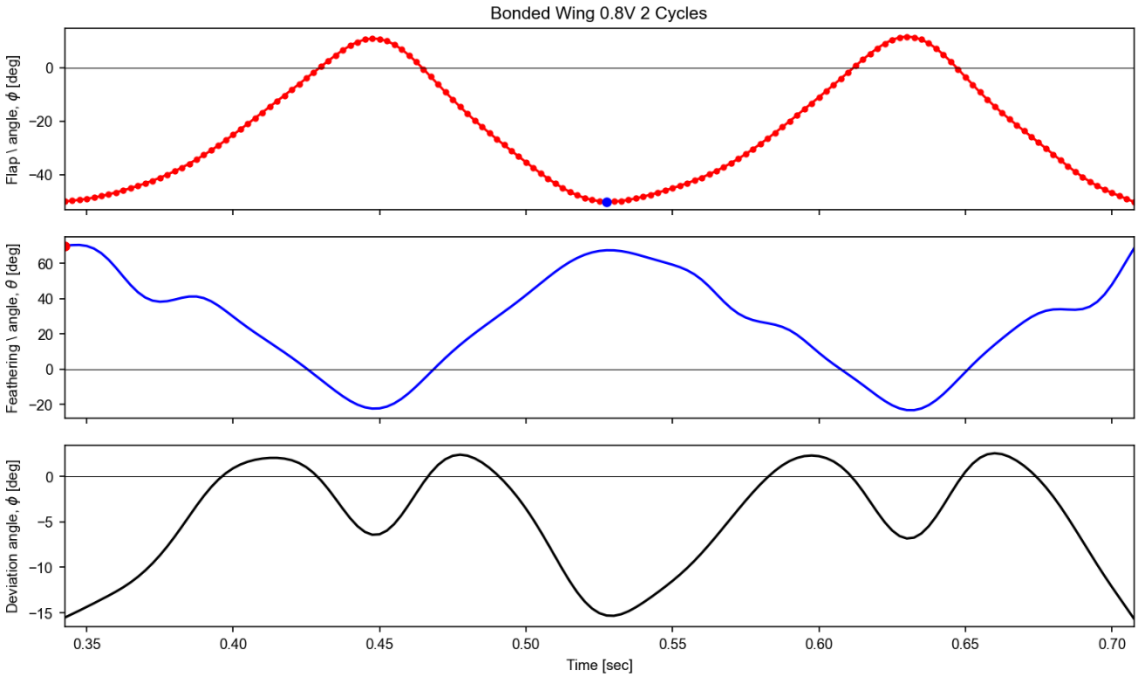

Figure A.19 Representative time history for 2 cycles of the bonded wing flapping with an input voltage of 0.8 V. The average feathering angle is 25.41° while the flapping frequency is 5.44 Hz. The peak-to-peak flapping amplitude is 61.87° while the peak-to-peak feathering amplitude is 93.76°.

Table A.7 Average feathering angles for the half-cycles of the two cycles for the bonded wing flapping with a voltage input of 0.8 V.

	Upstroke 1	Downstroke 1	Upstroke 2	Downstroke 2
Average Feathering Angle (°)	34.88	17.77	34.32	14.36

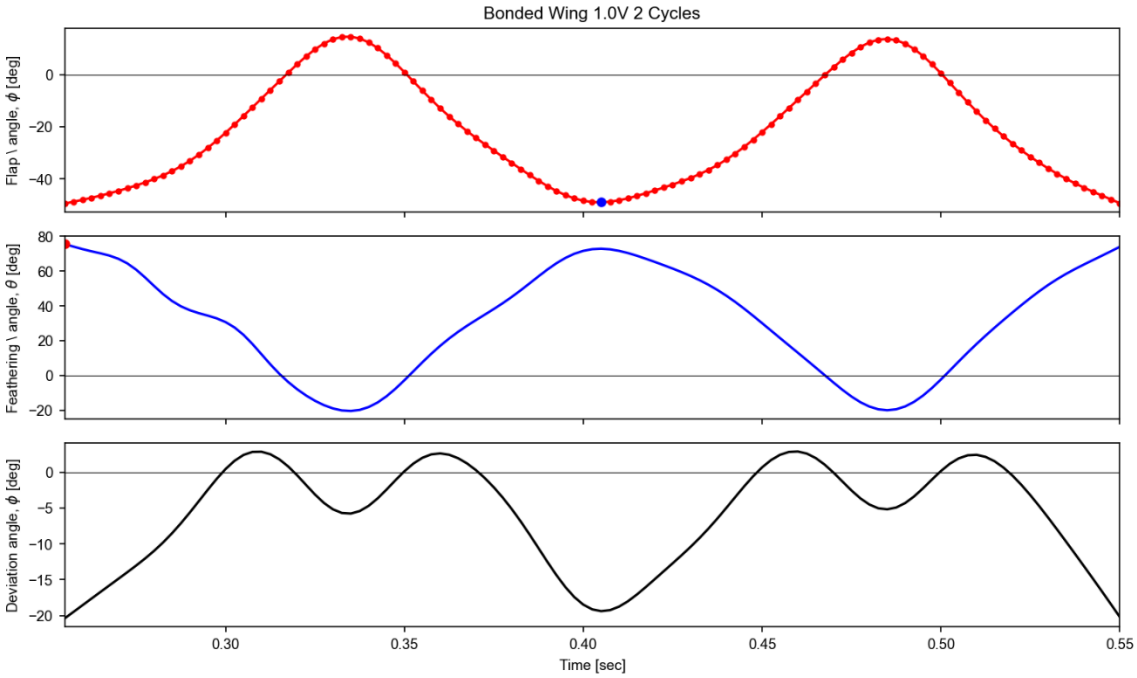

Figure A.20 Representative time history for 2 cycles of the bonded wing flapping with an input voltage of 1.0 V. The average feathering angle is 30.78° while the flapping frequency is 6.72 Hz. The peak-to-peak flapping amplitude is 64.04° while the peak-to-peak feathering amplitude is 95.97°.

Table A.8 Average feathering angles for the half-cycles of the two cycles for the bonded wing flapping with a voltage input of 1.0 V.

	Upstroke 1	Downstroke 1	Upstroke 2	Downstroke 2
Average Feathering Angle (°)	35.53	24.53	37.57	25.29

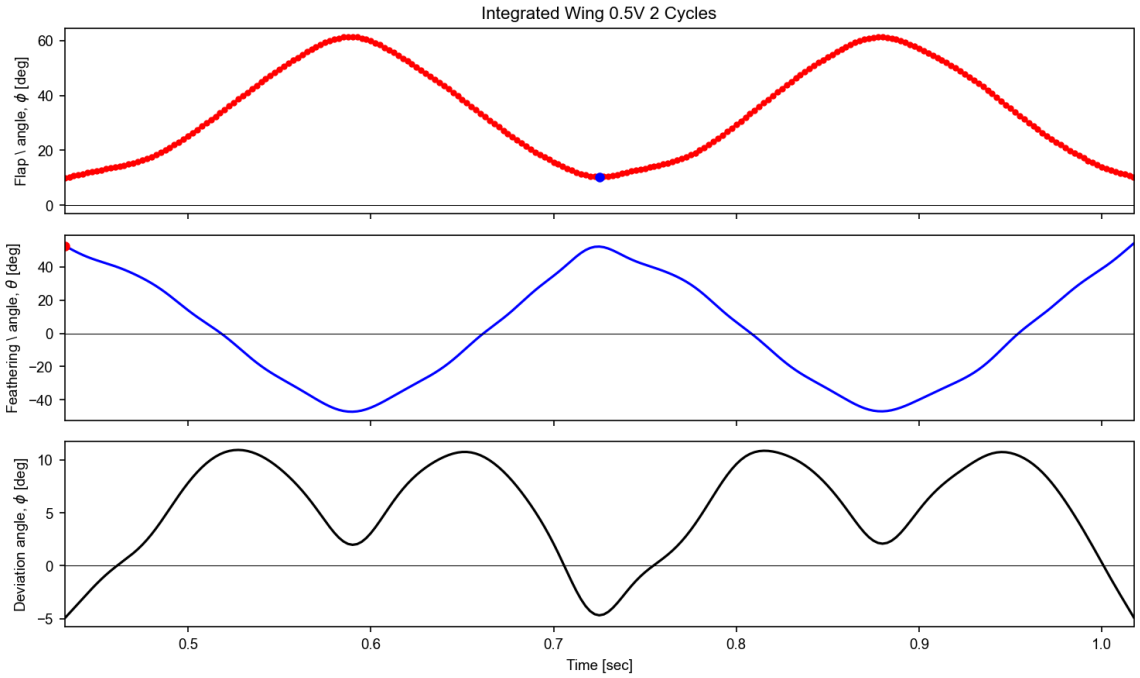

Figure A.21 Representative time history for 2 cycles of the integrated wing flapping with an input voltage of 0.5 V. The average feathering angle is 1.12° while the flapping frequency is 3.35 Hz. The peak-to-peak flapping amplitude is 51.33° while the peak-to-peak feathering amplitude is 102.82°.

Table A.9 Average feathering angles for the half-cycles of the two cycles for the integrated wing flapping with a voltage input of 0.5 V.

	Upstroke 1	Downstroke 1	Upstroke 2	Downstroke 2
Average Feathering Angle (°)	7.07	-6.44	9.96	-6.23

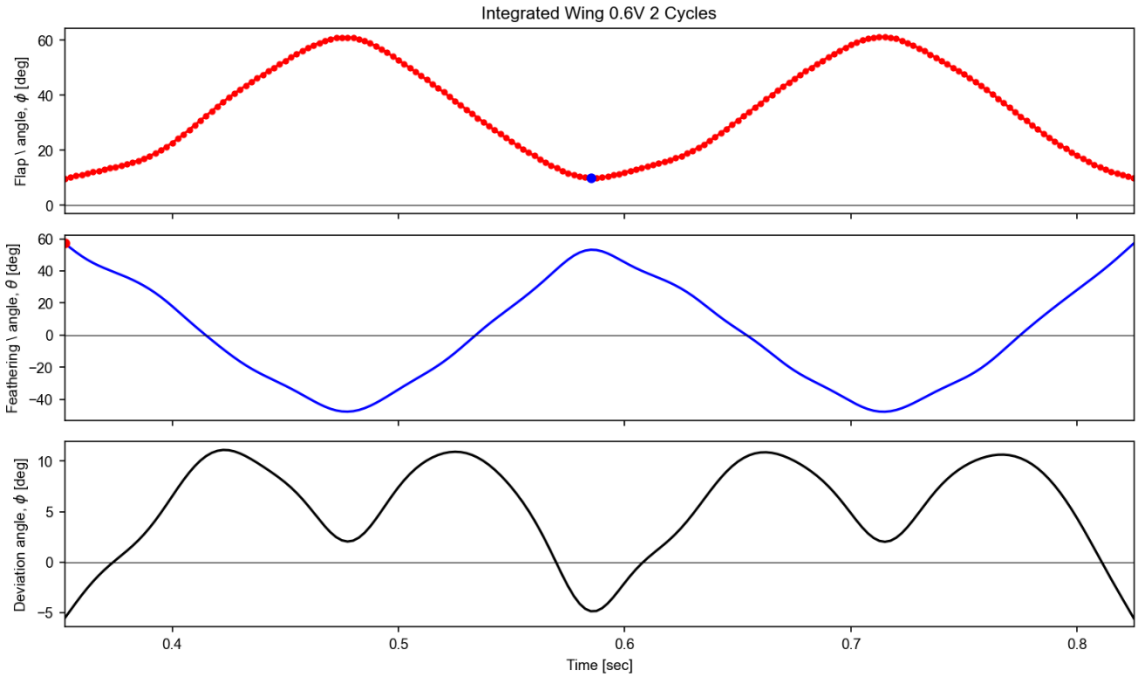

Figure A.22 Representative time history for 2 cycles of the integrated wing flapping with an input voltage of 0.6 V. The average feathering angle is 0.49° while the flapping frequency is 4.28 Hz. The peak-to-peak flapping amplitude is 51.54° while the peak-to-peak feathering amplitude is 105.16°.

Table A.10 Average feathering angles for the half-cycles of the two cycles for the integrated wing flapping with a voltage input of 0.6 V.

	Upstroke 1	Downstroke 1	Upstroke 2	Downstroke 2
Average Feathering Angle (°)	6.61	-5.43	5.76	-5.11

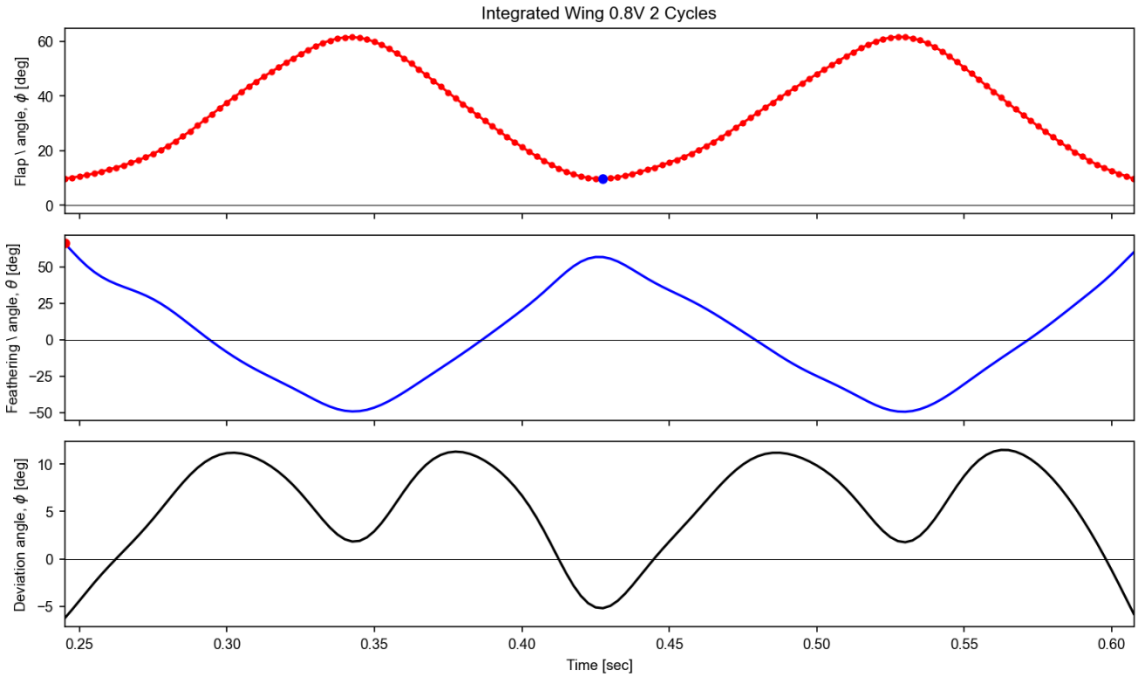

Figure A.23 Representative time history for 2 cycles of the integrated wing flapping with an input voltage of 0.8 V. The average feathering angle is 1.25° while the flapping frequency is 5.52 Hz. The peak-to-peak flapping amplitude is 52.10° while the peak-to-peak feathering amplitude is 116.93°.

Table A.11 Average feathering angles for the half-cycles of the two cycles for the integrated wing flapping with a voltage input of 0.8 V.

	Upstroke 1	Downstroke 1	Upstroke 2	Downstroke 2
Average Feathering Angle (°)	8.93	-6.23	7.38	-6.87

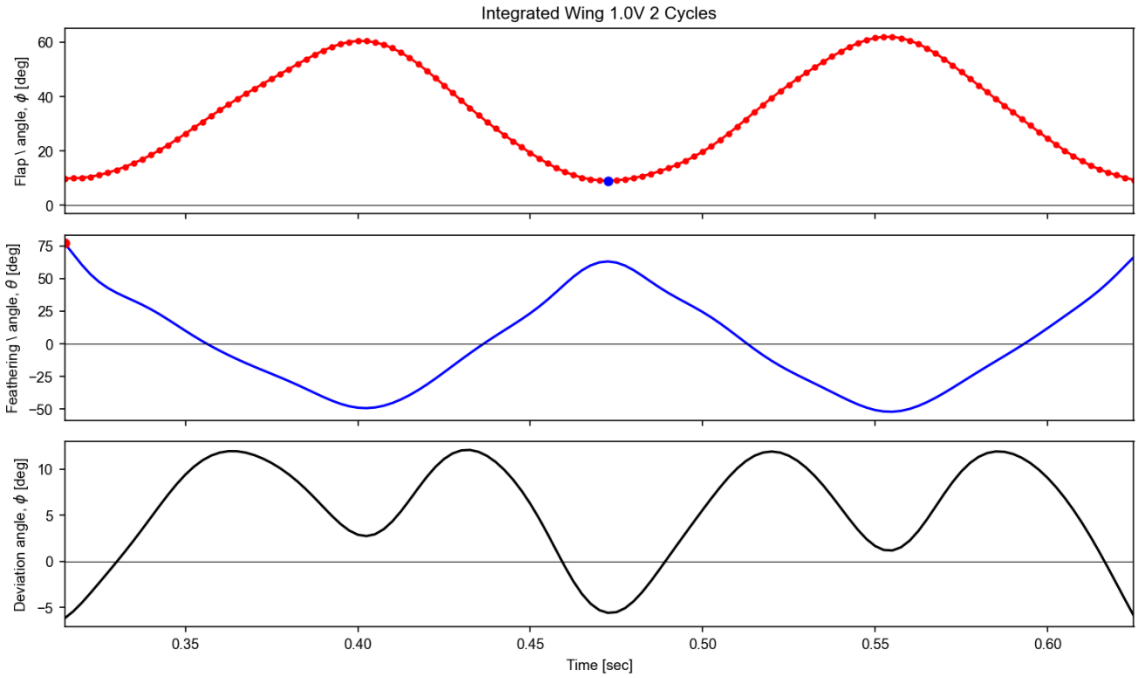

Figure A.24 Representative time history for 2 cycles of the integrated wing flapping with an input voltage of 1.0 V. The average feathering angle is 1.68° while the flapping frequency is 6.45 Hz. The peak-to-peak flapping amplitude is 53.08° while the peak-to-peak feathering amplitude is 129.74°.

Table A.12 Average feathering angles for the half-cycles of the two cycles for the integrated wing flapping with a voltage input of 1.0 V.

	Upstroke 1	Downstroke 1	Upstroke 2	Downstroke 2
Average Feathering Angle (°)	5.80	-0.55	5.22	-3.77

Appendix B. Additional Empirical Lift and Drag Time Histories

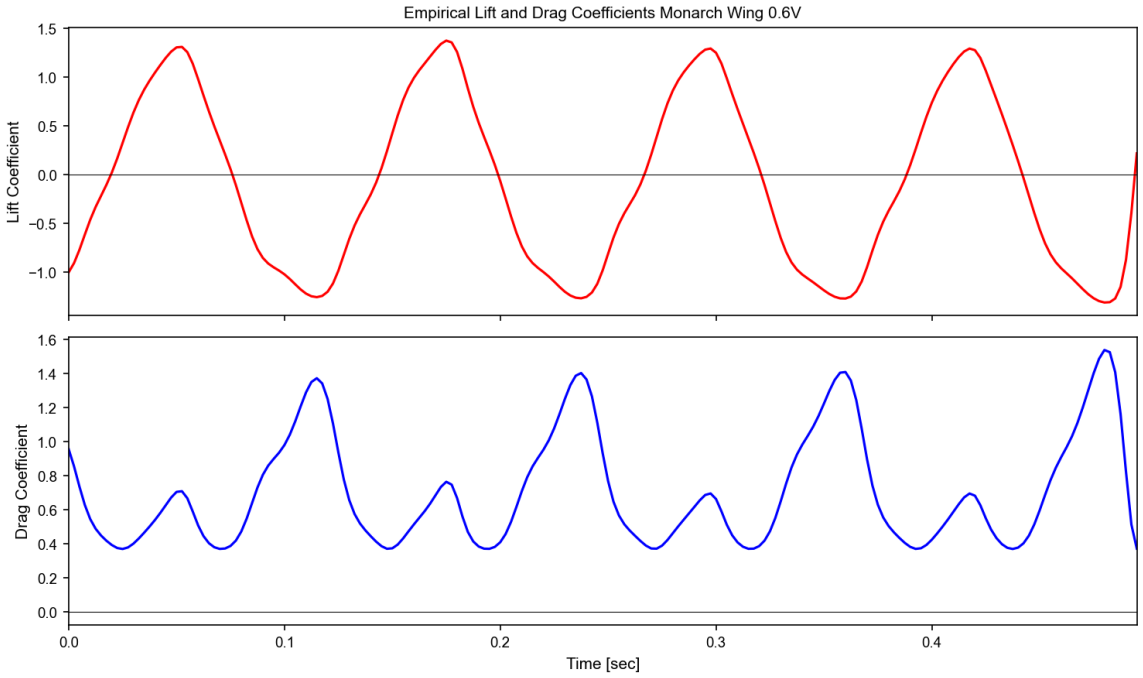

Figure B.1 Empirical lift and drag coefficient curves calculated from the feathering angle of a monarch wing flapping with an input voltage of 0.6 V. The average lift coefficient is -0.10, and the average drag coefficient is 0.71. The maximum lift coefficient is 1.4.

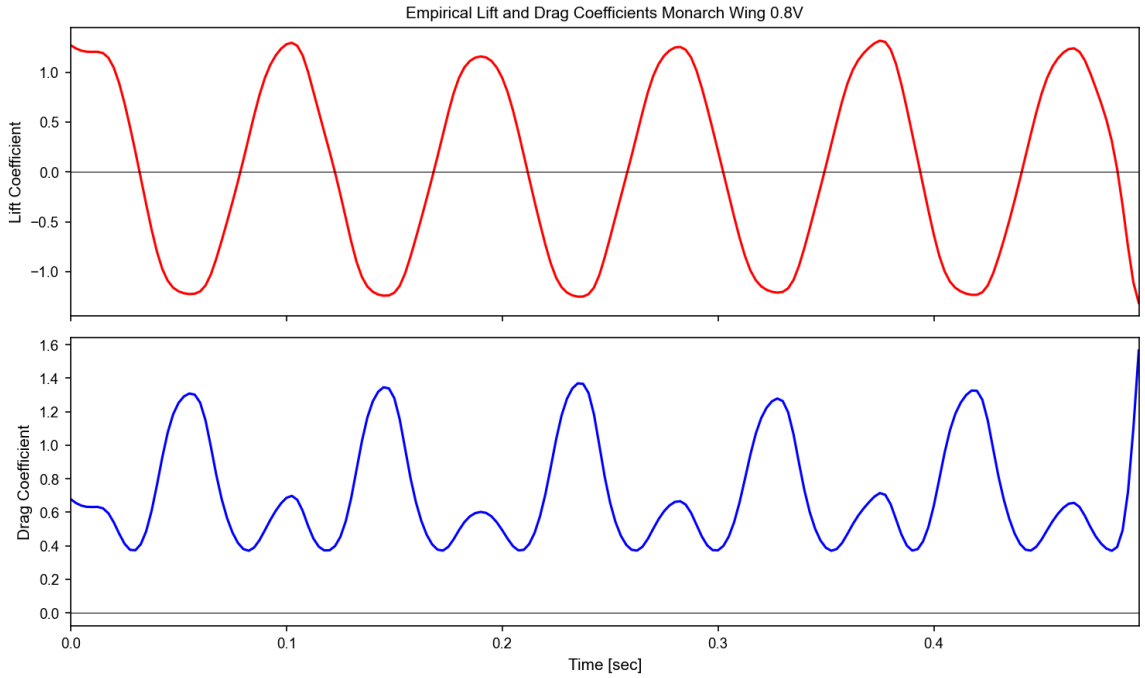

Figure B.2 Empirical lift and drag coefficient curves calculated from the feathering angle of a monarch wing flapping with an input voltage of 0.8 V. The average lift coefficient is 0.02, and the average drag coefficient is 0.70. The maximum lift coefficient is 1.3.

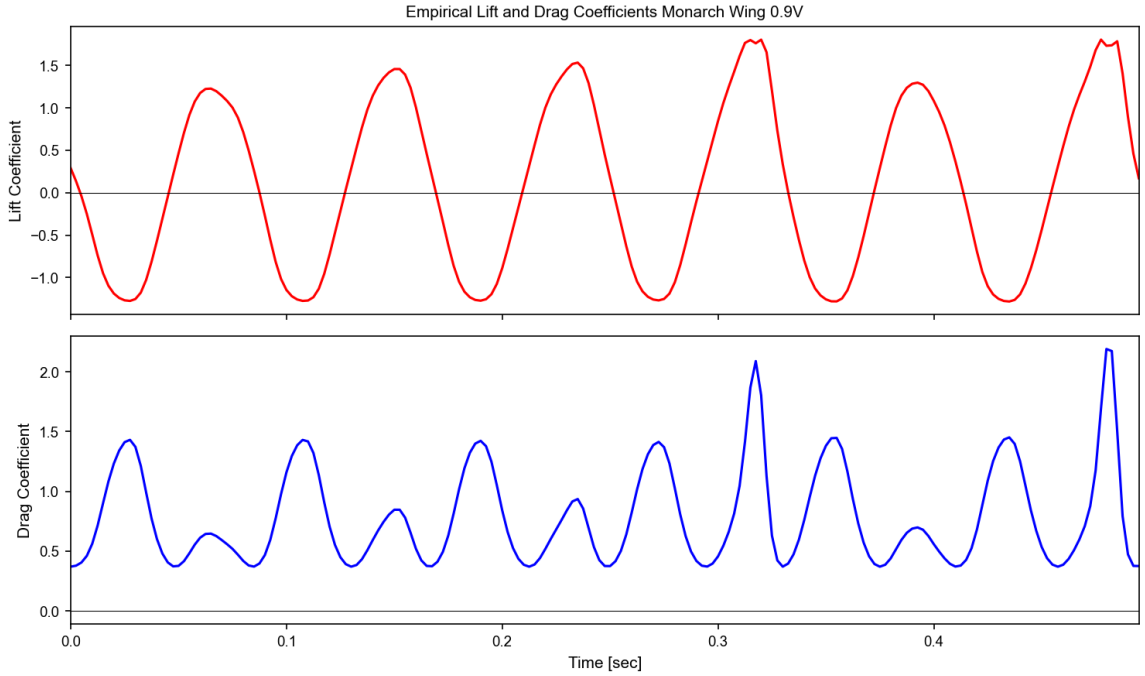

Figure B.3 Empirical lift and drag coefficient curves calculated from the feathering angle of a monarch wing flapping with an input voltage of 0.9 V. The average lift coefficient is -0.04, and the average drag coefficient is 0.79. The maximum lift coefficient is 1.8.

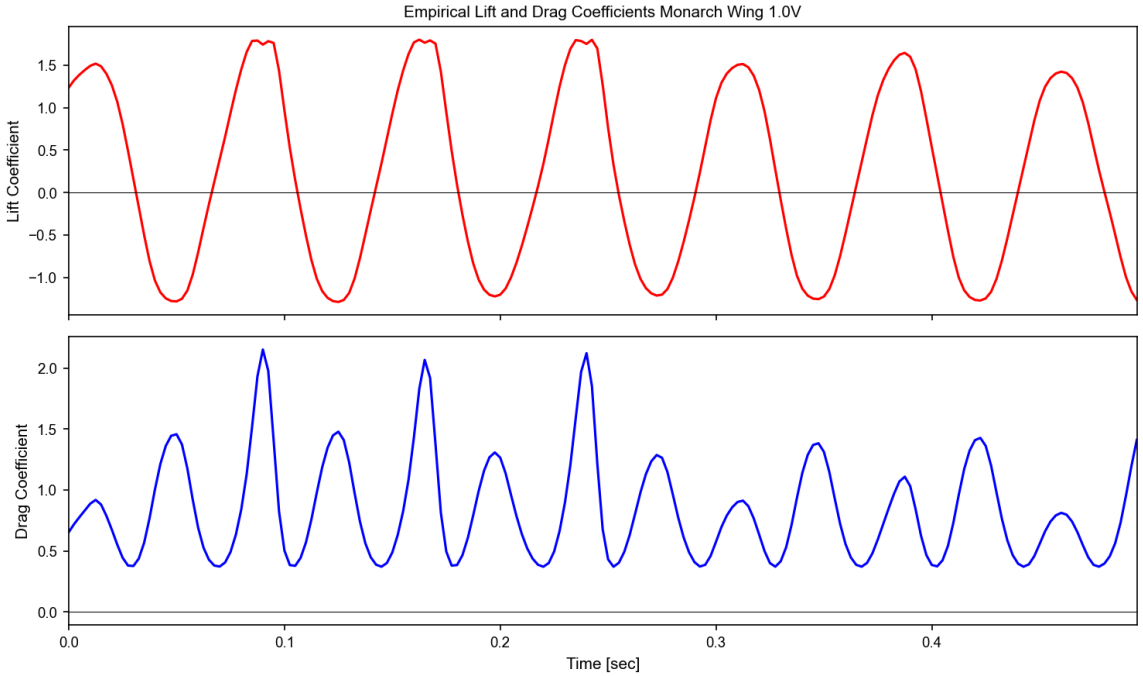

Figure B.4 Empirical lift and drag coefficient curves calculated from the feathering angle of a monarch wing flapping with an input voltage of 1.0 V. The average lift coefficient is 0.20, and the average drag coefficient is 0.84. The maximum lift coefficient is 1.8.

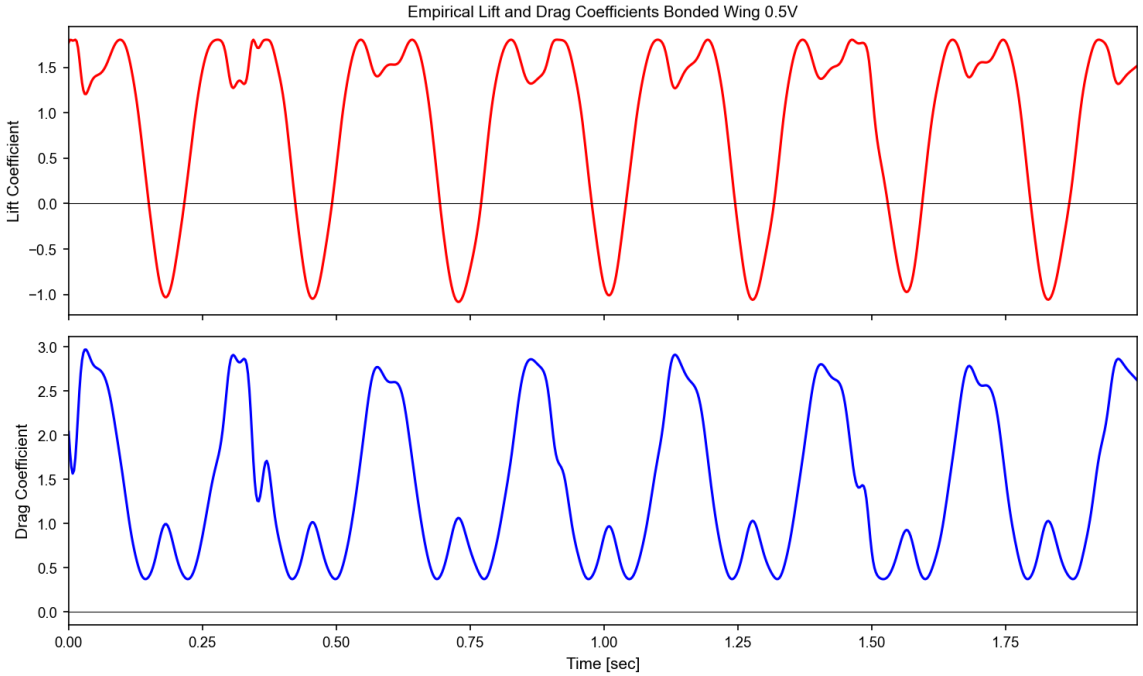

Figure B.5 Empirical lift and drag coefficient curves calculated from the feathering angle of the bonded wing flapping with an input voltage of 0.5 V. The average lift coefficient is 0.87, and the average drag coefficient is 1.39. The maximum lift coefficient is 1.8.

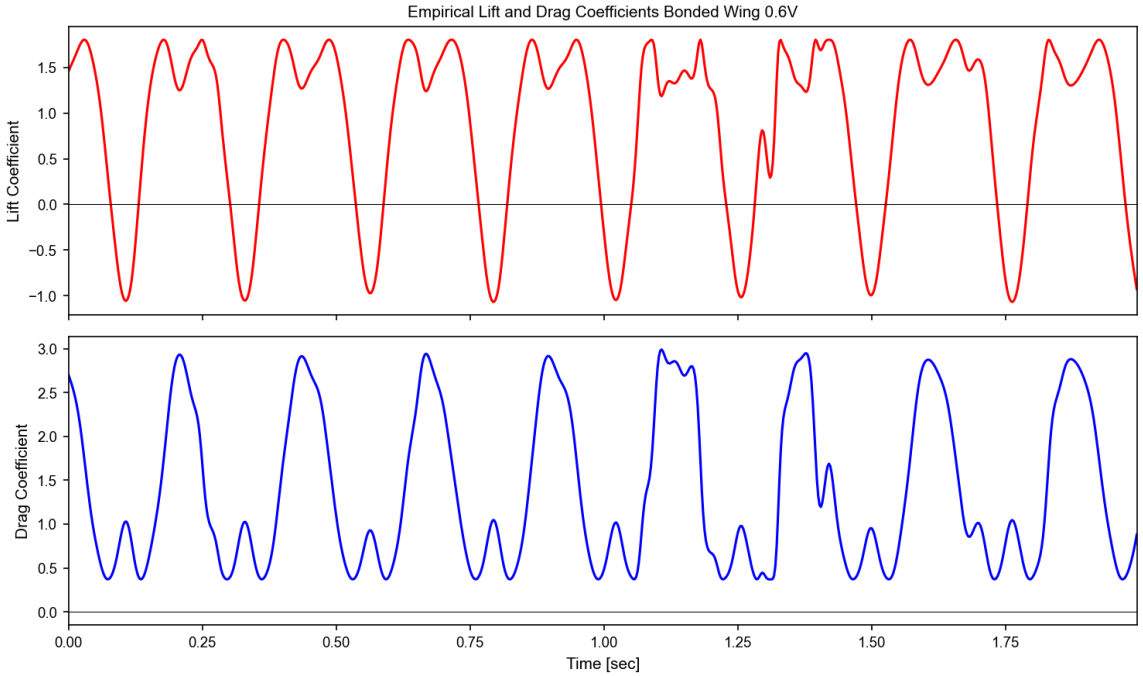

Figure B.6 Empirical lift and drag coefficient curves calculated from the feathering angle of the bonded wing flapping with an input voltage of 0.6 V. The average lift coefficient is 0.87, and the average drag coefficient is 1.38. The maximum lift coefficient is 1.8.

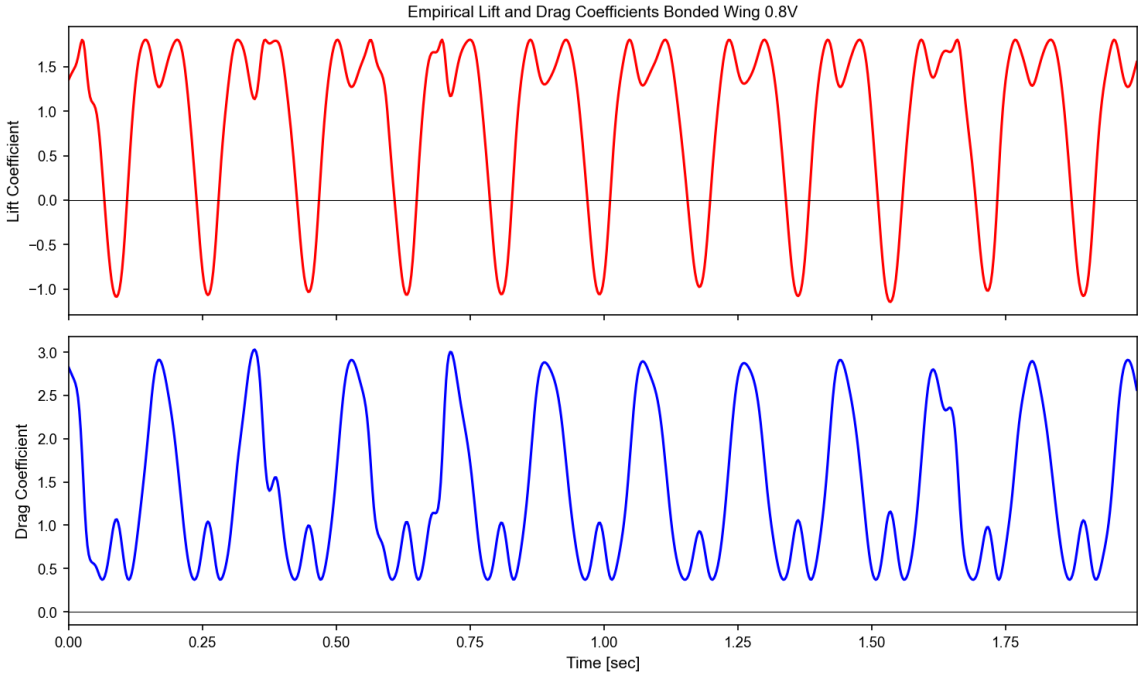

Figure B.7 Empirical lift and drag coefficient curves calculated from the feathering angle of the bonded wing flapping with an input voltage of 0.8 V. The average lift coefficient is 0.87, and the average drag coefficient is 1.38. The maximum lift coefficient is 1.8.

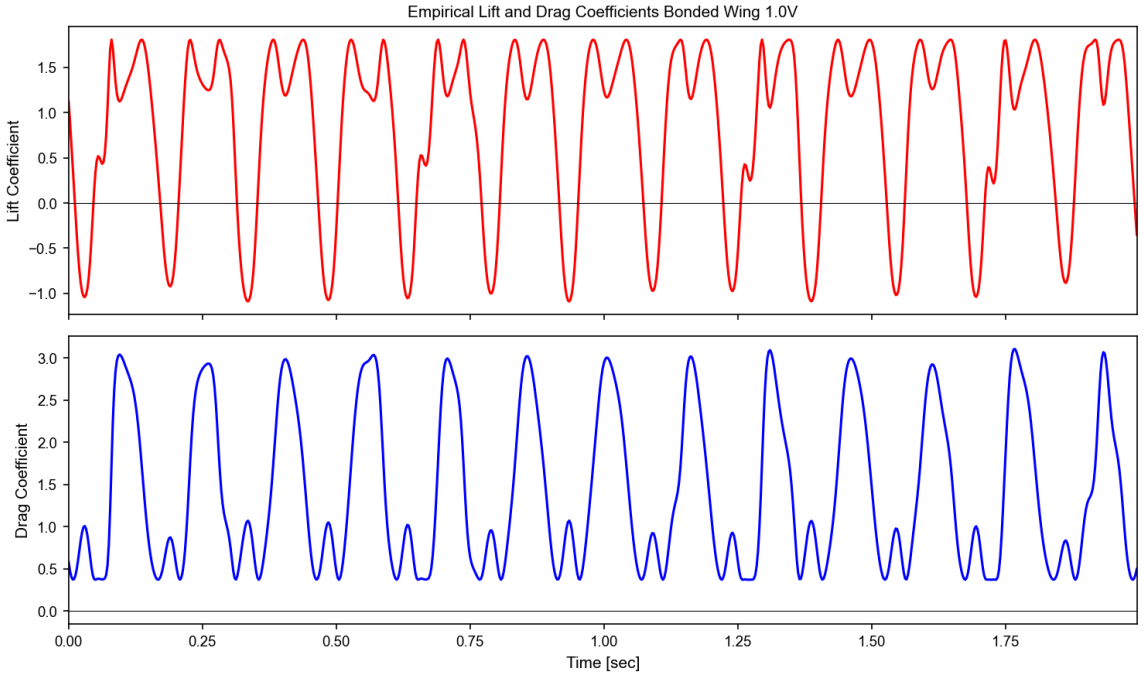

Figure B.8 Empirical lift and drag coefficient curves calculated from the feathering angle of the bonded wing flapping with an input voltage of 1.0 V. The average lift coefficient is 0.83, and the average drag coefficient is 1.40. The maximum lift coefficient is 1.8.

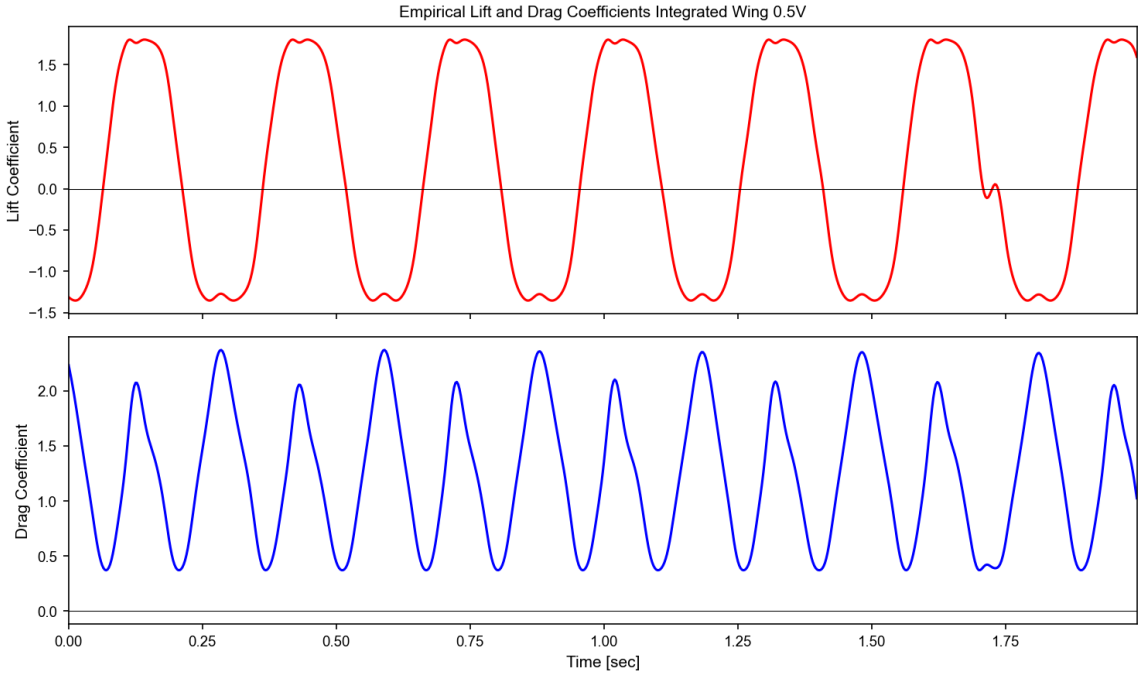

Figure B.9 Empirical lift and drag coefficient curves calculated from the feathering angle of the integrated wing flapping with an input voltage of 0.5 V. The average lift coefficient is 0.18, and the average drag coefficient is 1.24. The maximum lift coefficient is 1.8.

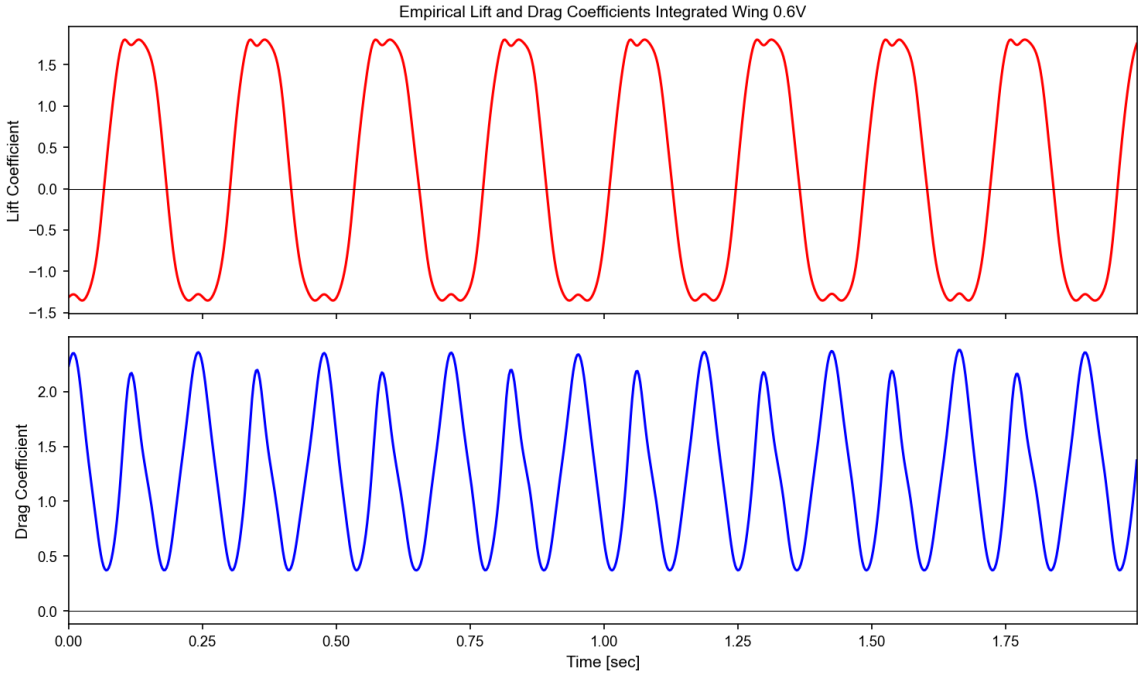

Figure B.10 Empirical lift and drag coefficient curves calculated from the feathering angle of the integrated wing flapping with an input voltage of 0.6 V. The average lift coefficient is 0.11, and the average drag coefficient is 1.26. The maximum lift coefficient is 1.8.

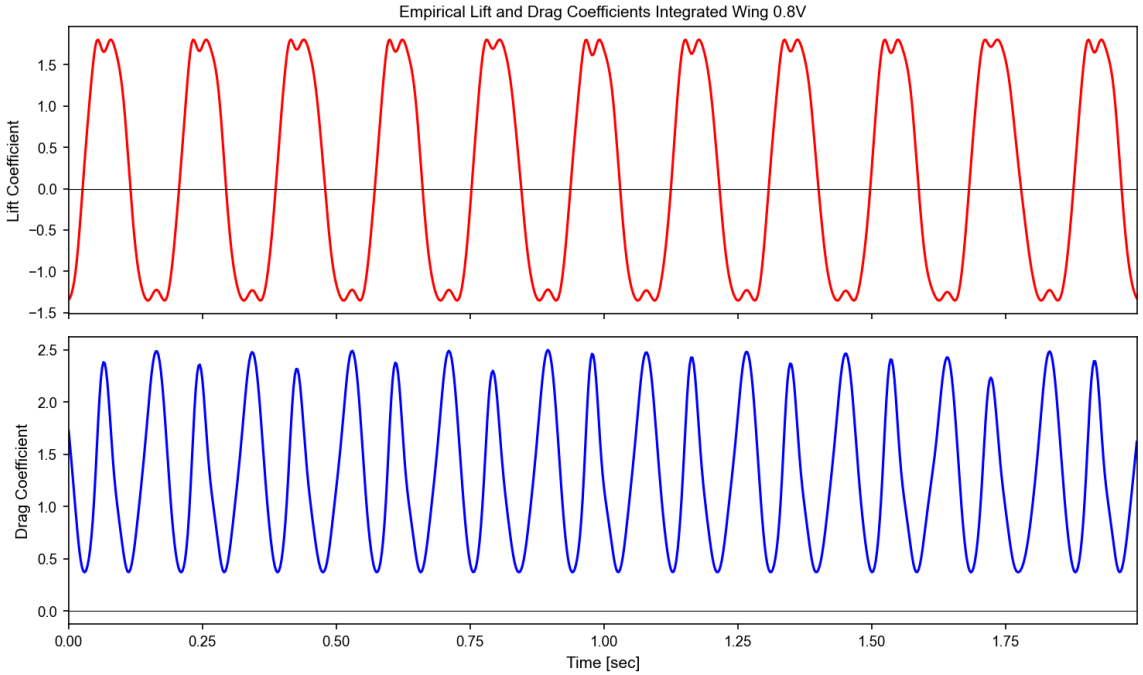

Figure B.11 Empirical lift and drag coefficient curves calculated from the feathering angle of the integrated wing flapping with an input voltage of 0.8 V. The average lift coefficient is 0.15, and the average drag coefficient is 1.29. The maximum lift coefficient is 1.8.

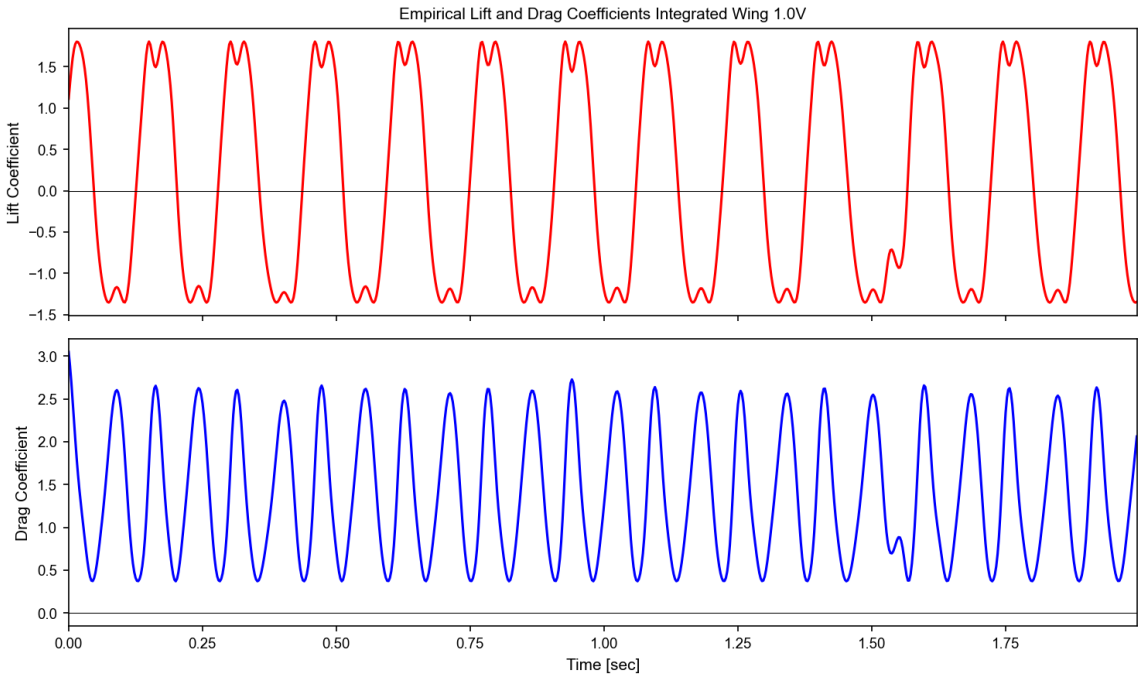

Figure B.12 Empirical lift and drag coefficient curves calculated from the feathering angle of the integrated wing flapping with an input voltage of 1.0 V. The average lift coefficient is 0.12, and the average drag coefficient is 1.39. The maximum lift coefficient is 1.8.